Monitoring of reducing conditions in soils and implications for biogeochemical processes

I n a u g u r a l - D i s s e r t a t i o n

zur

Erlangung des Doktorgrades

der Mathematisch-Naturwissenschaftlichen Fakultät

der Universität zu Köln

vorgelegt von

Kristof Dorau

aus Minden

Köln 2017

Berichterstatter:	Prof. Dr. Tim Mansfeldt
	PD Dr. Martin Kehl
Tag der mündlichen Prüfung:	13.04.2016

Summary

Reducing conditions in soils alter a variety of biogeochemical processes that affects the mobility of nutrients and pollutants, the emission of greenhouse gases, and the formation of redoximorphic features. Hence, a precise characterization and monitoring of reducing conditions is important for land use management and risk assessment. Conventionally, platinum (Pt) electrodes are used to measure the redox potential (E_H) for delineation of the soil redox status. In combination with a data-logger system the E_H can be monitored at high temporal resolution but with the shortcoming of cost-intensive technical equipment. Alternatively, the Indicator of Reduction In Soils (IRIS) method can be used to delineate soil reducing conditions that consists of synthesized iron (Fe^{III}) oxides coated onto white polyvinyl chloride (PVC) bars. The bars are installed for a period of 30 days in the soil and visually assessed for the effects of reduction by the depletion of the Fe^{III} oxide coating. Currently, a differentiation into redox classes of oxidizing (E_H > 300 mV; oxygen (O_2) is present in the soil), weakly reducing (E_H 300 to 100 mV; manganese ($Mn^{III,IV}$) oxide reduction), and moderately reducing (E_H 100 to –100 mV; Fe^{III} oxide reduction) soil conditions can only be achieved by Pt electrodes.

The objectives of this thesis are to investigate the temporal and spatial distribution of the E_H by different monitoring approaches. Automated Pt electrode measurements on hourly basis (2011 to 2014) were compared with measurements on a weekly basis (1990 to 1993) to query the benefit of high temporal resolution E_H monitoring. Additionally, the IRIS method was adopted by coating $Mn^{III,IV}$ oxides onto white PVC bars (in the following referred to as ‘Mn and Fe redox bars’) and evaluated for their potential to differentiate into weakly and moderately reducing soil conditions in field and laboratory experiments. An important characteristic of $Mn^{III,IV}$ and Fe^{III} oxides is their functioning as a sorbent for elements in soil solution. Therefore, the oxide coatings of previously field-installed redox bars were extracted and analyzed to investigate the element sorption behavior. Finally, long-term groundwater data (1997 to 2012) was analyzed to assess trends of the water table (WT) depth development along a 17 km^2 sized mesotrophic fen, which is relevant for the onset of reduction and with impact on the soil redox status. All field-experiments were conducted at different study sites in North-West Germany.

Daily E_H readings by Pt electrodes were sufficient to equally derive trends of the redox class distribution over time compared with hourly measurements but a loss of information occurred when weekly or monthly E_H readings were performed. Since fluctuations up to 540 mV were measured within a day, hourly readings were essential to identify biogeo-

chemical processes. Besides E_H measurements by Pt electrodes, it was possible to facilitate a durable $Mn^{III,IV}$ oxide coating onto white PVC bars enabling to monitor the soil redox status. Laboratory experiments at defined E_H-pH conditions went along with $Mn^{III,IV}$ oxide dissolution under weakly reducing conditions. The capillary fringe above the groundwater surface was identified as a hot spot for $Mn^{III,IV}$ oxide reduction with minor Fe^{III} oxide removal. Hence, the simultaneous application of Mn and Fe redox bars enabled to differentiate zones of weakly and moderately reducing soil conditions. It was found that the presence of ferrous Fe^{2+} (reductant) in soil solution mediated an abiotic redox reaction with the formation of durable Fe^{III} oxide coatings along Mn redox bars. Subsequently, $Mn^{III,IV}$ oxides (oxidant) transformed to manganous Mn^{2+} being removed from the PVC surface. The Fe precipitates and the remaining $Mn^{III,IV}$ oxide coating differed remarkably in color enabling to quantify the percentage area of these patterns over time. Thereby, temporally and spatially diverse pathways of Fe^{III} oxide forming processes can be studied. Selective chemical extraction of these oxide coatings along Mn redox bars verified a preferential sorption of cationic elements (e.g. copper, lead, zinc) to the surface of $Mn^{III,IV}$ oxides, whereas the positively charged surface of *in situ* formed Fe^{III} oxides were enriched in elements having an oxyanionic character (e.g. arsenic, molybdenum, phosphorus, vanadium). Moreover, *in situ* formed Fe^{III} oxides ('field'-Fe oxides) revealed higher element loadings compared with synthesized Fe^{III} oxides along Fe redox bars ('lab'-Fe oxides). In accordance with this finding, field-Fe oxides were solely composed of short-range ordered minerals exhibiting a higher sorption capacity. The WT depth was the main driver for the above-mentioned processes and controlled the (i) E_H dynamics, (ii) oxide removal along Mn and Fe redox bars, and (iii) element relocation into the topsoil by capillary rise. In this regard, WT depth readings along a mesotrophic fen indicated a lowering by on average 20 cm at 39 out of 46 monitoring wells. A meteorological forecast of the climatic water balance until the year 2100 indicated that the development of decreasing WT depths will be intensified. Obviously, this will have impact on the soil redox status and associated biogeochemical processes within the top soil.

Overall, monitoring by Mn and Fe redox bars improves the understanding of the spatial and temporal distribution of soil reducing conditions but does not capture the 'true' dynamic nature that can be determined by Pt electrodes. A continuous monitoring of the soil redox status by Pt electrodes or redox bars over decadal time scales is important to evaluate the impact of climate change on biogeochemical processes in waterlogged soils.

Zusammenfassung

Reduzierende Bedingungen in Böden beeinflussen eine Vielzahl von biogeochemischen Prozessen, welche für die Mobilität von Nähr- und Schadstoffen, die Emission von Klimagasen und die Entstehung von redoximorphen Merkmalen verantwortlich sind. Eine präzise Charakterisierung des Redox-Milieus ist daher wichtig für eine adäquate Landbewirtschaftung und Risikobewertung. Konventionell werden Platin (Pt)-Elektroden zur Messung des Redoxpotentiales (E_H) verwendet. In Kombination mit einem Datenlogger kann der E_H-Wert zeitlich hochauflösend gemessen werden, allerdings wird dafür kostenintensive Technik benötigt. Eine kostengünstige Alternative zum Nachweis reduzierender Bedingungen ist die Indicator of Reduction In Soils (IRIS)-Methode. Dabei werden weiße Polyvinylchlorid-Stäbe mit synthetisierten Eisen (Fe^{III})-Oxiden beschichtet und für 30 Tage im Boden installiert. Durch die reduktive Auflösung der Oxidbeschichtung können die Entfärbungsmuster quantifiziert werden. Derzeit ist es nur durch den Einsatz von Pt-Elektroden möglich, die Redoxklassen von oxidierenden (E_H > 300 mV; Sauerstoff (O_2) ist vorhanden), schwach (E_H 300 bis 100 mV; Mangan ($Mn^{III,IV}$)-Oxid Reduktion) und mäßig reduzierenden (E_H 100 bis –100 mV; Fe^{III}-Oxid Reduktion) Bedingungen in Böden zu unterscheiden.

Das Ziel dieser Arbeit ist es, die zeitliche und räumliche Verteilung des E_H in Böden durch verschiedene Monitoring-Verfahren zu untersuchen. Um die Vorteile von hochauflösenden E_H-Messungen mit Pt-Elektroden zu bewerten, wurde ein stündliches Messinterval (2011 bis 2014) mit einem wöchentlichen (1990 bis 1993) verglichen. Weiterhin wurde die IRIS-Methode durch die Verwendung von $Mn^{III,IV}$-Oxiden adaptiert und die Differenzierung von schwach und mäßig reduzierenden Bedingungen in Gelände- und Laborstudien evaluiert (im Folgenden als „Mn und Fe Redox-Stäbe“ bezeichnet). Die Sorption von Elementen aus der Bodenlösung an die Oberflächen von $Mn^{III,IV}$- und Fe^{III}-Oxiden ist eine wichtige Eigenschaft dieser Minerale. Um dies weitergehend zu untersuchen, wurde die Oxidbeschichtung von im Vorfeld installierten Redox-Stäben extrahiert und auf die Elementzusammensetzung hin analysiert. Abschließend wurden Langzeitmessungen (1997 bis 2012) des Grundwasserflurabstandes in einem 17 km^2 großen Niedermoor-Einzugsgebiet ausgewertet, um Trends im Pegelverlauf zu prognostizieren, welche eine besondere Relevanz für das Redox-Milieu haben. Alle Geländeuntersuchungen wurden in Nordwestdeutschland durchgeführt.

Stündliche und tägliche Messungen des E_H-Wertes mittels Pt-Elektroden waren ausreichend, um Trends in der Redoxklassen-Verteilung über die Zeit abzuleiten. Wöchentliche und monatliche Messungen führen jedoch zu einem Informationsverlust. Da Tages-

schwankungen von 540 mV gemessen wurden, ist es empfehlenswert auf stündlicher Basis zu messen, um biogeochemische Prozesse zu identifizieren. Mangan-Oxid beschichtete PVC-Stäbe dienten ebenfalls zum Nachweis reduzierender Bedingungen. Laborstudien unter definierten E_H-pH Bedingungen gingen mit einer Reduktion der $Mn^{III,IV}$-Oxide unter schwach reduzierenden Bedingungen einher. Geländeuntersuchungen haben gezeigt, dass besonders der Kapillarsaum oberhalb der Grundwasseroberfläche ein „hot spot" der $Mn^{III,IV}$-Oxid Reduktion war, bei nur geringer Fe^{III}-Oxid Entfärbung. Der simultane Einsatz von Mn und Fe Redox-Stäben ermöglicht es daher, schwach und mäßig reduzierende Bedingungen in Böden zu differenzieren. Die Gegenwart von Fe^{2+} (Reduktant) in der Bodenlösung verursachte eine abiotische Redoxreaktion mit der Bildung von Fe^{III}-Oxiden entlang der Mn Redox-Stäbe. Als Folge werden die $Mn^{III,IV}$-Oxide (Oxidant) zu Mn^{2+} reduziert und gehen in Lösung. Die $Mn^{III,IV}$- und Fe^{III}-Oxide unterschieden sich deutlich in der Farbe, welches weitergehende Studien zur räumlichen und zeitlichen Fe^{III}-Oxid Bildung ermöglicht. Durch den Einsatz einer selektiven Extraktionsmethode der Oxidbeschichtung konnte darüber hinaus nachgewiesen werden, dass $Mn^{III,IV}$-Oxide präferentiell kationische Elemente aus der Bodenlösung sorbieren (bspw. Kupfer, Blei und Zink), wohingegen anionische Elemente (bspw. Arsen, Molybdän, Phosphor, Vanadium) mit der positiv geladenen Oberfläche der *in situ* gebildeten Fe^{III}-Oxide assoziiert sind. Die sorbierten Elementgehalte an den *in situ* gebildeten Fe^{III}-Oxiden („Gelände Fe-Oxide") überstieg die der synthetisierten Fe^{III}-Oxide („Labor Fe-Oxide"). In Übereinstimmung mit diesem Befund waren die Gelände Fe-Oxide ausschließlich geringkristalliner Natur mit höheren Sorptionskapazitäten. Der Grundwasserflurabstand war der wichtigste Einflussfaktor für die genannten Prozesse und steuerte die (i) E_H-Dynamik, (ii) Oxidentfärbung an den Mn und Fe Redox-Stäben und (iii) Bodenlösungskonzentrationen bestimmter Elemente, die durch kapillaren Aufstieg in den Oberboden verlagert werden. In diesem Zusammenhang hat das Absinken des mittleren Grundwasserflurabstandes von 20 cm an 39 von 46 Pegeln des Niedermoor-Standortes eine besondere Bedeutung auf die biogeochemischen Prozesse im Oberboden.

Mangan und Fe Redox-Stäbe verbessern das Verständnis der räumlichen und zeitlichen Verteilung von reduzierenden Bedingungen in Böden. Die Entfärbungsmuster spiegeln jedoch nicht die „wahre" Redox-Dynamik wieder, wie sie mit Pt-Elektroden bestimmt werden kann. Ein Langzeit-Monitoring reduzierender Bedingungen durch Pt-Elektroden oder Redox-Stäbe ist sinnvoll, um bspw. den Einfluss des Klimawandels auf biogeochemische Prozesse in grundwasserbeeinflussten Böden zu beurteilen.

Acknowledgements

Without the wide-ranging support of many people around me, the preparation of this thesis would not have been possible. At first place, I want to express my gratitude to my advisor Prof. Dr. Tim Mansfeldt for his guidance and the ability to pursue my own ideas. Besides constructive discussions during numerous field trips, his enduring effort and support to implement many of the experiments helped me to stay focus.

Furthermore, I would like to express my gratitude to:

- PD Dr. Martin Kehl for co-supervising this thesis and valuable comments in advance,
- members of the research group Soil Geography / Soil Science (Corinna Földi, Karin Greef, Marius Gurk, Anne Kolvenbach, Max Lösse, Heike Mandt, Katrin Matern) for many stimulating talks and support in various ways,
- people from different institutions who contributed to the studies directly or were involved in the peer-review process (Ruth Bruker, Christoph Burow, Dr. Reiner Dohrmann, Dirk Esplör, Dr. Matthias Händel, Dr. Peter Held, Dr. Stephan Opitz, Dr. Stefan Roitsch, Dr. Stefan Wessel-Bothe),
- Michael Eickmeier, Henrik Gelhausen, Samuel Papenfuß, Marcel Possoch, and Julian Rölkens for their enthusiasm during their theses and their support,
- *Verein der Freunde und Förderer der Universität zu Köln* for financial support,
- Steffen Richter for deepening my electrotechnical knowledge, and
- Helge Aasen for being a companion (and many more on the course…).

I can be proud to have parents and grandparents, who supported me my entire life and never questioned my decisions. Finally, my motivation to keep on going – thank you Anne-Katrin.

Cologne, February 2016 Kristof Dorau

Contents

Figures

Tables

Chapter 1 Introduction

Reducing conditions in soils

Reducing conditions are widespread in terrestrial ecosystems and relate to soils that are temporarily or permanently water saturated (Ponnamperuma 1972). Suitable habitats to achieve reducing conditions are located in wetlands with low elevation and near-surface groundwater (Reddy and DeLaune 2008). The general term of "wetland" can be differentiated into more precise land classifications such as marshes, swamps, bogs, and fens. Wetlands play a unique role in regulating biogeochemical cycles as a critical feature of the global landscape. It is estimated that 6% of the Earth's land surface can be classified as wetland (Reddy and DeLaune 2008) illustrating the importance and all-round distribution of reducing conditions in soils.

The onset of reduction is the most important chemical change within soils (Ponnamperuma et al. 1967). Reduction, which is the gain or acceptance of an electron (e^-), and oxidation, which is the loss or donation of an electron, regulate many biogeochemical reactions in surface environments. Further, reduction-oxidation (redox) reactions always occur together and involve the transfer of electrons and protons (H^+) between the participating redox couples as shown by equation [1]:

$$Ox + mH^+ + ne^- \leftrightarrow Red \qquad \text{[Eq. 1]},$$

where *Ox* is the oxidized species, *m* and *n* is the number of H^+ and e^- involved in the reaction, and *Red* is the reduced species (DeLaune and Reddy 2005). During the transfer of electrons from a *Red* species (electron donor or reductant) to an *Ox* species (electron acceptor or oxidant), the oxidation number of the former compound is increased whereas the oxidation number of the latter compound is decreased. A prominent redox reaction is the process of carbon (C) fixation and oxygen (O_2) production by plants during photosynthesis. It can be expressed by the overall reaction

$$CO_2 + H_2O = CH_2O + O_2 \qquad \text{[Eq. 2]},$$

where CH_2O idealizes a carbohydrate. Carbon occurring in the soil organic matter (SOM) pool is the primary source of electrons and the most important electron donor. The SOM pool is continuously replenished by new inputs of roots, microbes, and dead plant matter and is important for microorganisms to obtain energy. However, to use the energy by the oxidation of SOM and by releasing carbon dioxide (CO_2), electron transfer to an acceptor is a prerequisite because free electrons do not exist in chemical reactions. If O_2 is available, it is used as terminal electron acceptor because it is most energy-efficient for heterotrophic microorganisms to reduce O_2 to water in the process of aerobic respiration (Glinski and Stepniewski 1985; Strawn et al. 2015). Soils are an open and porous system composed of solids, liquids, and gases and are in a continuous exchange of matter and energy

with the surrounding spheres. Flooding or other events cause water-saturation that hampers the replenishment of O_2 from the atmosphere, because O_2 diffusion rates through water-filled pores are slowed-down $3 \cdot 10^5$ times (Zausig et al. 1993) compared to air-filled pores. Hence, the availability of O_2 is in a transient state and not constant over time. Depending on various other external factors such as microbial population, soil temperature, organic amendments, CO_2 concentrations, bulk density and aggregate size, pH, and the presence of trace metals and pesticides (Glinski and Stepniewski 1985), the rate of O_2 exhaustion varies significantly between different soil types. A decrease to one-hundredth of the initial O_2 concentration was reported within 75 minutes after soil samples were water-saturated, which renders this process very dynamic (Scott and Evans 1955).

The redox status under which O_2 is present is termed “aerobic” or “oxidizing” and characterized by low electron availability, whereas the absence of O_2 is termed “anaerobic” or “reducing” with corresponding high electron availability (Essington 2015). Once the O_2 is depleted in the soil, obligate and facultative anaerobe microorganisms start using various other electron acceptors. The order is given by thermodynamics. Sequentially, pentavalent nitrogen (N^{V}) in nitrate (NO_3^-), tri- and tetravalent manganese ($Mn^{III,IV}$) in Mn oxides, trivalent iron (Fe^{III}) in Fe oxides, hexavalent sulfur (S^{VI}) in sulfate (SO_4^{2-}), and tetravalent carbon (C^{IV}) in carbon dioxide (CO_2), are reduced to their counterparts nitrous oxide (N_2O), elemental nitrogen (N_2), or ammonium (NH_4^+), manganous Mn^{2+}, ferrous Fe^{2+}, hydrogen sulfide (H_2S) and methane (CH_4) (Kirk 2004; Reddy and DeLaune 2008) (see Fig. 1.1 for illustration).

To quantify the reduction (or oxidation) intensity, the redox potential (E_H) scale in units of electrochemical energy (in V or mV) is used (DeLaune and Reddy 2005). It is a measure of the ability of elements to accept or donate electrons (Strawn et al. 2015). The E_H can be measured by connecting an inert platinum (Pt) electrode (‘working electrode’) with a ‘reference electrode’. When using the standard hydrogen electrode (SHE) as a reference electrode, which is composed of

- a Pt electrode,
- immersed into a 1 M H^+ containing solution (= pH 0),
- having a hydrogen gas (H_2) partial pressure of 1013 hPa,
- and a system temperature of 298.15 K (= 25 °C),

a standard reference is obtained with the reversible half-reaction of

$$H_2 = 2H^+ + 2e^- \qquad \text{[Eq. 3].}$$

The standard electrode potential (E^0) of the SHE serves as a reference base for any other chemical reaction and is per definition E^0 = 0 mV (Reddy and DeLaune 2008). Assuming the SHE connected to the Pt electrode and immersed into a solution containing the $Fe(OH)_3$–Fe^{2+} redox couple (at unit activity and equilibrium is attained), electrons start to flow and the measured E_H refers to the standard state potentials (Reddy and DeLaune 2008) of the involved species with the overall reaction of

$$Fe(OH)_3 + 3H^+ + e^- = Fe^{2+} + 3H_2O \qquad E^0 = 800 \text{ mV} \qquad \text{[Eq. 4].}$$

A relationship between redox potentials in soils and the participating oxidized and reduced species is derived by the Nernst equation (Strawn et al. 2015) with

$$E_H = E^0 - \frac{59}{n} log \frac{(Red)}{(Ox)} - \frac{m}{n} 59pH \qquad \text{[Eq. 5].}$$

Equation [5] reveals that a pH increase goes along with an E_H decrease. In nature, all redox reactions comprise the transfer of protons between the participating redox couples as demonstrated in equation [4]; one mol $Fe(OH)_3$ reduction consumes 3 mol of H^+. A predicted change of –59 mV per pH unit occurs, which is also included in equation [5] (called 'Nernst factor'). It is commonly used to adjust E_H data to pH 7 and remove pH variability between soils for the purpose of comparability (Bohn 1971). However, this value has little theoretical or experimental justification because E_H-pH slopes vary depending on the chemical system from –6 to –256 mV per pH unit (Fiedler et al. 2007). In soils, E_H ranges between 800 and –300 mV (Reddy and DeLaune 2008).

Analogous to the pH value, which describes the H^+ activity and is defined in terms of "mol H^+ L^{-1}", the pe value can be used to describe the electron activity. Both parameters can be considered to do thermodynamic work (Essington 2015; James and Brose 2012), even though the pe is not defined with "mol e^- L^{-1}". Such as pH, pe values range several orders of magnitude but unlike pH, it can have negative values (Essington 2015). Plotting of pe+pH data within a stability diagram enables to assess how redox conditions in soils alter the speciation of elements under consideration. A relation between pe and the SHE potential can be obtained by the expression

$$E_H = \frac{RTln10}{F} pe \qquad \text{[Eq. 6],}$$

with R being the natural gas constant (8.3145 J mol^{-1} K^{-1}), T being the temperature in Kelvin (25 °C = 298.15 K), F being the Faraday constant (96,484.56 C mol^{-1}). Substitution for F and R in equation [6] yields

$$E_H = 59.16pe \qquad \text{[Eq. 7],}$$

with E_H being expressed in mV. Hence, redox relationships and the abundance of electrons within the soil environment can be described either by the pe (electron activity) or the E_H (electrode potential) (Lindsay 1979). It should be noted that E_H can be measured directly within the soil as a cell potential and with respect to the SHE potential, whereas pe values for redox systems can only be calculated in terms of E^0 data or by conversion from E_H data. Reddy and DeLaune (2008) state that from a practical point of view the application of E_H is simpler with a wider applicability compared with the concept of pe. However, Lindsay (1979) encourages the use of pe+pH instead of E_H, because it partitions the H^+ ions into those involved in the redox reaction and those related with the acid-base concept, which simplifies the theoretical use of redox reactions.

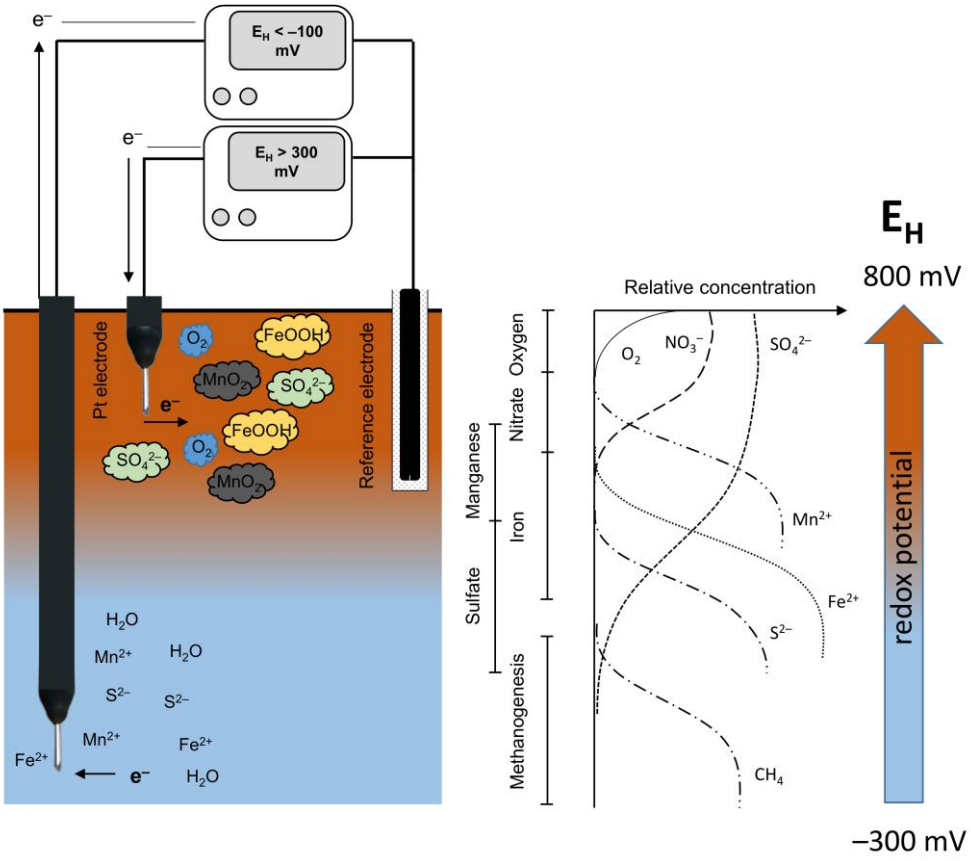

Figure 1.1 The illustration to the left shows the principle of E_H measurements performed in an oxidizing (E_H > 300 mV) and in a strongly reducing (E_H < –100 mV) soil environment with the corresponding distribution of electron acceptors (O_2, MnO_2, FeOOH, SO_4^{2-}) and their reduced equivalent (H_2O, Mn^{2+}, Fe^{2+}, S^{2-}) in the surrounding of the Pt tip. The graph to the right displays the relative concentration of electron acceptors as a function of time (and depth) after a flooding event; prerequisite is an unlimited supply of electron donors as food source. The subsequent order of oxidized and reduced species in the graph is related to the 'sequential reduction sequence' occurring in soils (adapted from Fiedler et al. 2007; Reddy and DeLaune 2008; Strawn et al. 2015).

The redox status of a soil is important and related to various fields of environmental issues regarding the release of greenhouse gases (Yu and Patrick 2004), metal mobility (Hindersmann and Mansfeldt 2014), nutrient availability (Peretyazhko and Sposito 2005), and pedogenesis (Bouma 1983). Hence, the assessment and characterization of reducing conditions is important for scientists, stakeholders and practitioners dealing with the abovementioned topics. According to the sequential use of prominent electron acceptors (Fig. 1.1), redox classes of

- oxidizing (E_H > 300 mV; O_2 is present in the soil),
- weakly reducing (E_H 300 to 100 mV; NO_3^- and $Mn^{III,IV}$ oxide reduction),
- moderately reducing (E_H 100 to –100 mV; Fe^{III} oxide reduction), and
- strongly reducing (E_H < –100 mV; SO_4^{2-} and CO_2 reduction)

can be deduced (Reddy and DeLaune 2008). This classification will be applied in the following thesis (please note that the classification in Chapter 2 is slightly different and obtained from Zhi-Guang 1985). It is more precise than, for instance, the classification according to the National Committee for Hydric Soils (2015; NTCHS). One feature of the NTCHS concept to characterize whether a soil is reduced is based on the empirical stability line for the Fe^{3+}–Fe^{2+} redox couple defined by the equation

$$E_H = 595 - (60pH) \quad \text{[Eq. 8]}.$$

If the measured soil E_H is underneath the E_H-pH stability line of equation [8] for at least 14 consecutive days, the soil can be considered reducing and defined as ‘hydric soil’ (NTCHS 2015). However, it seems reasonable to use a more precise classification because various geochemical processes are induced within a distinct redox class. Figure 1.2 attributes findings of environmental relevance linked to either weakly, moderately, or strongly reducing soil conditions (please note the overlapping areas and keep in mind that these processes are not separated by a sharp E_H boundary). Under weakly reducing conditions, the reductive dissolution of $Mn^{III,IV}$ oxides with the subsequent release of potentially sorbed, hazardous elements such as cobalt (Co) and molybdenum (Mo) (Fig. 1.2) is enhanced. However, moderately reducing soil conditions favor the reduction of arsenic (As)-hosting Fe^{III} oxides and increase the As availability in soil solution. Both oxides are important interfaces and scavengers for pollutants as well as nutrients (Komárek et al. 2013; Smedley and Kinniburgh 2002). Besides the effect of E_H and pH on metal-hosting oxides, numerous trace elements are *directly* influenced by electron transfer reactions that alters their toxicity and sorption characteristics e.g. chromium (Cr^{III} and Cr^{VI}), As (As^{III} and As^{V}), antimony (Sb^{III} and Sb^{V}), and selenium (Se^0, Se^{-II}, Se^{IV}, Se^{VI}) (Essington 2015). Furthermore, soil reducing conditions alter denitrification and the formation of the potent greenhouse gas

nitrous oxide (N_2O) under weakly reducing conditions, whereas the formation of CH_4 is achieved by and restricted to strongly reducing conditions (Yu and Patrick 2004). Hence, a binary classification of oxidizing or reducing by the Fe^{3+}–Fe^{2+} stability line [Eq. 8] is too simplified. It would be more appropriate to differentiate redox classes as illustrated in Fig. 1.2. Overall, a comprehensive understanding of the recording, monitoring, and interpretation of reducing conditions in soils is crucial, especially in distinguishing the zones of weakly and moderately reducing conditions.

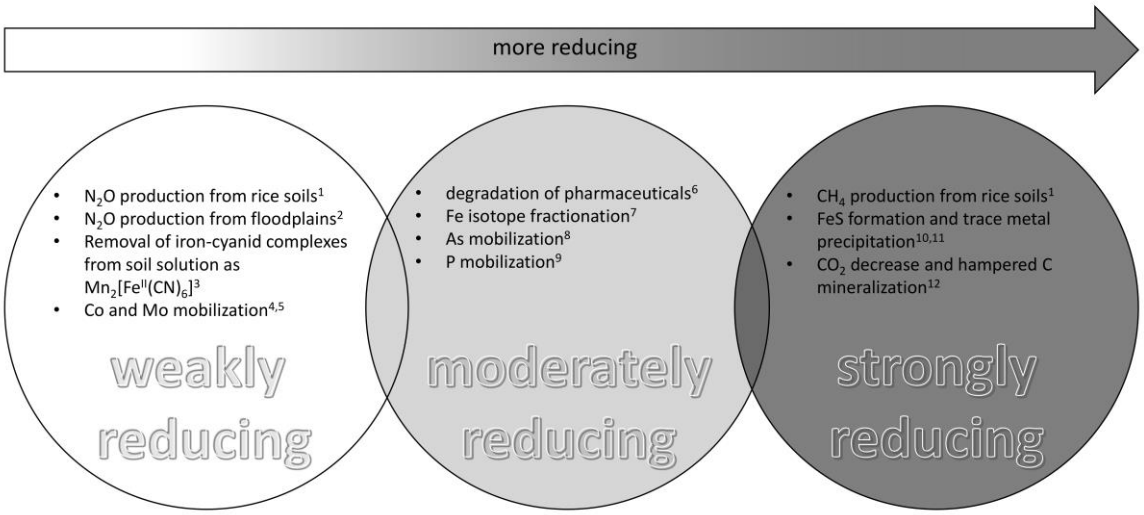

Figure 1.2 Biogeochemical processes associated to the onset of weakly, moderately and strongly reducing soil conditions. The literature overview integrates laboratory and field experiments in the subsequent order (please see indices) from: [1]Yu and Patrick 2004; [2]Shrestha et al. 2014; [3]Rennert and Mansfeldt 2005; [4]Matern and Mansfeldt 2015; [5]Hindersmann and Mansfeldt 2014; [6]Dalkmann et al. 2013; [7]Schuth et al. 2015; [8]Mansfeldt and Overesch 2013; [9]Peretyazhko and Sposito 2005; [10]Schieber 2011; [11]Morse et al. 1999; [12]Picek et al. 2000.

Methods to characterize reducing conditions in soils

Several methods are available to identify, characterize, and sometimes monitor soil reducing conditions. A simple field method comprises the use of dyes that react with Fe^{2+} in soil solution to color compounds. It is common to use 2,2' dipyridyl (Childs 1981) or potassium ferrocyanide (Ringrose-Voase and Humphreys 1993). Although it is a simple method, harmful chemicals are a prerequisite and it provides only a snapshot of the *in situ* reducing conditions. Moreover, the redox status can only be classified in terms of Fe^{III} reduction by the presence of Fe^{2+}. A differentiation of redox classes is therefore not possible (Table 1.1).

Table 1.1 Comparison of available methods to characterize soil reducing conditions. The abbreviations for the distinct categories indicate: Y = yes, NA = not applicable, N = no.

	Dyes[1]	Pt electrodes[2]	TEAPs[3]	OXC[4]	Fe nail[5]	SPP[6]	IRIS[7]
Harmful chemicals	Y	N	Y	Y	N	N	N
Expensive	N	Y	Y	Y	N	N	N
Self-manufacturing	NA	Y	NA	NA	Y	Y	Y
Lab equipment	Y	N	Y	Y	N	Y	Y
Monitoring	N	Y	Y	Y	Y	Y	Y
Redox classes	N	Y	Y	Y	N	N	N

[1] (Childs 1981; Ringrose-Voase and Humphreys 1993)
[2] (Gillespie 1920; Ponnamperuma 1972)
[3] Terminal electron-accepting processes (Chapelle et al. 1995)
[4] Oxidative capacity (Scott and Morgan 1990)
[5] (Owens et al. 2008)
[6] Striated polymer plates (Fakih et al. 2008)
[7] Indicator of Reduction in Soils (Jenkinson and Franzmeier 2006)

As previously mentioned, inert metal electrodes can be used to determine the oxidation-reduction status of a soil. Classically, a Pt tipped electrode is used in combination with a reference electrode, e.g. silver/silver chloride (Ag/AgCl) but a calomel (Hg/Hg_2Cl_2) electrode can also be used (Fiedler et al. 2007). Previous studies demonstrated that Pt electrodes (Mansfeldt 1993) and the reference electrode (Farrell et al. 1991) can be self-manufactured. Together with data logger equipment, monitoring on high temporal scale is possible and a differentiation of redox classes can be achieved (Table 1.1). The first E_H monitoring campaign using Pt electrodes was initiated in the 1920s (Gillespie 1920). Despite the long history and several successful applications in environmental sciences (Patrick and Turner 1968; Rezanezhad et al. 2014; Yu et al. 2001), this method comprises some restrictions that have to be kept in mind (see Whitfield (1974) for a detailed discussion):

- the redox couple (e.g. Fe^{3+}–Fe^{2+}) must be electroactive and the electron transfer rapid and reversible,
- species concentrations in soil solution must be greater than around 10^{-5} M (Bohn 1971),
- species adsorption onto the Pt tip surface has to be avoided because it alters the measured electrode potential, and most importantly,
- redox reactions must be in chemical equilibrium.

These prerequisites must be fulfilled for Nernstian behavior. However, in most cases it cannot be achieved under natural conditions. The fact that most redox reactions are biologically mediated with enzyme and cellular based processes make the recording and interpretation of E_H data very complicated. Though, E_H as a master variable is important to predict the speciation and mobility of elements and a continuous recording is useful to understand redox related processes (Strawn et al. 2015).

Another approach to characterize the redox status is called terminal electron-accepting processes (TEAPs), which involves simultaneous measurements of concentrations by electron acceptors (e.g. dissolved O_2, NO_3^-, SO_4^{2-}), intermediate products (dissolved H_2), and reduced species (e.g. Fe^{2+}, dissolved H_2S) along a redox gradient (Chapelle et al. 1995). It was applied for groundwater systems and provides a better understanding of redox processes on the large scale, contrary to pedological systems, where the focus of interest is in a smaller vertical and horizontal scale. Another approach is based on the concept of oxidative capacity (OXC), which integrates the major oxidized and reduced species to a single conservative parameter after defining an electron reference level (e.g. HS^-) (Scott and Morgan 1990). Both, TEAPs and OXC, comprise intensive water and soil analyses, which restricts the use of both approaches as an easy to handle field method for characterizing the soil redox status. Other available tools to infer the O_2 concentration comprise the use of polished Fe nails (Owens et al. 2008) or to install striated polymer plates (SPP; dimension of 2 · 2 cm) coated with synthesized ferrihydrite into the topsoil (Fakih et al. 2008). A differentiation of redox classes is not possible using either the former or the latter method and additionally, the latter one comprises the use of a handheld X-ray fluorescence (XRF) pistol to evaluate depletion of the Fe^{III} oxide coating and deduce reducing conditions that might not be available to many users.

A method to test whether a soil is in a reduced state uses white polyvinyl chloride (PVC) bars with a coating of synthesized Fe^{III} oxides (comparable to the use of SPP). The method is called Indicator of Reduction In Soils (IRIS) (Jenkinson and Franzmeier 2006). The Fe^{III} oxide coating acts as an electron acceptor and reveals the white PVC underneath by the removal of the oxide coating under reducing conditions. The depletion can be digitally analyzed or visually assessed to delineate the *in situ* distribution of soil reducing conditions. The more depleted the coating is, after 30 days of being installed, the more reducing the soil environment is where the bars were installed. This approach has a major advantage due to the simple implementation and the use of low cost equipment, it does not include the use of harmful chemicals, and it enables monitoring of soil reducing conditions up to 50 cm depth (whereas polished Fe nails and SPP are restricted to a small vertical profile).

Overall, monitoring of redox classes can only be achieved by the use of Pt electrodes for the soil environment. It is apparent by this brief literature review that there is an emerging need for improved methods to monitor the redox status of a soil.

Manganese and iron oxides in the soil environment

Manganese is considered to be a micronutrient and therefore an essential element for plants, animals, and human beings (Strawn et al. 2015). Its content in the lithosphere is

about 900 mg kg^{-1}, whereas contents in soils range from 20 to 3,000 mg kg^{-1} with on average 600 mg kg^{-1} (Lindsay 1979). Manganese forms hydrated oxides with three oxidation states of Mn^{II}, Mn^{III}, Mn^{IV} (Lindsay 1979). Birnessite (δ-MnO_2) is a prominent example in soils. Contrary to pure chemical systems with well known E^0 values, the redox chemistry of $Mn^{III,IV}$ oxides is particularly complicated due to a (i) broad-range from micro- to macrocrystalline phases, (ii) non-uniform stoichiometric formula (e.g. $MnO_{1.2\text{-}2.0}$), (iii) incorporation of ions into the crystal lattice (e.g. Al^{3+} and PO_4^{3-}), and (iv) co-precipitation with SOM or clay minerals (Brümmer 1974). Furthermore, (v) the presence of Mn^{2+} in soil solution is also driven by de-/sorption processes from carbonates, sulfides, and phosphates (Brümmer 1974), leading only to a qualitative interpretation of measured E_H data to predict Mn^{2+} concentrations in soil solution (Bohn 1970). Besides the reductive dissolution (electron promoted) of $Mn^{III,IV}$ oxides, proton- and ligand-promoted reactions also play an important role with the fastest dissolution rates occurring for electron transfer reactions and the slowest for proton-promoted reactions (Martin 2005). Manganese oxides are involved in many soil chemical processes such as metal ion sorption (Loganathan and Burau 1973) and related redox reactions with metal ions. They are powerful oxidizers (next to O_2) and known to oxidize Co^{II} to Co^{III}, Cr^{III} to Cr^{VI}, and As^{III} to As^{V} (summarized by Negra et al. (2005)). Finally, they serve as terminal electron acceptors for microbial and root mediated respiration of SOM (Tebo et al. 2005) and their pigmenting power enables classification of soils (IUSS Working Group WRB 2014). In a study by Canfield et al. (1993), it is estimated that one atom of Mn is 100 to 300 times oxidized and reduced before ultimately being buried into Danish coastal sediments, demonstrating the active role and catalytic reactions of these important soil constituents.

Iron oxides are the most abundant metallic oxides in the soils environment (Schwertmann and Taylor 1989). Such as Mn, Fe is essential for all organisms and thus considered a micronutrient (Strawn et al. 2015). The content of the lithosphere is about 51,000 mg kg^{-1} with a wide range for soils of 7,000 to 550,000 mg kg^{-1} and on average 38,000 mg kg^{-1} (Lindsay 1979). In soils, 16 Fe mineral phases are known and characterized at present, most of them occurring in the trivalent state (ferric Fe or Fe^{III}) (Cornell and Schwertmann 2003). Various forms of oxides, hydroxides, and oxyhydroxides exist but they will be collectively referred to as 'Fe^{III} oxide' in this thesis (analogous to '$Mn^{III,IV}$ oxide'). The broad variety and pathways of Fe^{III} oxide formation under natural conditions makes it complicated to apply thermodynamic concepts for the prediction of a distinct species (see previous paragraph; bullet points i to v). Owing to their high crystallization energy, they form minute crystals in natural environments that results in high specific surface areas of > 100 m^2 g^{-1} (Cornell and Schwertmann 2003). This renders them effective sorbents and scavengers

for toxic trace metals (e.g. As; Smedley and Kinniburgh 2002), nutrients (e.g. P; Peretyazhko and Sposito 2005), organic pollutants (e.g. glyphosate; Piccolo et al. 1994), and dissolved organic carbon (DOC; e.g. humic or fulvic acids; Zhou et al. 2001). Even at low concentrations, their pigmenting power determines the color of many soils which is important for soil classification (IUSS Working Group WRB 2014; Schwertmann and Taylor 1989).

As already outlined in the previous chapters, an outstanding feature of both elements (Mn and Fe) is their ability to function as an electron acceptor under soil reducing conditions. When the soil E_H decreases towards 300 to 100 mV, $Mn^{III,IV}$ oxides start to reductively dissolve before Fe^{III} oxides according to the sequential reduction sequence (Ponnamperuma 1972). This can be explained by the higher electrode potential of $Mn^{III,IV}$ oxides [Eq. 9], compared with short-range ordered [Eq. 10] and more crystalline [Eq. 11] Fe^{III} oxides. As long as $Mn^{III,IV}$ oxides are present, the soil E_H remains at the potential of the redox couple and only decreases to the next redox couple when the oxidant is depleted (= the soil is not 'poised' anymore by the redox couple; Strawn et al. 2015).

$$MnO_2 + 2e^- + 4H^+ \quad = Mn^{2+} + 2H_2O \qquad E^0 = 520 \text{ mV (at pH 7)} \qquad \text{[Eq. 9]}$$

$$Fe(OH)_3 + e^- + 3H^+ = Fe^{2+} + 2H_2O \qquad E^0 = -71 \text{ mV (at pH 7)} \qquad \text{[Eq. 10]}$$

$$FeOOH + e^- + 3H^+ \quad = Fe^{2+} + 2H_2O \qquad E^0 = -230 \text{ mV (at pH 7)} \qquad \text{[Eq. 11]}$$

Besides the redox behavior, there are other mineralogical differences between $Mn^{III,IV}$ and Fe^{III} oxides. For instance, the point of zero charge (PZC) of birnessite (pH 1.5 to 2.8) compared with ferrihydrite (pH 7 to 9) and goethite (pH 7.5 to 9), as well as the active surface area that is in the range of 100 to 200 $m^2\ g^{-1}$ compared with 20 to 100 and up to 400 $m^2\ g^{-1}$ differs significantly for the distinct minerals, respectively (Strawn et al. 2015). Finally, birnessite (darkish-brown), ferrihydrite (reddish) and goethite (yellowish) can be differentiated by their color.

The distribution of $Mn^{III,IV}$ and Fe^{III} oxides in the soil profile is an important characteristic to classify soils. The reductive dissolution and translocations favors the development of redoximorphic features, e.g. by *gleyic* (water saturation due to groundwater) or *stagnic* (water saturation due to stagnant water) color patterns. According to the World Reference Base for Soil Resources, four of 32 reference soil groups can be classified by the presence of redoximorphic features (IUSS Working Group WRB 2014). The extent of these soil groups captures 1,085 million ha (Mha) and makes up 7.75% of the Earth's land surface, which illustrates the importance and all-round distribution of reducing conditions in soils (Kirk 2004).

Scope of the thesis

As previously outlined, various biogeochemical processes are induced by the onset of reduction and the E_H, in addition to the pH, is considered to be a master variable in soils. The E_H dynamics render a characterization of the soil redox status and an interpretation of the data challenging for scientists. Numerous publications deal with measurements of the E_H. Most of them are related to medical health issues, where E_H is used to characterize processes in cells or the plasm, but there is also an emerging number of studies in soil sciences. Whereas the number of studies in soil sciences were below 50 articles per year in 2003, it exponentially increased to 260 articles in 2015 (Fig. 1.3). Most of these articles monitor the E_H by the use of Pt electrodes but other simple and robust field methods for monitoring are desired, particularly to differentiate weakly and moderately reducing conditions.

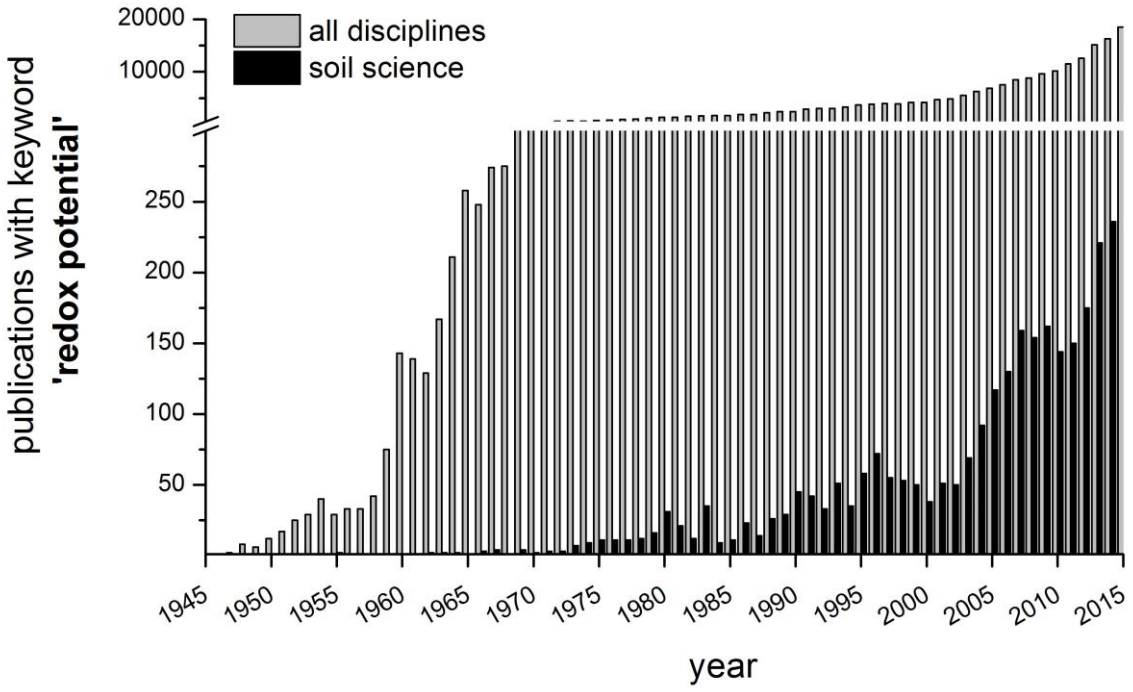

Figure 1.3 Literature overview of peer-reviewed articles dealing with E_H measurements for the period from 1945 to 2015. The data displays matches for all disciplines (Physical Sciences and Engineering, Life Sciences, Health Sciences, Social Sciences and Humanities; n = 214,174) and soil science (n = 3,057) in particular using the keyword 'redox potential'. (source: http://www.sciencedirect.com/)

This thesis aims to enhance the knowledge of the temporal and spatial distribution of reducing conditions in soils by the use of different approaches. Besides the recording of the E_H using **Pt electrodes**, Fe oxide-coated PVC bars (IRIS method) were manufactured and used in field-experiments to characterize the soil redox status. Analogous to the IRIS

method, a birnessite-type $Mn^{III,IV}$ oxide was synthesized in the laboratory and coated onto white PVC bars. Henceforth, the term **redox bars** is introduced and accounts for the use of both, Mn and Fe oxide-coated PVC bars. Especially the use of Mn redox bars is a novelty, because a documentation to manufacture these bars was missing in literature and a comparison with Fe redox bars is not available. Using both oxide coatings for monitoring purposes in the field might enable to differentiate between weakly and moderately reducing soil conditions. To bridge this scientific gap and improve this monitoring approach is of utmost importance, because a differentiation into redox classes is only possible by the use of Pt electrodes at present. Another pioneering aspect of this thesis is to investigate the sorption behavior of elements in soil solution to these man-made minerals, by extracting and analyzing the oxide coating of previously field-installed redox bars. This aspect has environmental relevance, as *in situ* techniques to collect freshly formed mineral phases and determine element sorption behavior are scarce in literature. Finally, as the water table (WT) depth is one of the main drivers to stimulate the onset of reduction, long-term groundwater data was evaluated using a versatile and robust geostatistical algorithm called '**Seasonal and Trend decomposition using Loess**' (STL) to assess increasing or decreasing trends in groundwater level. This issue is not directly associated to the monitoring of soil reducing conditions but the results have an impact on redox induced processes, as the groundwater surface can be considered as an interface between aerobic (oxidizing) and anaerobic (reducing) conditions.

The objectives of this thesis are as follows:

a) Comparison of the E_H dynamics between two monitoring campaigns (1990 to 1993; 2011 to 2014) using permanently installed Pt electrodes
b) Manufacturing and evaluation of Mn redox bars
c) Monitoring and differentiation into weakly and moderately reducing soil conditions by Mn and Fe redox bars
d) Investigation of selective element sorption to the oxide coating of redox bars
e) Evaluation of the WT depth development under the aspect of climate change

Study areas and project implementation

Figure 1.4 shows the geographical position of study sites in north-west Germany. All study sites are characterized by near-surface and strongly fluctuating WT depths. Prior to this thesis, the study sites **Speicherkoog** (Chapter 2; Mansfeldt 1993, 2003, 2004; Mansfeldt and Blume 2002) and **Lavesum** (Chapter 3, 4, and 5; Mansfeldt and Overesch 2013;

Mansfeldt et al. 2012; Schuth et al. 2015) were studied intensively for the effects of different redox conditions on the speciation of As, soil solution composition, and pathways of Fe^{III} oxide formation. These investigation showed that variations from oxidizing to strongly reducing conditions occur on an annual basis, rendering these study sites very suitable for the planned objectives a) to d). Previous reports and management strategies for the study site **Bastauwiesen** (Chapter 6) were conducted by the organization *Biologische Station Minden-Lübbecke e.V.*, who also provided the data for the groundwater monitoring campaign. The final objective e) was conducted at this study site.

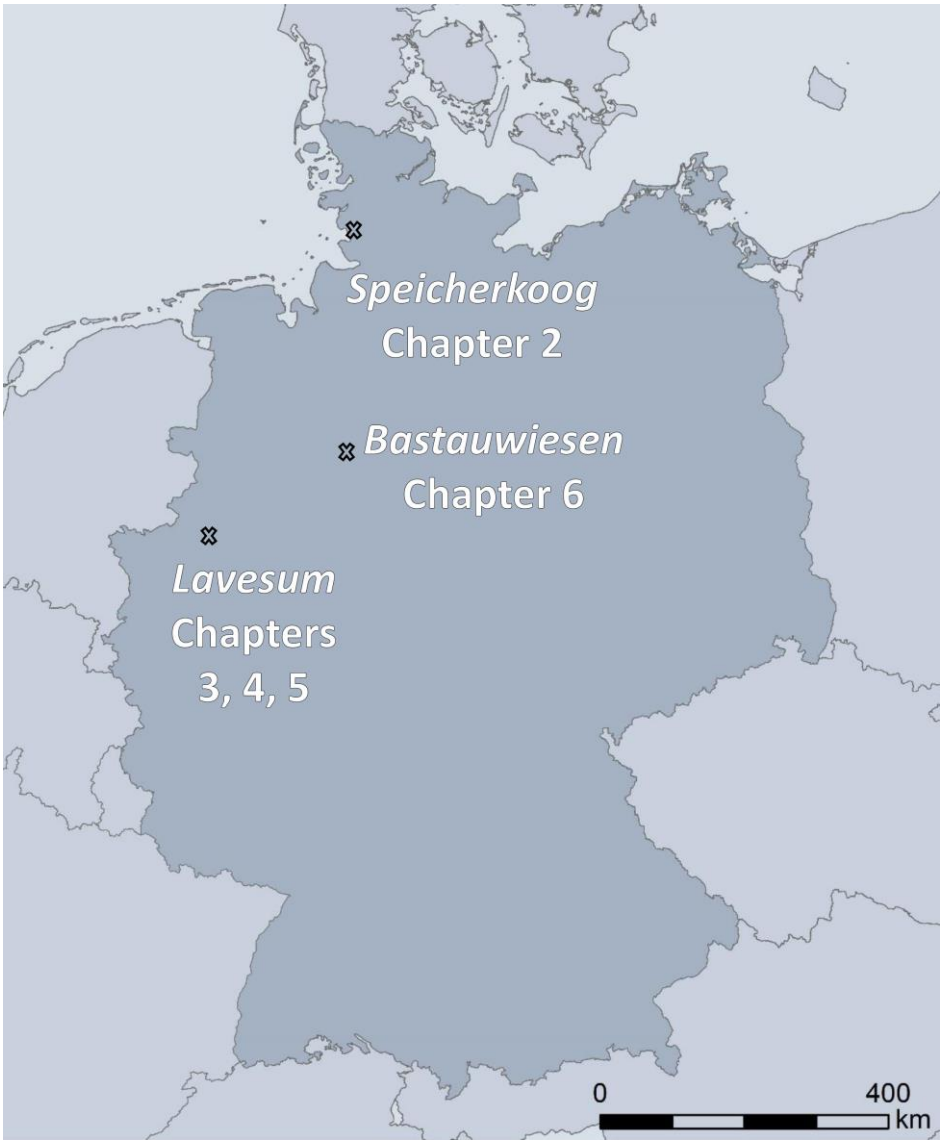

Figure 1.4 Location of study sites in Germany where field-experiments were conducted (includes data from gadm.org).

Chapter 2 Comparison of redox potential dynamics in a diked marsh soil: 1990 to 1993 versus 2011 to 2014

Journal of Plant Nutrition and Soil Science (2016) 179(5): 641–651

Co-author: Tim Mansfeldt

Formatting and orthography of the manuscript is adapted to the dissertation style.

Abstract

As revealed by an earlier study, young diked marsh soils on the west coast of Schleswig-Holstein (Germany) are characterized by pronounced redox potential (E_H) dynamics. Since soil forming processes occur over a short period of time in these man-made environments, the impact of pedogenesis on E_H was examined by comparing the E_H dynamics measured from November 1989 to October 1993 (weekly measurements) with those measured from November 2010 to October 2014 (hourly measurements) at the same study site in Polder Speicherkoog, Northern Germany. In addition, the necessity for high resolution E_H measurements was assessed as well as the impact of climate change on E_H. Redox potentials were determined in both monitoring campaigns with permanently installed platinum electrodes at 10, 30, 60, 100, and 150 cm soil depths. Soil properties were determined in November 1989 and in August 2013. In 24 years of soil formation, bulk density was demonstrated to increase by 28.5% and 33.3% in 10 and 20 cm depths, respectively, and the sulfide-bearing Protothionic horizon lowered from 105 to 135 cm below surface level. Overall, E_H dynamics were similar at all soil depths during both study periods with topsoil compaction not affecting E_H. Annual alterations of E_H were primarily driven by the variable climatic water balance (CWB) and by the corresponding water table (WT) fluctuations. These fluctuations resulted in occasional aeration of the subsoil and subsequent oxidation of sulfides. A forecast of CWB to 2100 predicts an intensified WT drawdown by elevated evapotranspiration rates that should amplify sulfide oxidation. To deduce the soil redox status on a seasonal or annual scale, readings taken at daily intervals are sufficient. To identify biogeochemical processes, it is necessary to monitor E_H on an hourly basis because increases in E_H values of up to 540 mV have been observed within a 24 hour period in temporarily waterlogged horizons.

Key words: marsh soil, monitoring, redox potential (E_H), pedogenesis, soil heterogeneity

Introduction

Determination of the oxidation–reduction (redox) status of a soil and identification of dominant redox processes is of great concern and has been practiced for more than 80 years (Gillespie, 1920). Spatial and temporal distributions of reducing conditions in the field can be assessed by installation in the soil of an inert metal electrode (e.g., platinum, Pt) and a reference electrode (e.g., silver/silver chloride, Ag/AgCl). The potential difference between the electrodes can then be determined using a potentiometer to produce readings in mV (Patrick et al., 1996). This reading is called the redox potential (E_H) and is a classic measure of reducing soil conditions that affects processes resulting in the release of potent greenhouse gases, controls the mobility of nutrients and pollutants, and alters soil formation. Hence, knowledge of the E_H dynamics in temporarily water saturated soils is important for stakeholders and practitioners, e.g., dealing with the reconstruction of wetlands or to assess associated biogeochemical processes.

Various studies have already dealt with in situ monitoring of E_H in field applications, with installation times of up to five years and at various monitoring frequency intervals ranging from hourly to monthly (DeLaune et al., 1983; Faulkner and Patrick, 1992; Austin and Huddleston, 1999; Fiedler, 2000; Teichert et al., 2000; Mansfeldt, 2003). However, none of these studies integrated the impact of pedogenesis on E_H development. The intensity and development of E_H depends on various time-dependent and external conditions (Glinski and Stepniewski, 1985). Since these properties (e.g., soil moisture) vary significantly in space and time, the investigation of reducing conditions in soils is a challenge for scientists worldwide. Redox potential measurements using Pt electrodes are at best interpreted as ‘‘semi-quantitative expressions of mixed potentials in a non-equilibrium environment’’ (Austin and Huddleston, 1999) and therefore, the use of E_H classes over the use of numerical values is encouraged. Soils that undergo frequent changes from oxidizing (E_H > 400 mV) via weakly reducing (E_H 400 to 200 mV) and moderately reducing (E_H 200 to –100 mV) to strongly reducing (E_H < –100 mV) soil conditions, and vice versa, are located within diked marshes (Mansfeldt, 1993, 2003, 2004). In these unique man-made environments, soil-forming processes can be studied over years to decades due to special features of the parent material (Schroeder and Brümmer, 1969). This contrasts to many other soil environments, e.g., highly weathered soils in tropical regions with low rates of soil formation (Pillans, 1997). Diking and drainage of near-surface groundwater plays a crucial role for pedogenetic processes in marshes (Kuntze, 1986). These processes comprise (1) compaction and (2) desalination of the topsoil, (3) mineralization of ‘‘marine’’ derived organic matter, and (4) soil acidification by oxidation of sulfide-bearing minerals that is con-

comitant with the (5) dissolution of carbonate minerals (Brümmer et al., 1971; Müller-Ahlten, 1994a, 1994b; Mansfeldt and Blume, 2002). It is expected that climate change will affect these pedogenetic processes and soil properties, but few attempts have been made to evaluate consequences for coastal marsh soils (Blume and Müller-Thomsen, 2007).

Technical progress in monitoring soil E_H has evolved enormously over the last two decades of data acquisition, especially since electrodes for continuous monitoring of soil E_H have become commercially available to the public (Vorenhout et al., 2004). In remote areas (as typified by the present study site), data transmission via General Packet Radio Service (GPRS) to a web-based server together with less expensive data storage enables the study of E_H interaction with meteorological and hydrological parameters. As a further advantage, technical improvements with regard to sampling frequency of E_H measurements have made tremendous advancements towards the minute interval (Shoemaker et al., 2013). However, little is known about the benefit and advantage of gathering information by performing E_H measurements at a high (e.g., hourly or daily) monitoring frequency interval compared with measurements at a low (e.g., weekly or monthly) monitoring frequency interval.

In this study, manual E_H readings taken on a weekly basis from November 1989 to October 1993 (referred to as hydrological years 1990 to 1993) were compared with automated E_H readings taken on an hourly basis from November 2010 to October 2014 (referred to as hydrological years 2011 to 2014) at Polder Speicherkoog in Schleswig-Holstein, Northern Germany. Each set of readings was obtained from permanently installed Pt electrodes. Soil chemical and physical properties were measured during both monitoring campaigns. The objectives were (1) to assess the impact of pedogenesis (i.e., 24 years of soil formation) on the E_H dynamics; (2) to examine the benefit of E_H measurements on a high frequency basis; and (3) to address the impact of climate change using a forecast of the climatic water balance (CWB) to the year 2100 to evaluate future scenarios for soil pedogenesis and E_H dynamics in these coastal marsh areas.

Materials and methods

Study site

The monitoring campaign was carried out at Polder Speicherkoog, situated 30 km north of the river Elbe in Schleswig-Holstein, Northern Germany (54°8‘1“ N, 8°58‘28“ E; 0.5 m.a.s.l.). The Polder is part of the Meldorf Bight and was diked in 1978. The monitoring station is 3 km from the shoreline and belongs to a non-cultivated field embedded in an

agrarian landscape. At the study site, the typical vegetation consists of willow bushes (Salix ssp.), elder bushes (Sambucus nigra), and fireweed (Epilobium angustifolium) (Mansfeldt, 2003). The E_H monitoring was performed in a soil developed from calcareous marine deposits originating from the Dunkirk transgression between 0 to 100 AD (Hoffmann, 1991). According to FAO (IUSS Working Group WRB, 2014) the soil is a Calcaric Gleysol (Eutric).

Data collection and soil properties 1990 to 1993

Detailed information about the monitoring campaign from November 1989 to October 1993 is presented in Mansfeldt (1993, 2003). Briefly, the monitoring campaign was based on the following approach: E_H was monitored in quintuplicate with permanently installed Pt electrodes at 10, 30, 60, 100, and 150 cm depths on a weekly basis. The Pt electrodes were self-made with a Pt wire (2 mm diameter, 20 mm length) welded on a copper (Cu) wire and connected to a Cu lead. The electrode body was embedded into an acrylic tube (8 mm diameter, variable length, depending on the measurement depth) and coated with a ceramic jacket at the Pt and Cu wire section to prevent intrusion of water (Pfisterer and Gribbohm, 1989). The Pt electrode cables were labeled at the end and fed into a waterproof container in which E_H readings were taken manually by connecting a portable pH meter to the Cu wire with the support of an alligator clip (Mansfeldt, 2003). The water table (WT) depth was measured concomitantly with E_H readings on a weekly basis, within a 200 cm (50 mm diameter) perforated polyvinyl chloride pipe.

A few meters adjacent to the monitoring plot, disturbed and undisturbed soil samples were taken in November 1989 from an excavated soil profile to determine soil physical and chemical properties as follows: soil pH was measured potentiometrically using a glass electrode in a 0.01 mol L^{-1} calcium chloride ($CaCl_2$) solution in twofold repetition. Undisturbed soil samples were taken with steel cylinders (100 cm^3), weighed after saturation within a water bath and weighed again after incubation at 105°C for 24 h to determine soil porosity (pore soil volume per total soil volume) and bulk density (mass of dry soil per unit bulk volume) in eightfold repetition. The grain size distribution was obtained by the sieve and settling method. Total carbon (TC) was determined by dry combustion of the material at 1,200°C (TR 3600 Deltronik). Inorganic carbon (IC) was determined by adding perchloric acid ($HClO_4$; 15%) to the samples, which were preheated to 60°C within the same analyzer to detect CO_2 by Coulomb electrochemical titration. Organic Carbon (OC) was calculated as the difference between TC and IC. Iron oxides (Fe_d) were extracted using dithionite-citrate-bicarbonate (DCB) and the solution analyzed for total iron (Fe) concentrations via flame atomic absorption spectroscopy (Mansfeldt, 1994, 2003). Reduced inorganic sulfur (S) was determined on fresh material immediately postsampling as chromium-reducible

S using a distillation apparatus according to Wieder et al. (1985). Each of these parameters were determined in twofold repetition.

Data collection and soil properties 2011 to 2014

The study site was located 10 meters adjacent to that of the initial monitoring campaign. All instruments were installed within a 2 · 2 m plot in March 2010. Readings were stored in a data logger (enviLog Maxi, ecoTech, Bonn, Germany) and transmitted at 8 h intervals to a web-based server via GPRS/Internet. Monitoring operations were carried out as follows: soil E_H was measured with permanently installed Pt electrodes (ecoTech, Bonn, Germany) in threefold repetition at 10, 30, 60, 100, and 150 cm monitoring depths. An Ag/AgCl electrode (ecoTech, Bonn, Germany; 3 M KCl internal electrolyte) was placed in a salt bridge to act as the reference electrode in the middle of the measuring plot around which the working electrodes were placed in a stellar configuration. This configuration of the electrodes is nearly the same as that implemented by the initial campaign over 1990 to 1993, with the exception of the smaller-sized Pt tip (1 mm diameter, 10 mm length). The electrode potential was adjusted by adding +207 mV (deviation of the reference electrode against the standard hydrogen electrode) to calculate the E_H. The WT depth was determined in a 2.0-m perforated polyvinyl chloride tube using a relative pressure sensor (PDLR, ecoTech, Bonn, Germany). All measurements and calculations were performed on an hourly basis and converted to daily, weekly, monthly and annual averages or sums. XLSTAT-Pro (Addinsoft V.2014.1.05.) software was used to statistically analyze the dataset.

In August 2013, 24 years after the initial monitoring campaign, disturbed and undisturbed soil samples were taken to evaluate changes in the most important soil chemical and physical properties. The soil pH was measured potentiometrically using a glass electrode in a 0.01 mol L^{-1} $CaCl_2$ solution mixed 5:1 with soil (v/v). In addition, undisturbed soil samples were taken with 250 cm^3 steel cylinders in eightfold repetition per observation depth and saturated in a water bath in the laboratory, and then weighed before and after drying at 105°C for 24 h to calculate the soil bulk density and porosity. Grain size distribution was determined by the sieve and settling method, TC was measured by dry combustion with a CNS analyzer (Vario EL cube, Elementar, Hanau, Germany), IC was measured by dry combustion after adding hydrochloric acid (HCl), and OC determined from the difference between TC and IC. Iron oxides of homogenized and air-dried samples were extracted using dithionite-citrate-bicarbonate (DCB) (Mehra and Jackson, 1960). The extracts were measured afterwards via flame atomic absorption spectroscopy (iCE 3000 series, Thermo Scientific, Waltham, USA). Reduced inorganic S was determined as mentioned above.

Replicates of measurements for each parameter were equal to the period from 1990 to 1993.

Climatic water balance and forecast

For both measuring campaigns, precipitation and meteorological data were taken as a daily sum or mean value from the weather station Cuxhaven (15 km southwards) (German Meteorological Service, 2009; Potsdam Institute for Climate Impact Research, 2013).

The Haude formula was used to calculate rates of evapotranspiration in mm d^{-1} according to:

$$PET_{Haude} = f \cdot e_s \left(1 - \frac{F}{100}\right) \quad [1],$$

with f being a plant specific coefficient for grassland (Loepmeier, 1994); es is the water vapor saturation deficit (hPa) for air at 14:00 CET; and F is the relative humidity (%). The vapor pressure deficit was calculated using the maximum air temperature (T), which is assumed to be equal to the air temperature at 14:00 CET, according to:

$$e_s = 6.11 \cdot e^{\frac{(17.62T)}{(243.12+T)}} \quad [2].$$

The climatic water balance (CWB) was calculated as the difference between the monthly sums of precipitation and PET_{Haude}. A forecast of air temperature, relative humidity, and precipitation to 2100, based on the regional climate model STAR (Orlowsky et al., 2008; German Meteorological Service, 2009; Potsdam Institute for Climate Impact Research, 2013) was used to evaluate the possible occurrence of changes, e.g., towards drier summers. Based on the data, the CWB was calculated in the same manner as previously described. Scenarios account for the Representative Concentration Pathways (RCPs) 2.6 and 8.5 that describe the possible range of radiative forcing with 2.6 and 8.5 W m^{-2} proposed by the Intergovernmental Panel on Climate Change.

Results

Soil properties

No significant change of pH values was identified between the two monitoring campaigns (as evident by the two-tailed t-test at the 5% significance level) and a slightly alkaline soil reaction indicates that calcareous material is still present at the study site (Table 2.1).

Table 2.1 Selected soil properties in the E_H measurement depth of the monitoring campaign from 1990 to 1993 and from 2011 to 2014. The two monitoring sites were within 10 m of each other.

	Sampling 1989							Sampling 2013						
Depth (cm)	pH[a]	Bulk density (g cm^{-3})	Porosity (cm^3 cm^{-3})	Clay	OC[b]	IC[c]	Fe_d[d]	pH	Bulk density (g cm^{-3})	Porosity (cm^3 cm^{-3})	Clay	OC	IC	Fe_d
					(g kg^{-1})							(g kg^{-1})		
10	7.0±0.1	0.84±0.12	0.651±0.078	260±5.9	26.5±0.89	3.0±0.87	8.77±0.19	7.1±0.1	1.08±0.03	0.533±0.005	250±0.5	28.6±0.92	2.1±1.31	8.22±0.07
20	7.1±0.1	0.87±0.14	0.649±0.091	250±4.0	19.5±1.01	3.5±0.77	11.90±0.07	7.3±0.1	1.16±0.01	0.513±0.007	210±8.0	17.5±0.11	4.6±0.55	8.23±0.09
30	7.2±0.1	1.29±0.22	0.520±0.051	80±1.5	9.0±0.23	4.5±0.23	3.12±0.07	7.4±0.1	1.29±0.02	0.467±0.013	220±16	9.7±0.47	5.0±0.50	5.11±0.12
60	7.3±0.1	1.43±0.17	0.456±0.032	30±2.0	7.2±0.09	5.7±0.31	0.85±0.05	7.4±0.1	1.41±0.03	0.450±0.001	110±1.5	4.6±0.01	5.9±0.19	1.92±0.02
100	7.3±0.1	1.42±0.11	0.420±0.046	40±1.3	2.8±0.12	5.1±0.36	1.65±0.23	7.6±0.1	1.54±0.02	0.446±0.015	60±2.0	2.6±0.11	5.5±0.12	1.54±0.03
150	7.3±0.1	1.41±0.14	0.468±0.023	90±2.3	3.7±0.19	4.7±0.67	1.45±0.11	7.6±0.1	1.54±0.01	0.435±0.008	50±2.0	2.0±0.01	5.7±0.04	0.95±0.06
60[f]	-[e]	-[e]	-[e]	-[e]	-[e]	-[e]	-[e]	7.5±0.1	-[e]	-[e]	200±4.9	7.4±0.17	5.5±0.38	2.48±0.05
60[g]	-[e]	-[e]	-[e]	-[e]	-[e]	-[e]	-[e]	7.5±0.1	-[e]	-[e]	70±2.1	2.7±0.28	4.5±0.27	1.03±0.01

[a] 0.01 M $CaCl_2$ (1:5 ratio)
[b] Total Organic Carbon
[c] Total Inorganic Carbon
[d] Dithionite-citrate-bicarbonate extractable Fe
[e] Not determined
[f] Clay lens at 60 cm monitoring depth
[g] Sandy material at 60 cm monitoring depth

Compared with the 1990 to 1993 monitoring campaign, the bulk density increased at depths of 10 and 20 cm by 28.5% and 33.3%, respectively, but remained constant in the subsoil. Accompanying the changes of bulk density, the porosity decreased in these depths from 0.651 $cm^3\ cm^{-3}$ to 0.533 $cm^3\ cm^{-3}$ and from 0.649 $cm^3\ cm^{-3}$ to 0.513 $cm^3\ cm^{-3}$, respectively (Table 2.1). The porosity decreased slightly at 30 cm, but no change of bulk density and porosity occurred at 60, 100, and 150 cm depths. Clay contents were similar in the topsoil (10 and 20 cm) and the bottom of the soil profile but differed at 30 and 60 cm depths. The OC content gradually decreased from the top 26.5 (28.6) g OC kg^{-1} soil to the bottom 3.7 (2.0) g OC kg^{-1} soil of the soil profile in 1989 (2013), whereas the IC content gradually increased from the top 3.0 (2.1) g IC kg^{-1} soil to the bottom 4.7 (5.7) g IC kg^{-1} soil of the soil profile. These findings demonstrate that over 24 years of soil formation (1989 to 2013), the OC and IC content remained stable over time (Table 2.1). However, the OC and clay contents were found to be subject to small-scale variations. This is corroborated by the results obtained from the steel cylinders placed at 60 cm depth during soil sampling in August 2013. A small clay lens originating from a mid-Holocene marine transgression was found to be 2 cm thick and contained elevated OC and clay contents (7.4 g kg^{-1} and 200 g kg^{-1}, respectively) compared with respective values from the surrounding sandy soil in the steel cylinder (2.7 g kg^{-1} and 70 g kg^{-1}) and with the values for 100 cm depth (2.6 g kg^{-1} and 60 g kg^{-1}) (Fig. 2.1, Table 2.1).

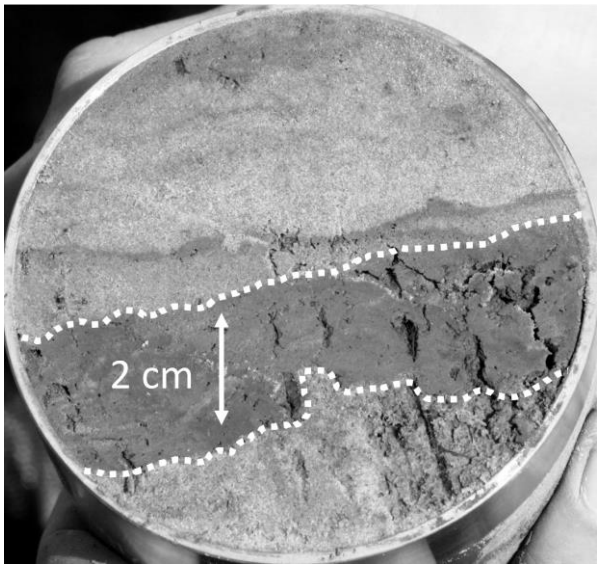

Figure 2.1 Soil core taken in August 2013 at 60 cm depth. The dashed white line indicates a clay lens originating from mid-Holocene marine transgression.

The DCB-extractable Fe contents were highest in the topsoil and decreased towards the bottom of the soil profile. Depth-dependent differences of Fe_d contents between the two monitoring campaigns are likely to be the result of variations in clay content as indicated

by the strong correlation between Fed and clay ($r = 0.86$, $p = 0.002$, $n = 8$), since the oxidic Fe fraction of a soil correlates with the clay content (Cornell and Schwertmann, 2003).

Climatic water balance and water table depth

Mean annual air temperatures of 8.8°C and precipitation of 805 mm during the reference period from 1961 to 1990, together with cool summers and mild winters, characterize the climate of the Polder Speicherkoog. The CWB ranged between 285 mm and 663 mm during both monitoring campaigns with an above average dry year in 1992 and an above average rainfall year in 1993 for the earlier monitoring campaign. Also, 2014 can be considered as a dry year with significantly higher evapotranspiration rates compared with the reference period (Table 2.2).

Table 2.2 Annual sums of precipitation, evapotranspiration, climatic water balance and mean annual water table depth of the monitoring campaigns during the hydrological years 1990 to 1993 and 2011 to 2014 (hydrological year is from November, 1 to October, 31). In addition, normal climatic conditions for the periods from 1961 to 1990 and 2071 to 2100 are presented for comparison. The future scenarios account for an anthropogenic radiative forcing of 2.6 W m^{-2} and 8.5 W m^{-2}.

Year	Precipitation	PET_{Haude}[a] (mm $year^{-1}$)	CWB[b]	WT[c] depth (cm below ground)
1961 to 1990	805	269	536 (325[d]/209[e])	–
1990	831	295	535	–75
1991	797	293	503	–69
1992	657	372	285	–102
1993	952	289	663	–92
2011	833	310	523	–68
2012	871	285	586	–67
2013	778	258	520	–73
2014	752	356	396	–91
2071 to 2100 (RCP2.6[f])	860	321	539 (348/191)	–
2071 to 2100 (RCP8.5[g])	755	394	361 (274/87)	–

[a] Evapotranspiration according to Haude
[b] Climatic water balance
[c] Water table
[d] Hydrological winter (November, 1 to April, 30)
[e] Hydrological summer (May, 1 to October, 31)
[f] Representative Concentration Pathways with a radiative forcing of 2.6 W m^{-2}
[g] Representative Concentration Pathways with a radiative forcing of 8.5 W m^{-2}

According to the climate projection from 2071 to 2100 under the RCP2.6 scenario, the annual CWB remains constant compared with the 30-year reference period from 1961 to 1990, with a slight shift towards drier summers (May to October) (Table 2.2). This development is intensified under the RCP8.5 scenario with a CWB of only 361 mm y^{-1}, due to a lowering of annual precipitation and enhanced evapotranspiration rates. A decrease of the CWB under this scenario has to be highlighted during the hydrological summer.

Typically for all years, in spring (April to May) the WT decreased because of the partial negative CWB when evapotranspiration exceeded precipitation but increased in early fall

(October to November) when the water demand of the vegetation declined and evapotranspiration decreased (Fig. 2.2). This annual pattern caused seasonal fluctuations of the WT depth from –10 cm in the winter to –200 cm below ground in the summer. The annual cycle of enhanced evapotranspiration (data not shown) from 1990 to 1993 is similar to the development from 2011 to 2014, but the CWB varied significantly for individual months between both periods. For instance, the dry summer of 1992 with a CWB of –81 mm in June (Fig. 2.2a) differed remarkably from the moist and mild conditions with 63 mm in June 2013 (Fig. 2.2c). The impact of water deficiency indicated by the long-lasting dry period from June to September 1992 favored a more intense WT drawdown that remained at lower than –200 cm below ground for a 4-month period (Fig. 2.2b). In contrast, the mean WT depth remained at –126 cm below ground for the corresponding period in 2013 (Fig. 2.2d).

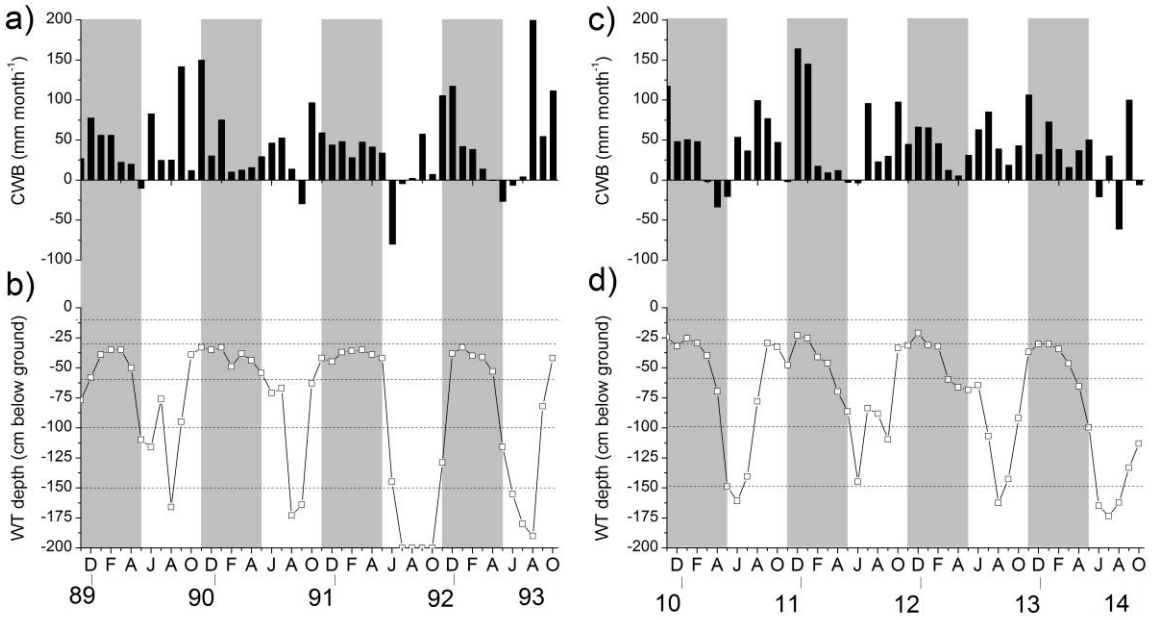

Figure 2.2 Dynamics of the monthly climatic water balance (CWB) and water table (WT) depth during the hydrological years 1990 to 1993 (a and b) and 2011 to 2014 (c and d). The dashed lines (b and d) indicate the E_H recording depths at 10, 30, 60, 100 and 150 cm depths and the shaded areas indicate the period from November to April (grey) and from May to October (white) of each hydrological year.

Soil redox potentials

Figures 2.3a to 2.3e illustrate the E_H dynamics during the initial campaign. Mean E_H values ranged from 547 mV at 10 cm to –84 mV at 150 cm (Fig. 2.3, Table 2.3). The soil was oxidized at the 10 cm monitoring depth throughout the study period (E_H > 400 mV). Variations of E_H occurred at 30 cm with distinct patterns characteristic of oxidizing soil conditions in the summer, to weakly reducing soil conditions in the winter (Fig. 2.3b).

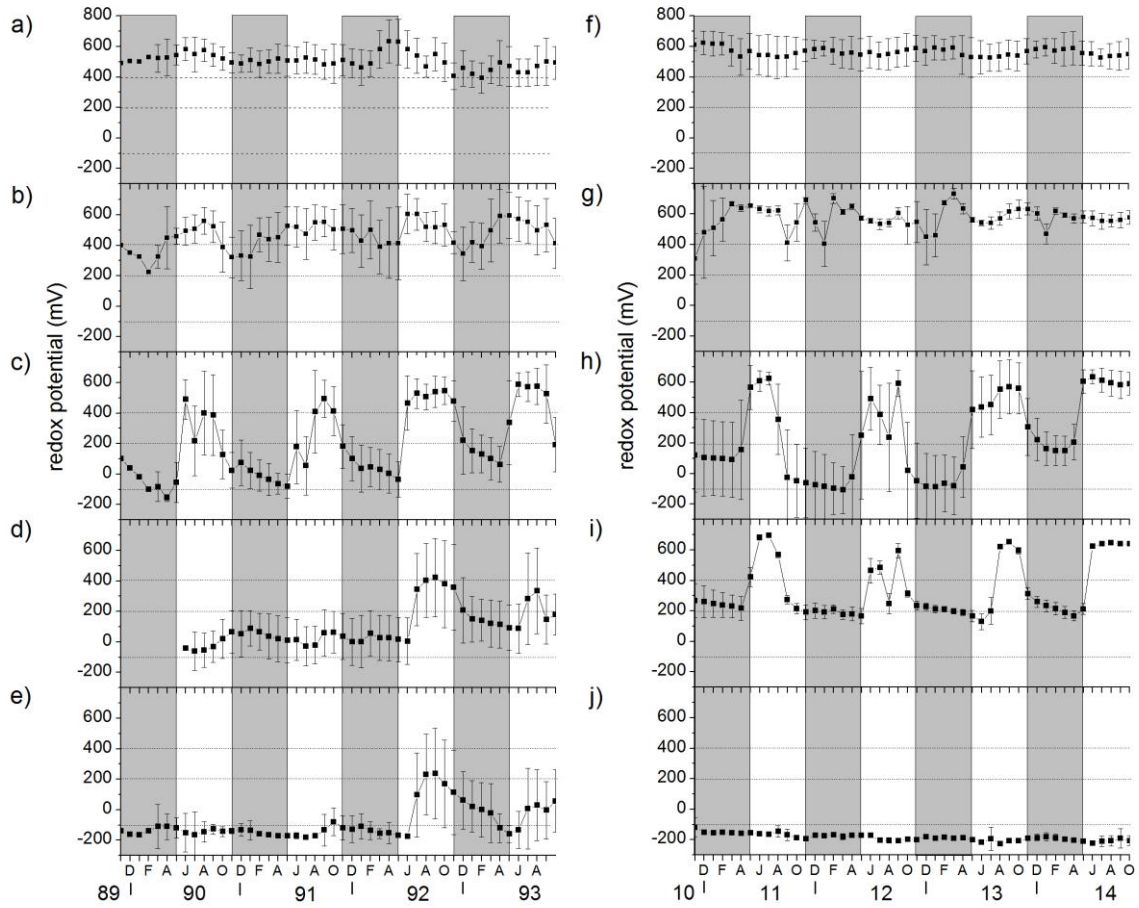

Figure 2.3 Dynamics of redox potentials (E_H) during the hydrological years 1990 to 1993 (a to e) and 2011 to 2014 (f to j) at 10, 30, 60, 100 and 150 cm depths, respectively. The dashed lines indicate the redox classes of oxidizing (> 400 mV), weakly reducing (400 mV to 200 mV), moderately reducing (200 mV to –100 mV), and strongly reducing (< –100 mV) soil conditions according to Zhi-Guang (1985). The E_H dynamics are presented as monthly means with the corresponding standard deviation for measurements in quintuplicate on weekly basis for the initial monitoring campaign and in triplicate on hourly basis for the latter.

This pattern was even more pronounced at monitoring depths of 60 cm and 100 cm on an annual basis. At 100 cm (150 cm), the redox status was at moderately (strongly) reducing soil conditions for 80% (71%) of the time, but increased in the summer of 1992 to weakly reducing conditions (Fig. 2.3d, e, Table 2.3). From 2011 to 2014, mean E_H values were in the range of 573 mV to –184 mV (Table 2.3). Oxidizing soil conditions prevailed at 10 cm depth throughout the study period and annual E_H fluctuations at 30, 60, and 100 cm monitoring depths approximate the fluctuations of the initial monitoring campaign. A high standard deviation revealed differences of the E_H readings between individual electrodes from November 2010 to April 2011 at 60 cm depth (Fig. 2.3h) with differences ranging from strongly to weakly reducing soil conditions. Strongly reducing soil conditions prevailed throughout the study period at 150 cm. The standard deviations were significantly lower at

10 and 150 cm depths compared to the soil depths at 30, 60, and 100 cm, respectively (Table 2.3). Overall, the soil profile can be separated into an oxidized horizon (10 cm), a predominantly oxidized horizon with seasonal reducing conditions (30 cm), an intermittent reduced horizon with strong seasonal variations (60 and 100 cm), and a permanently reduced horizon (150 cm). The E_H data for both monitoring campaigns were very similar at a monitoring depth of 10 cm (Table 2.3) in accordance with the E_H dynamics (Fig. 2.3a, f, Table 2.3). Although the mean E_H and the standard deviation were very similar at 60 cm during both campaigns (Table 2.3), the monthly standard deviation was different and more pronounced during the hydrologic winters from 2011 to 2014 (Fig. 2.3c, h). During the initial campaign, E_H at 30 cm and 100 cm depths remained at a lower level, expressed by differences in mean E_H values of 430 mV to 573 mV and 116 mV to 341 mV, respectively (Table 2.3). Until June 1992, E_H levels at 150 cm were identical for both monitoring campaigns with an E_H of –161 mV to –184 mV. However, the E_H increase in June 1992 resulted in significant differences for the selected statistical parameters (Fig. 2.3e, j, Table 2.3; proven by the two-tailed t-test at the 5% significance level).

Temporal resolution of redox potential measurements

To assess the possible necessity and benefit resulting from high-resolution E_H measurements, the following program of investigation was undertaken. For the campaign from 2011 to 2014, hourly E_H readings were compared with those obtained at a daily, weekly, and monthly interval by examining their redox class distribution. Arbitrarily, for the daily data, the E_H measured at 8 am of each day was chosen, for the weekly data, the E_H measured at 8 am of each Monday of the week, and for the monthly data the E_H measured at 8 am of each first Monday of the month. Since E_H fluctuations are subject to different time scales (Fiedler et al., 2007), the dataset was analyzed for the total period (hydrologic years 2011 to 2014), a seasonal period (hydrologic summer 2011) and an event-based period (July and August 2012) (Fig. 2.4). For the total, seasonal, and event-based periods, no significant differences in the redox class distribution were apparent between hourly and daily measurement intervals across all depths. This was also valid at 10, 30, and 150 cm monitoring depths when weekly and monthly readings are given additional consideration. In contrast, at 60 and 100 cm, the redox class distribution differed between the hourly and daily interval, and the weekly and monthly interval. A lowering of the measurement interval resulted in a faulty description of the redox class distribution, considering hourly readings as the ‘true’ representation of the E_H dynamics for the corresponding periods.

Table 2.3 Comparison of selected statistical redox potential (E_H) data and distribution of redox classes between the monitoring campaigns from 1990 to 1993 and from 2011 to 2014 at 10, 30, 60, 100 and 150 cm monitoring depths.

	1990 to 1993							2011 to 2014						
	Mean	Min	Max	Ox[a]	Weak[b]	Mod[c]	Strong[d]	Mean	Min	Max	Ox	Weak	Mod	Strong
	E_H (mV)			(%)				E_H (mV)			(%)			
10	547±84[e]	377	761	98	2	0	0	562±44	373	702	100	0	0	0
30	430±137	28	739	75	23	0	0	573±112	125	779	98	2	0	0
60	233±273	–199	724	29	8	56	2	254±293	–144	684	35	15	48	2
100	116±221	–207	645	5	15	80	0	341±199	81	702	31	46	23	0
150	–84±171	–276	603	0	4	25	71	–184±30	–243	–32	0	0	0	100

[a] oxidizing; E_H > 400 mV
[b] weakly reducing; E_H 400 to 200 mV
[c] moderately reducing; E_H 200 to –100 mV
[d] strongly reducing; E_H < –100 mV
[e] standard deviation

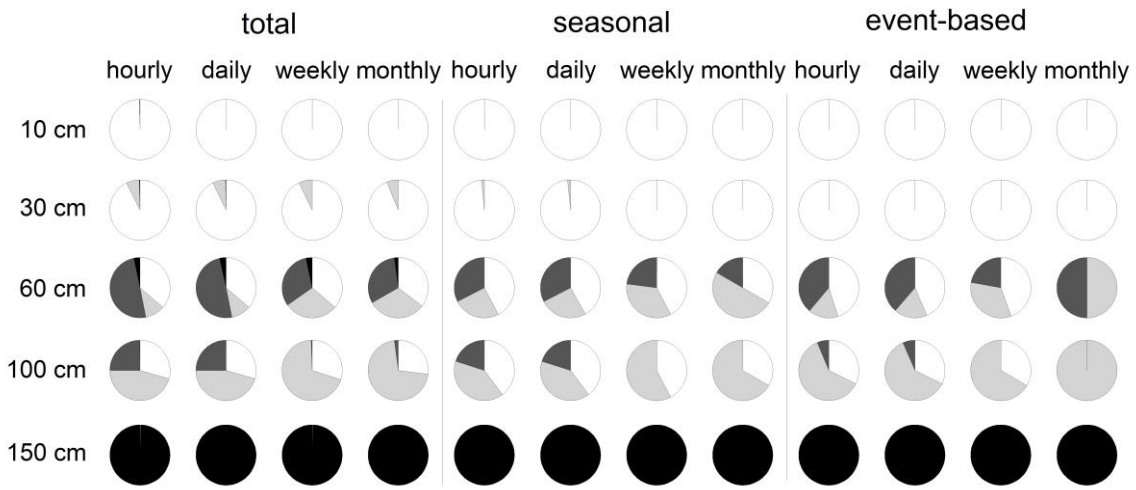

Figure 2.4 Comparison of the redox class distribution on an hourly, daily, weekly and monthly basis measurement intervals (columns) for the E_H recorded at depths of 10, 30, 60, 100 and 150 cm (lines) for the total (hydrological year 2011 to 2014), seasonal (hydrological summer 2011), and event-based (July and August 2012) time-scale. The pie charts display the percentage of oxidizing (> 400 mV; white), weakly reducing (400 mV to 200 mV; light grey), moderately reducing (200 mV to –100 mV; grey), and strongly reducing (< –100 mV; black) soil conditions according to Zhi-Guang (1985).

To obtain an insight into the temporal variability of the E_H, we checked for the whole study period the E_H of the single electrodes in the 60-cm depth which revealed the largest oscillations in E_H. Figure 2.5 displays such an example of the E_H dynamics by illustrating the response of the Pt electrode to aeration as a function of declining WT. E_H started to rise from –90 mV at 1 am towards 450 mV at 12 am and over a 24 h period achieved a range of 540 mV. The E_H increase for this period amounts to 22.5 mV h^{-1} exemplifying short-term fluctuations.

Discussion

Comparison of E_H data and soil properties

Despite the fact that E_H measurements are subject to several limitations (Ponnamperuma, 1972), numerous publications have already demonstrated the linkage to abiotic processes, such as aeration (Mansfeldt, 2003) as well as the specific impact of redox classes on distinct soil processes (Yu et al., 2001). The maximum WT rise (data not shown) was above the 10 cm monitoring depth during both monitoring campaigns, but did not facilitate reducing conditions. It was not possible to assess any impact of the capillary fringe on stimulating the onset of reducing conditions in the topsoil. Hence, oxygen (O_2) replenishment via diffusion from the atmosphere was demonstrated as sufficient and exceeded O_2 consumption (Fig. 2.3a, f). Diking (in 1978) and drainage favored a lowering of WT depths within the Polder Speicherkoog that subsequently conformed to unsaturated soil conditions in

the topsoil. An increase of the bulk density, with a decrease of the air-filled porosity at 10, 20, and 30 cm depths (Table 2.1) verified the process of compaction from 1989 onwards. Reszkowska et al. (2011) concluded that a decrease of the air-filled porosity, along with a decrease of the air-conductivity, hampers aeration of the soil. These conditions lead to lowered pathways for gas transport with existing O_2 consumption mediated by existing microbial and root-based mechanisms. However, no assessment was made of any impact on E_H development at these depths or on the subsoil (i.e., at depths of 60, 100, and 150 cm). The annual E_H pattern, with reducing soil conditions in the winter and oxidizing soil conditions in the summer is evident for both study periods at 30, 60, and 100 cm monitoring depths and is related to phases of water saturation caused by the setting of the WT. To achieve oxidizing conditions, it takes on average 4, 10, and 11 d after the WT declined underneath the corresponding E_H measurement depth in 30, 60, and 100 cm depth for the study period from 2011 to 2014.

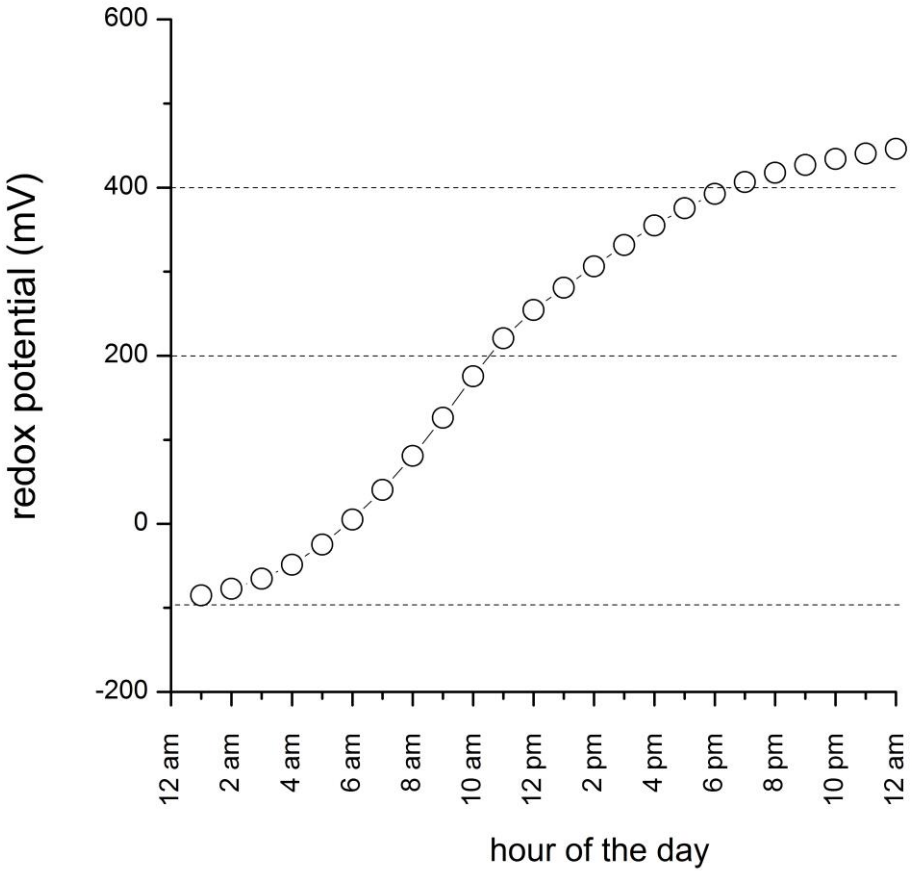

Figure 2.5 Redox potential (E_H) dynamics for a single platinum electrode at 60 cm depth on an hourly basis for a 24 h period on August 24, 2011. The dashed lines indicate the redox classes of oxidizing (> 400 mV), weakly reducing (400 mV to 200 mV), moderately reducing (200 mV to –100 mV), and strongly reducing (< –100 mV) soil conditions according to Zhi-Guang (1985).

Furthermore, the position of the WT to facilitate oxidizing conditions in these measurement depths was at –33, –75, and –137 cm below ground, respectively. Both results indicate that it takes longer to facilitate oxidizing soil conditions with decreasing soil depth because of microbial and root mediated O_2 consumption during the transport from the atmosphere to the Pt electrode. Besides this biotic process, gas transport over a longer distance through a porous system will take more time than over a shorter distance, which is also reflected by the data. The absence of E_H fluctuations at 100 cm depth from June 1990 to May 1992 can be explained by this process (Fig. 2.3d), even though the WT was below this depth for a short period (Fig. 2.2b). It has not been possible to assess the relationship between a response of the Pt electrode to aeration and the setting of the WT for the period from 1990 to 1993 because of the coarse measurement interval. In contrast to the period from 2011 to 2014, in which strongly reducing conditions continuously occurred at 150 cm depths, there was a significant increase of E_H, especially during July to September 1992, but also during July to October 1993 (Fig. 2.3e, Table 2.3). Such a change in the redox conditions of the subsoil should have influenced black colored Fe(II) sulfide minerals (FeS). The presence of these minerals is a heritage of the Wadden Sea and originates from sulfate (SO_4^{2-}) reduction. Sulfate is abundant in interstitial seawater and with divalent Fe forms various FeS minerals, giving the former Wadden Sea sediments the typical black coloring. These minerals are very sensitive to oxidation. Aeration of deeper soil horizons is associated with the construction of dikes from 1978 and the corresponding drainage for agricultural purposes and with declining WT in the summer time. Consideration of these processes has led to the following proposed sequence of events: (1) O_2 diffusion into deeper soil depths, (2) oxidation of insoluble black-colored sulfide to soluble SO_4^{2-}, (3) translocation of SO_4^{2-} downwards to the WT and its subsequent removal via groundwater from the soil profile, and (4) change of color leaving greyish soil particles behind. Whereas the sulfide-bearing Protothionic soil horizon (IUSS Working Group WRB, 2014) (Gr horizon according to the German soil classification; AG Boden, 2005) was closer to the soil surface before diking and drainage, i.e., at –105 cm below ground in November 1989 (11 years after diking), this has declined to –135 cm in August 2013 (35 years after diking). This observation corresponds to a FeS oxidation rate of 1.3 cm y^{-1}. A reduction of monosulfidic S at a depth of 150 cm from 275 mg S^{2-}-S kg^{-1} (1989) to 112 mg S^{2-}-S kg^{-1} (2013) also underlines these pedogenetic processes of diminishing FeS concentrations as a result of prolonged periods of aeration. Under reducing conditions, major discrepancies between monthly E_H measurements for individual Pt electrodes were evident at 60 cm from 2011 to 2014, contrary to the former campaign where the standard deviation was less pronounced (Fig. 2.3c, h). It is assumed that the clay lens in Fig. 2.1 is responsible for this pattern. Higher OC and clay contents presumably caused stronger reducing conditions around the

Pt electrode (as a result of higher microbial activity and soil moisture), supporting the assumption that one out of three Pt tips dips into the clay lens and, in general, causes strongly reducing soil conditions (Fig. 2.3h). In this regard, a continuous placement of Pt electrodes in the soil is encouraged because frequent manual installation and de-installation of electrodes, even when care is taken that the electrodes are placed at the same monitoring depth, can lead to measurements reflecting soil heterogeneity which will be reflected over time.

Measurement interval of redox potential

Various studies have demonstrated the variability of E_H over small distances (Yang et al., 2006). In addition, redox conditions are known to be heterogeneous on a temporal scale and therefore manual measurements performed over discrete time intervals may not be able to capture the 'true' redox dynamic. During the hydrological summers from 2011 to 2014, E_H increases at 60 and 100 cm depths occurred regularly, but with annual differences. The significance of temporal variation was particularly noticeable in August 2012 when the sharp decrease from 480 mV to 250 mV at 100 cm (Fig. 2.3i) was observed to be followed by a steep increase to 600 mV. Such variations in the E_H regime could easily be overlooked if only monthly readings are obtained. Even when weekly measurements are made, information about the temporal distribution between weakly and moderately reducing soil conditions would be lost at monitoring depths of 60 and 100 cm where WT fluctuations were present (Fig. 2.4). This indicates that these time intervals are not sufficient to derive trends of redox class distribution. Careful consideration should therefore be given to establishing a precise moment for measurement in the monitoring program (e.g., for sampling of soil solution). Nevertheless, even daily E_H readings can be subject to shortcomings. Characterization of the soil redox status in the field at 7 am (40 mV) compared with 8 pm (420 mV) (Fig. 2.5), will lead to a faulty and misleading interpretation of the in situ biogeochemical conditions.

Redox potential measurements and implications for marsh soil development

The presence of sulfide minerals might alter the E_H reading by pushing the measured E_H values to more negative potentials when PtS is formed along the electrode tip surface (Whitfield, 1974). This theoretical limitation must be rejected for the study site, because sulfate-reducing bacteria require a readily available carbon source (e.g., acetate as an electron donor), which was only present during the period of deposition of marine sediments and is no longer available at these depths. Hence, the diminishing of sulfide concentrations is a non-reversible process, even though SO_4^{2-} was detected at 150 cm depth at concentrations of up to 650 mg L^{-1} (Mansfeldt, 2004). It is assumed that elemental sulfur

(S^0) formed during FeS oxidation at first remains at the mineral surface whilst soluble Fe^{2+} is subsequently leached into soil solution (Nordstrom, 1982). The measured E_H displays potentials driven by the redox couple FeS-S^0 (Whitfield, 1974). In this regard, a lowering of the FeS-containing Gr horizon from 105 to 135 cm might offer an explanation for why the mean E_H values from 1990 to 1993 (Fig. 2.3d) remain constantly below the E_H values from 2011 to 2014 at the 100 cm monitoring depth (Fig. 2.3i). The only proof of this assumption would be to continue monitoring of the E_H development at 150 cm to assess whether or not the E_H is altered by the decreasing Protothionic soil horizon over the next few years to decades. The CWB forecast indicates that this process is likely to occur because the precipitation pattern and the PET_{Haude} indicate drier summers. The intensified WT drawdown would concur with prolonged periods of aeration in previously water-saturated soil environments (Dorau et al., 2015). Picek et al. (2000) demonstrated in laboratory soil incubation experiments that a change from reducing to oxidizing soil conditions results in elevated OC mineralization rates and enhanced CO_2 evolution, demonstrating the need to assess whether similar results are attained under field conditions during extended periods of aeration in the future. This process is not relevant for the study site by low OC contents but of relevance for other settings such as fens and bogs. Continuous monitoring of E_H by the use of permanently installed Pt electrodes is therefore of utmost importance in linking a change of environmental conditions to E_H development and vice versa.

Conclusions

A comprehensive understanding of biogeochemical processes in soils implies knowledge of the redox status. Soil chemical (OC content, FeS, pH) and physical properties (bulk density, porosity) have to be considered as a transient state within dynamic marsh ecosystems. As evident by this study, a linkage to E_H dynamics can only be achieved when Pt electrodes are placed permanently in the soil to differentiate whether variations of the E_H dynamics are either caused by the re-installation of the electrodes or by changes of soil properties. Redox potential measurements on an hourly and daily basis described the redox class distribution equally well during the study period from 2011 to 2014, but a loss of information occurred when weekly and monthly readings were performed. The findings demonstrate the need to measure E_H on an hourly basis, because fluctuations across three redox classes within 24 h were apparent. According to meteorological forecasts, enhanced evapotranspiration rates favor an intensified water table drawdown during the hydrological summer, which also results in prolonged periods of aeration and therefore extends the

timeframe and extent for oxidizing soil conditions. This favors and accelerates topsoil compaction in marsh ecosystems and has implications for metastable minerals sensitive to oxidation.

Acknowledgements

This study was financially supported by Verein der Freunde und Förderer der Universität zu Köln. We kindly thank Julian Rölkens and Marcel Possoch for assistance during the sampling campaign in August 2013 and Karin Greef (University of Cologne) for support in the laboratory. Furthermore, Dr. Stefan Wessel-Bothe, ecoTech Bonn, is thanked for technical support. We thank two anonymous reviewer for their recommendations to improve the quality of the article.

References

AG Boden (2005): Bodenkundliche Kartieranleitung. 5th ed., Schweizerbarth, Stuttgart, Germany.

Austin, W. E., Huddleston, J. H. (1999): Viability of permanently installed platinum redox electrodes. *Soil Sci. Soc. Am. J.* 63, 1757–1762.

Blume, H. P., Müller-Thomsen, U. (2007): A field experiment on the influence of the postulated global climatic change on coastal marshland soils. *J. Plant Nutr. Soil Sci.* 170, 145–156.

Brümmer, G., Grunwaldt, H. S., Schroeder, D. (1971): Beiträge zur Genese und Klassifizierung der Marschen II. Zur Schwefelmetabolik, in Schlicken und Salzmarschen. *Z. Pflanzenernähr. Bodenk.* 129, 92–108.

Cornell, R. M., Schwertmann, U. (2003): The iron oxides: structure, properties, reactions, occurences and uses. Wiley-VCH, Weinheim, Germany p. 703.

DeLaune, R. D., Smith, C. J., Patrick, W. H. (1983): Relationship of marsh elevation, redox potential and sulfide to *Spartina alterniflora* productivity. *Soil Sci. Soc. Am. J.* 47, 930–935.

Dorau, K., Gelhausen, H., Esplör, D., Mansfeldt, T. (2015): Wetland restoration management under the aspect of climate change at a mesotrophic fen in Northern Germany. *Ecol. Eng.* 84, 84–91.

Faulkner, S. P., Patrick, W. H. (1992): Redox processes and diagnostic wetland soil indicators in bottomland hardwood forests. *Soil Sci. Soc. Am. J.* 56, 856–865.

Fiedler, S. (2000): In situ long-term-measurement of redox potential in redoximorphic soils, in Schüring, J., Schulz, H. D., Fischer, W. R., Böttcher, J., Duijnisveld, W. H. M.: Redox: fundamentals, processes and applications. Springer-Verlag, Heidelberg, Germany pp. 81–93.

Fiedler, S., Vepraskas, M. J., Richardson, J. L. (2007): Soil redox potential: importance, field measurements and observations, in Sparks, D. L.: Advances in Agronomy. Elsevier Academic Press Inc, San Diego, US, pp. 1–54.

German Meteorological Service (2009): Daten der Klimastationen des Deutschen Wetterdienstes, Offenbach, Germany.

Gillespie, L. J. (1920): Reduction potentials of bacterial cultures and of water-logged soils. *Soil Sci.* 9, 199–216.

Glinski, J., Stepniewski, W. (1985): Soil aeration and its role for plants. CRC Press, Boca Raton, USA p. 229.

Hoffmann, D. (1991): Sea level changes at the Schleswig-Holsteinian North Sea coast during the last 3000 years. *Quatern. Int.* 9, 61–65.

IUSS Working Group WRB (2014): World reference base for soil resources 2014. *World Soil Resources Reports*. 106, FAO, Rome.

Kuntze, H. (1986): Soil reclamation, improvement, recultivation and conservation in Germany. *Z. Pflanzenernähr. Bodenk.* 149, 500–512.

Loepmeier, F. J. (1994): Berechnung der Bodenfeuchte und Verdunstung mittels agrarmeteorologischer Modelle. *Z. Bewässerun.* 29, 157–167.

Mansfeldt, T. (1993): Redoxpotentialmessungen mit dauerhaft installierten Platinelektroden unter reduzierenden Bedingungen. *Z. Pflanzenernähr. Bodenk.* 156, 287–292.

Mansfeldt, T. (1994): Schwefeldynamik von Böden des Dithmarscher Speicherkoogs und der Bornhöveder Seenkette in Schleswig-Holstein. Schriftenreihe Institut für Pflanzenernährung und Bodenkunde. University of Kiel, Germany. 28, 1–154.

Mansfeldt, T. (2003): In situ long-term redox potential measurements in a dyked marsh soil. *J. Plant Nutr. Soil Sci.* 166, 210–219.

Mansfeldt, T. (2004): Redox potential of bulk soil and soil solution concentration of nitrate, manganese, iron and sulfate in two Gleysols. *J. Plant Nutr. Soil Sci.* 167, 7–16.

Mansfeldt, T., Blum,, H. P. (2002): Organic sulfur forms in mineral top soils of the marsh in Schleswig-Holstein, Northern Germany*. J. Plant Nutr. Soil Sci.* 165, 255–260.

Mehra, O. P., Jackson, M. L. (1960): Iron oxide removal from soils and clays by a dithionite-citrate system buffered with sodium bicarbonate. *Clay Clay Miner.* 7, 317–327.

Müller-Ahlten, W. (1994a): Zur Genese der Marschböden. I. Der Einfluß von Sediment- und Bodengefüge. *Z. Pflanzenernähr. Bodenk.* 157, 1–9.

Müller-Ahlten, W. (1994b): Zur Genese der Marschböden. II. Kalksedimentation, Entkalkung. *Z. Pflanzenernähr. Bodenk.* 157, 333–343.

Nordstrom, D. K. (1982): Aqueous pyrite oxidation and the consequent formation of secondary iron minerals, in Kittrick, J. A., Fanning, D. S., Hosner, L. R.: Acid sulfate weathering. Soil Science Society of America: Madison, USA pp. 37–56.

Orlowsky, B., Gerstengarbe, F. W., Werner, P. C. (2008): A resampling scheme for regional climate simulations and its performance compared to a dynamical RCM. *Theor. Appl. Climatol.* 92, 209–223.

Patrick, W. H., Gambrell, R. P., Faulkner, S. P. (1996): Redox measurements of soils, in Sparks D. L.: Methods of soil analysis: chemical methods part 3. Soil Science Society of America and American Society of Agronomy: Madison, USA pp. 1255–1273.

Pfisterer, U., Gribbohm, S. (1989): Zur Herstellung von Platinelektroden für Redoxmessungen. *Z. Pflanzenernähr. Bodenk.* 152, 455–456.

Picek, T., Šimek, M., Šantrůčková, H. (2000): Microbial responses to fluctuation of soil aeration status and redox conditions. *Biol. Fert. Soils.* 31, 315–322.

Pillans, B. (1997): Soil development at snail's pace: evidence from a 6 Ma soil chronosequence on basalt in North Queensland, Australia. *Geoderma* 80, 117–128.

Ponnamperuma, F. N. (1972): The chemistry of submerged soils. *Adv. Agron.* 24, 29–96.

Potsdam Institute for Climate Impact Research (2013): STARS Klimaszenarien, Potsdam, Germany.

Reszkowska, A., Krümmelbein, J., Gan, L., Peth, S., Horn, R. (2011): Influence of grazing on soil water and gas fluxes of two Inner Mongolian steppe ecosystems. *Soil Till. Res.* 111, 180–189.

Schroeder, D., Brümmer, G. (1969): Beiträge zur Genese und Klassifizierung der Marschen. I. Problematik der Marschen-Genese und -Klassifizierung und Untersuchungen zum Ca/Mg-Verhältnis. *Z. Pflanzenernähr. Bodenk.* 122, 228–249.

Shoemaker, C., Kroger, R., Reese, B., Pierce, S. C. (2013): Continuous, short-interval redox data loggers: verification and setup considerations. *Environ. Sci.: Processes Impacts.* 15, 1685–1691.

Teichert, A., Böttcher, J., Duijnisveld, W. H. M. (2000): Redox measurements as a qualitative indicator of spatial and temporal variability of redox state in a sandy forest soil,

in Schüring, J., Schulz, H. D., Fischer, W. R., Böttcher, J., Duijnisveld, W. H. M.: Redox: fundamentals, processes and applications. Springer-Verlag, Berlin Heidelberg, Germany pp. 95–109.

Vorenhout, M., van der Geest, H. G., van Marum, D., Wattel, K., Eijsackers, H. J. P. (2004): Automated and continuous redox potential measurements in soil. *J. Environ. Qual.* 33, 1562–1567.

Whitfield, M. (1974): Thermodynamic limitations on the use of the platinum electrode in E_H measurements. *Limnol. Oceanogr.* 19, 857–865.

Wieder, R. K., Lang, G. E., Granus, V. A. (1985): An evaluation of wet chemical methods for quantifying sulfur fractions in freshwater wetland peat. *Limnol. Oceanogr.* 30, 1109–1115.

Yang, J., Hu, Y., Bu, R. (2006): Microscale spatial variability of redox potential in surface soil. *Soil Sci.* 171, 747–753.

Yu, K. W., Wang, Z. P., Vermoesen, A., Patrick, W. H., Van Cleemput, O. (2001): Nitrous oxide and methane emissions from different soil suspensions: effect of soil redox status. *Biol. Fert. Soils.* 34, 25–30.

Zhi-Guang, L. (1985): Oxidation-reduction potential, in Tian-Ren Y. E.: Physical chemistry of paddy soils. Springer-Verlag, Berlin, Germany pp. 1–26.

Chapter 3 Manganese Oxide–Coated Redox Bars as an Indicator of Reducing Conditions in Soils

Journal of Environmental Quality (2015) 44: 696–703

Co-author: Tim Mansfeldt

Formatting and orthography of the manuscript is adapted to the dissertation style.

Abstract

Identification of reducing conditions in soils is of concern not only for pedogenesis but also for nutrient and pollutant dynamics. We manufactured manganese (Mn) oxide–coated polyvinyl chloride bars and proved their suitability for the identification of reducing soil conditions. Birnessite was synthesized and coated onto white polyvinyl chloride bars. The dark brown coatings were homogenous and durable. As revealed by microcosm devices with adjusted redox potentials (E_H), under oxidizing conditions (E_H ~450 mV at pH 7) there was no Mn-oxide removal. Reductive dissolution of Mn-oxides, which is expressed by the removal of the coatings, started under weakly reducing conditions (E_H ~175 mV) and was more intensive under moderately reducing conditions (~80 mV). According to thermodynamics, the removal of Mn-oxide coatings (225 $mm^2\ d^{-1}$) exceeded the removal of iron (Fe)-oxide coatings (118 $mm^2\ d^{-1}$) in soil column experiments. This was confirmed in a soil with a shallow and strongly fluctuating water table where both types of redox bars were inserted. Consequently, it was possible to identify reducing conditions in soils using Mn-oxide–coated bars. We recommend this methodology for short-term monitoring because tri- and tetravalent Mn is the preferred electron acceptor compared with trivalent Fe, and this additionally offers the possibility of distinguishing between weakly and moderately reducing conditions. If dissolved Fe^{2+} is abundant in soils, the possibility of nonenzymatic reduction of Mn has to be taken into account.

Introduction

Reduction (i.e., the gain, or acceptance, of an electron) and oxidation (i.e., the loss, or donation, of an electron) are important chemical reactions in soil environments. Because free electrons do not exist in chemical reactions, reduction–oxidation (redox) reactions always occur together.

The most important source of electrons in soils is reduced carbon (C) occurring in the soil organic matter. Metabolizing plant roots and microorganisms enzymatically oxidize the reduced C forms. Electrons released during the oxidation of C are transferred to elemental oxygen (O, which occurs as the dioxygen molecule O_2), which, in turn, is reduced to water (H_2O). Hence, O_2 acts as the terminal electron acceptor. Soil redox conditions under which O_2 is available are termed “aerobic” or “oxidizing” and are characterized by low electron availability. The O_2 pool of soils is continuously replenished by O_2 diffusion through soil pores as long as they are filled with air. When filled with water, the O_2 diffusion is extremely slow, and, depending on metabolic activity, the soil O_2 pool is more or less rapidly exhausted. Soil redox conditions under which O_2 partial pressure is low or O_2 is absent are termed “anaerobic” or “reducing” and are characterized by high electron availability. Under reducing soil conditions, elements other than O are used as terminal electron acceptors, including pentavalent nitrogen (N^{V}) in nitrate, tri and tetravalent manganese ($Mn^{III,IV}$) in Mn-oxides, trivalent iron (Fe^{III}) in Fe-oxides, hexavalent sulfur (S^{VI}) in sulfate, and tetravalent C (C^{IV}) in carbon dioxide (CO_2). Although some overlap may occur, the use of the different electron acceptors is a stepwise one and is known as the “sequential reduction sequence” (Ottow, 2011; Ponnamperuma, 1972). Redox conditions of soils are classically assessed by measuring the redox potential (E_H). According to the preferential electron acceptor in use, a more precise classification of the different redox conditions (at pH 7) can be deduced and is used in the following text (e.g., Reddy and DeLaune, 2008): “oxidizing,” where the E_H is > 300 mV and O_2 is predominant; “weakly reducing,” where E_H ranges from 300 to 100 mV and nitrate and $Mn^{III,IV}$ are reduced; “moderately reducing,” where E_H ranges from 100 to –100 mV and Fe^{III} is reduced; and “strongly reducing,” where the E_H is less than –100 mV and sulfate and CO_2 are reduced.

In their oxidized species, Fe and Mn occur as strongly colored oxides in soils, whereas under reducing conditions these oxides are reductively dissolved, liberating their water-soluble reduced counterparts, ferrous Fe (Fe^{2+}) and manganous Mn (Mn^{2+}). Typically, repeated changes in oxidation and reduction are reflected in special patterns of soil color, which are called “redoximorphic features.” The occurrence of redoximorphic features is

used in many national and international soil classification systems to infer reducing conditions in soils (e.g., Ad-hoc-AG Boden, 2005; Isbell, 2002; IUSS Working Group, 2006; Soil Survey Staff, 2010). However, because soil color does not necessarily reflect the current redox conditions in soils (e.g., due to the intrinsic color of parent materials of soil formation, higher content of organic matter, or preservation of relict redox conditions), methods of recording reducing conditions in soils are necessary. Both oxides are important not only for the genesis and classification of soils but also for the chemistry of many elements. For instance, Fe-oxides act as a strong adsorbent for toxic (semi)metals (e.g., arsenic) (Bowell, 1994) or for nutrients (e.g., phosphate) (Peretyazhko and Sposito, 2005), and, by their reductive dissolution, the adsorbed compounds may be released. Despite the low abundance of Mn-oxides in soils, their oxidizing power and their function as an adsorbent renders them important soil constituents (Crowther et al., 1983; Kay et al., 2001; Manceau et al., 2002). Furthermore, the range of weakly reducing conditions is the range of formation of the potent greenhouse gas nitrous oxide (N_2O) (Yu and Patrick, 2004). In this regard, a comprehensive understanding of the monitoring and interpretation of reducing conditions in soils is crucial, especially for distinguishing the zones of weakly and moderately reducing conditions.

Several field methods are available to identify reducing soil conditions, including the use of dyes (Childs, 1981), the determination of the E_H (Fiedler et al., 2007; Patrick et al., 1996), the terminal electron-accepting processes approach (Gao et al., 2002), and the concept of oxidative capacity (Gao et al., 2002). Although these methods have their own merits, they also have significant disadvantages because, for example, they provide only snap-shots and require laborious sampling and intensive chemical analyses or the use of expensive equipment. A new field method of identifying reducing conditions in soils, called the Indicator of Reduction in Soils (IRIS), was introduced by Jenkinson (2002) and Jenkinson and Franzmeier (2006) and adapted by Rabenhorst and Burch (2006) and Castenson and Rabenhorst (2006). Synthesized Fe-oxides are coated on polyvinyl chloride (PVC) tubes, which are inserted for a distinct period in the soil. If O_2 is depleted due to water saturation, the Fe^{III} on the PVC tube is reduced to soluble Fe^{2+}. After removing the tubes from the soil, they can be visually assessed for the effects of reduction due to the depletion of the oxide coating. Striated polymer plates coated with ferrihydrite are also in use (Fakih et al., 2008). Meanwhile, the IRIS technique is one of three methods within the framework of the Hydric Soil Technical Standard for proving the presence of reducing soil conditions (National Technical Committee for Hydric Soils, 2007).

Stiles et al. (2010) introduced PVC tubes coated with synthesized Mn-oxides, called the Manganese Indicator of Reduction in Soils (MIRIS). The results indicate that MIRIS tubes

are a suitable tool in alkaline soil environments (pH > 8), inhibiting Fe reduction, or at locations where the installation time is not sufficient to remove the Fe-oxide coating. The advantages of Mn oxides as an alternative electron acceptor are their suitability for application in alkaline soils, their good contrast with the white PVC surface, and the shorter time interval when Mn reduction takes place. However, the manufacture of MIRIS tubes has some general restrictions regarding the abrasion of the coating and the synthesis of the Mn-oxides (McKenzie, 1971; Stiles et al., 2010). Currently available methods for synthesizing birnessite [(Na, Ca, MnII)$Mn_7O_4 \cdot 2.8H_2O$)], a common Mn-oxide of soils, in the laboratory are time consuming and have some disadvantages such as high temperatures (60–400 °C), long reaction times (up to 90 d), and the use of strong acids and bases in closed systems (Ching et al., 1997; Ma et al., 1999; McKenzie, 1971; Zhang et al., 2012), which effectively limits the MIRIS technology. Recently, Händel et al. (2013) introduced a new method to synthesize birnessite in the laboratory. This method is simple, fast, and reliable. We adopted this method and manufactured birnessite-coated PVC bars to indicate reduction in soils (called “Mn-oxide-coated redox bars”). The objectives of this study are (i) to report on how to manufacture Mn-oxide-coated redox bars and test their durability, (ii) to adopt the bars in microcosm experiments under defined redox conditions to evaluate Mn reduction, (iii) to validate the rate of depletion for Mn-oxide- and Fe-oxide-coated bars in laboratory soil column experiments, and (iv) to prove the application in field experiments.

Materials and Methods

Synthesis of Birnessite and Fe-Oxides

Birnessite was synthesized according to Händel et al. (2013). Briefly, we added 1 mL of sodium lactate ($C_3H_5O_3Na$, 50%) to 100 mL of 63.3 mmol L^{-1} $KMnO_4$ solution. The suspension was stirred for 2 h, centrifuged for 15 min at 5300 g, washed five times with deionized water to remove residual salts, and freeze dried for storage. X-ray powder diffraction pattern was recorded using X-ray diffraction (XRD) (X’Pert PRO MPD theta–theta, PANalytical) with cobalt Ka radiation. The XRD pattern (Supplemental Fig. 3.S1) is very similar to the synthesized material described by Händel et al. (2013). By following the above-mentioned procedure, 621 mg of the very fine-grained material should be obtained. However, during the removal of salts via centrifugation, washing the suspension, and decanting the supernatant, the turbidity between each step increased, and loss of birnessite in suspension occurred. Hence, 100 mL $KMnO_4$ yielded 437 mg of birnessite, which is two thirds of the mass reported by Händel et al. (2013). To minimize the loss of birnessite, we recommend centrifuging the suspension with a larger centrifugal force.

Iron-oxide-coated bars were used to compare the oxide removal with that of Mn-oxide-coated bars. We synthesized ferrihydrite by titrating a 0.5 mol L^{-1} solution of $FeCl_3$ to pH 12 with 1 mol L^{-1} KOH. The suspension was stored for 7 d in an opaque glass bottle until the desired goethite content of 30 to 40% was obtained via mineralogical alteration (Rabenhorst and Burch, 2006). The Fe-oxides were applied to the PVC bars in the same manner as the Mn-oxides (see below). It is possible to use a hot-air gun for a few seconds to dry the coating lengthwise or to air-dry the bars overnight. To validate the recommended ratio between ferrihydrite and goethite, acid-oxalate extraction to determine the quantity of ferrihydrite (Schwertmann, 1964) and dithionite-citrate-bicarbonate (DCB) extraction to determine the total Fe content were performed (Mehra and Jackson, 1960). The Fe_o/Fe_d was 0.76, indicating that the major fraction was short-range ordered and oxalate-extractable ferrihydrite, whereas goethite represents a minor fraction.

Applying the Birnessite onto the Bars

Before the Mn-oxides were applied to the white PVC bar (21 mm diameter) (Co. Kunststoffe Jansen GmbH), the freeze-dried powder was pulverized in an agate mortar for 2 min because some larger aggregates (< 10 mm) were visible after the drying process. Roughening of the PVC surface is an important step and improved when fine sandpaper (400 grit) is used. This leads to a better adherence of the Mn-oxide coating than when the surface is roughened with coarse sandpaper (< 100 grit). If the PVC surface is not well sanded, hydrophobicity, similar to the lotus effect, is observed. Hence, it is fundamental to roughening the PVC surface as long as the original smooth surface is not visible anymore. The powder was suspended with a ratio of 100 mg birnessite to 1 mL deionized water, which resulted in the desired viscosity. It is advisable to dip the soft foam brush into the suspension, wrap it around the bar, and facilitate a lengthwise coating with pressure. In our experience, a used foam performed better than a new one. Rubbing along the PVC surface should be performed for at least 30 s until the residual water of the suspension at the foam brush evaporates or diffuses inside the foam, leaving the Mn-oxide particles behind. Facilitating the coating with pressure will enhance the contrast and the durability of the Mn-oxide coating. We recommend drying the coating by moving a hot-air gun (300 °C, 300 L min^{-1}) (Mannesmann) lengthwise (45 s for a 50-cm coated surface and 5 cm distance to the PVC) without drying a single spot too long to prevent mineralogical alteration of Mn-oxide. We could not assess a change of crystallinity as long as the surface temperature was < 200 °C (Supplemental Fig. 3.S2). With 437 mg of Mn-oxides, 0.17 m^2 of PVC bars can be coated.

Checking the Adherence of Birnessite onto the PVC Bars

To test the durability of the Mn-oxide coating, one redox bar was set in a water bath with deionized water of 6 cm depth for 10 d, and one bar was set in acidified hydroxylamine hydrochloride (AAH) solution (0.1 mol L^{-1} $HONH_2 \cdot HCl$ in 0.01 mol L^{-1} HNO_3 [pH 2]) for 5 min. Additionally, we wiped a finger along the coated bar and classified the adherence of the Mn-oxides into categories from 1 (paint wipes off when applying slight pressure) to 5 (paint does not wipe off when applying firm pressure) as classified by Rabenhorst and Burch (2006).

Laboratory Experiment at Fixed Redox Conditions in Soil Suspensions

To validate the reductive dissolution behavior of the Mn-oxide-coated redox bars, experiments were performed at a fixed E_H using a microcosm reactor. This device was adapted from Patrick et al. (1973) and allows the E_H to be controlled. The E_H can be regulated by adding N_2 or filtered ambient air. Our modified system was presented in detail in Mansfeldt and Overesch (2013). Therefore, 1.2 kg of air-dried arable topsoil (< 2 mm; Ap horizon; pH in $CaCl_2$–extract 6.2; 19.1 g kg^{-1} organic C; loamy sand) and 6 L of deionized water were continuously stirred in a sealed glass vessel at 20 to 22 °C. The Mn-oxide-coated bars were screwed into the plastic lid and protruded into the soil suspension. Three microcosms were incubated for 8 d. One microcosm was adjusted to oxidizing conditions (~450 mV, O_2 is present), the second to weakly reducing conditions (~175 mV, O_2 becomes exhausted and Mn reduction takes place), and the third to moderately reducing conditions (~80 mV, no O_2 present and slight Fe reduction takes place). After the incubation period, the redox bars were removed and visually inspected for Mn-oxide removal.

Laboratory Column Experiment

For the soil column experiment, we used the same arable topsoil as in the microcosm experiment. Four PVC columns (220-mm height) were filled with the soil up to 200 mm, resulting in a bulk density of 1.5 Mg m^{-3}. Then, four Mn-oxide- or Fe-oxide-coated redox bars of 220 mm length were pushed into each column. The columns were placed in a water bath having a water level of 100 mm. By using this experimental setup, we wanted to validate the hypothesis that Mn is preferentially reduced compared with Fe. The adjustment of the water table (WT) to the middle of the soil column should separate the redox bars into an aerobic (upper 100 mm; O_2 enters the pores via diffusion) and an anaerobic part (lower 100 mm; pores are water saturated and O_2 content is low) with a transition zone caused by the capillary fringe. We placed the water bath in a climate chamber (KB400 incubator, Binder) and incubated it at 24 °C to stimulate microbial activity. Before inserting the bars into the soil columns, we predrilled a hole to reduce abrasion. After 7, 14, 21, and

28 d of incubation, two Mn-oxide-coated and two Fe-oxide-coated bars were carefully removed from the columns. A picture was taken of each 120° section, and the distorted images were cropped together and analyzed for the depleted area. This was performed using an image retouching and editing tool (GIMP v.2.8.4). Binary images were made by using the threshold tool to separate the PVC bars into depleted and nondepleted areas (Rabenhorst, 2010). Afterward, the bars were reinserted into the soil columns to prevent enhanced O_2 diffusion. They were not considered for further analysis.

Field Application

Field application of the Mn- and Fe-oxide-coated bars was performed at a site with shallow and strongly fluctuating WTs in Lavesum, North Rhine-Westphalia, Germany (51°48.898 N, 007°12.997 E). The soil is a Haplic Gleysol (Petrogleyic) according to the WRB system (IUSS Working Group, 2006), which developed from Holocene fluvial material showing loamy texture overlaying glaciofluvial sands. Because of glaciofluvial processes, a microrelief developed with height differences varying from 47.6 to 49.0 m asl. More site and soil data are presented by Mansfeldt and Overesch (2013) and Mansfeldt et al. (2012). To validate the hypothesis that reducing conditions are induced by water-filled pores and therefore affect depletion patterns along redox bars, we chose three plots at which to insert the bars: an elevated dry plot, an intermediate plot where the WT was shallow but the plot was not flooded, and a periodically flooded plot on lower terrain. The WT was measured in a groundwater well (PDLR 70, EcoTech) at the intermediate plot. We assumed the WT depths of the dry and flooded plots by extrapolating the measured data to the soil level at the site using a digital elevation model derived by airborne laser scanning (GEOBASIS NRW). The accuracy of the data is ±10 mm in height. Water table depth and soil temperature (temperature lance with RS 485 interface, UIT) were recorded every 10 min during the study period from 19 Mar. to 20 Apr. 2013. We assumed that soil temperature was the same for all plots. To minimize abrasion and loss of oxide coatings from the surface due to scratching, a push probe with a soil auger of the same length and width was predrilled into the soil. The PVC bars were cut to 600 mm length with the lower 500 mm coated and were carefully inserted without rotating to a depth of 500 mm. We cautiously removed the bars from the soil by digging a hole close by and gently pushing the bars to the side. Adhering soil material was removed from the PVC surface with tap water. The redox bars were stored dry afterward.

Results and Discussion

Manufacturing

Figure 3.1 presents three Mn-oxide-coated bars. Bar A shows the appearance just after manufacture. The color was dark brown (mean RGB of 98, 78, and 55 derived from image analysis).

Figure 3.1 Manganese-oxide-coated redox bars without any treatment after manufacturing (A), with the lower 6-cm set in deionized water for 10 d (B), and with the lower 6-cm set in 0.1 mol L^{-1} hydroxylamine hydrochloride/0.01 mol L^{-1} nitric acid solution for 5 min (C).

The Mn-oxide-coated bars showed a homogenous coating, which is important for further analysis. When the coated bars were dried, the durability of the coating was excellent, which corresponds to category 5 of the classification introduced by Rabenhorst and Burch (2006) (i.e., paint does not wipe off when applying firm pressure). Furthermore, when exposed to water, the Mn-oxides were not removed by dissolution or displacement (Fig. 3.1B). No depletion was visible, nor was the darkness or brightness changed after 10 d of storage in water. Manganese oxides can be dissolved by chemical reductants. In the protocol of Chao (1972), an AAH solution is used to selectively extract Mn-oxides from soils

and sediments. Only 5 min after setting the bar into this solution, the Mn-oxides were completely dissolved, leaving the white PVC surface behind (Fig. 3.1C). The simple removal of Mn-oxides is resource friendly because the redox bars can be used several times after field installation. Hence, the consumption of material can be reduced during monitoring campaigns.

Microcosm Experiment

Figure 3.2 and Supplemental Fig. 3.S3 present the results of the E_H measurements in the microcosms. To achieve and maintain the desired E_H range, air had to be pumped from time to time to adjust the microcosm to oxidizing conditions. To the microcosm adjusted to weakly reducing conditions, air (when the E_H dropped too much) or N_2 (when the E_H increased too much) was continuously added, which explains the saw-tooth pattern of the E_H. The microcosm adjusted to moderately reducing conditions received only N_2 and was characterized by a continuous decrease of E_H. Figure 3.3 illustrates the bars before and after the microcosm experiment. The hypothesis that no reductive dissolution of Mn-oxides takes place when the E_H is in an oxidizing range can be confirmed by the appearance of the Mn-oxide-coated bar presented in Fig. 3.3A: the brightness did not change, nor were any depletion patterns visible. In contrast, a change in brightness occurred under weakly reducing conditions because the brownish birnessite became a little transparent, showing the white PVC surface (Fig. 3.3B). We assume that under weakly reducing conditions the O_2 partial pressure continuously decreased to zero and that under low O_2 contents facultative living microorganisms had already oxidized the organic matter by using the synthesized birnessite as an electron acceptor according to, for example,

$$CH_3COO^- + 4MnO_2 + 3H_2O \rightarrow 4Mn^{2+} + 2HCO_3^- + 7OH^- \quad [1]$$

where acetate represents the electron donator.

As shown by Gotoh and Patrick (1972), the transformation of Mn-oxides at pH 6.0 to 8.0 takes place at E_H of 200 to 300 mV. Under stronger reducing conditions, the transformation of Mn-oxides to Mn^{2+} is accelerated. This coincides with the appearance of bar C (Fig. 3.3) because the coating became more transparent due to an intensified reduction of Mn under moderately reducing conditions. Furthermore, the intensified reduction under moderately reducing conditions is reflected by the increased pH because reduction is a proton-consuming process (Eq. [1] and Fig. 3.2b).

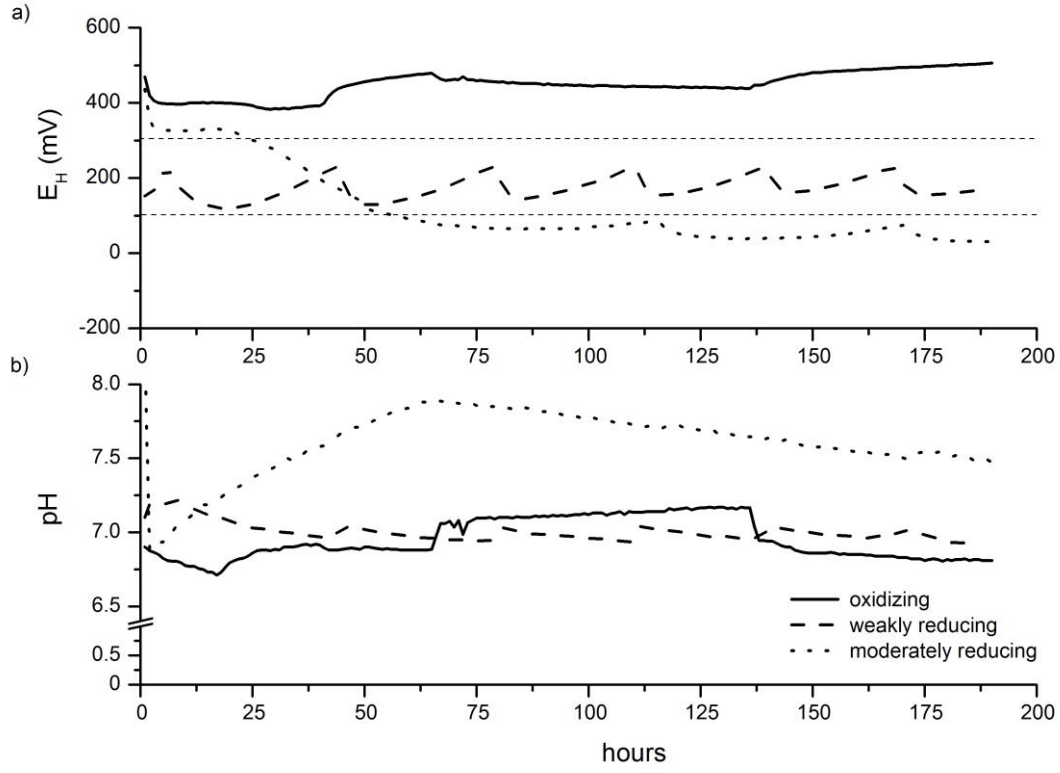

Figure 3.2 Development of the redox potential (E_H) (a) and the pH (b) in microcosm experiments adjusted to oxidizing (~450 mV), weakly reducing (~175 mV), and moderately reducing (~80 mV) conditions during the course of 8 d. The dashed line in (a) indicates the boundary between oxidizing and weakly reducing conditions and between weakly and moderately reducing conditions.

Soil Column Experiment

Table 3.1 shows the results of the soil column experiment. After 7 d, the mean depletion of areas of the Mn-oxide-coated bars was nearly identical above and below the WT at about 55%. Hence, no difference due to the level of the WT was visible. In contrast, the depletion patterns along the Fe-oxide-coated bars reflected the level of the WT because only 6.1% of the Fe-oxides was removed above the WT, whereas 30.8% was removed below the WT. After 14 d, the Mn-oxide coatings were nearly completely dissolved apart from a thin zone on the upper parts of the bars where O_2 could have entered.

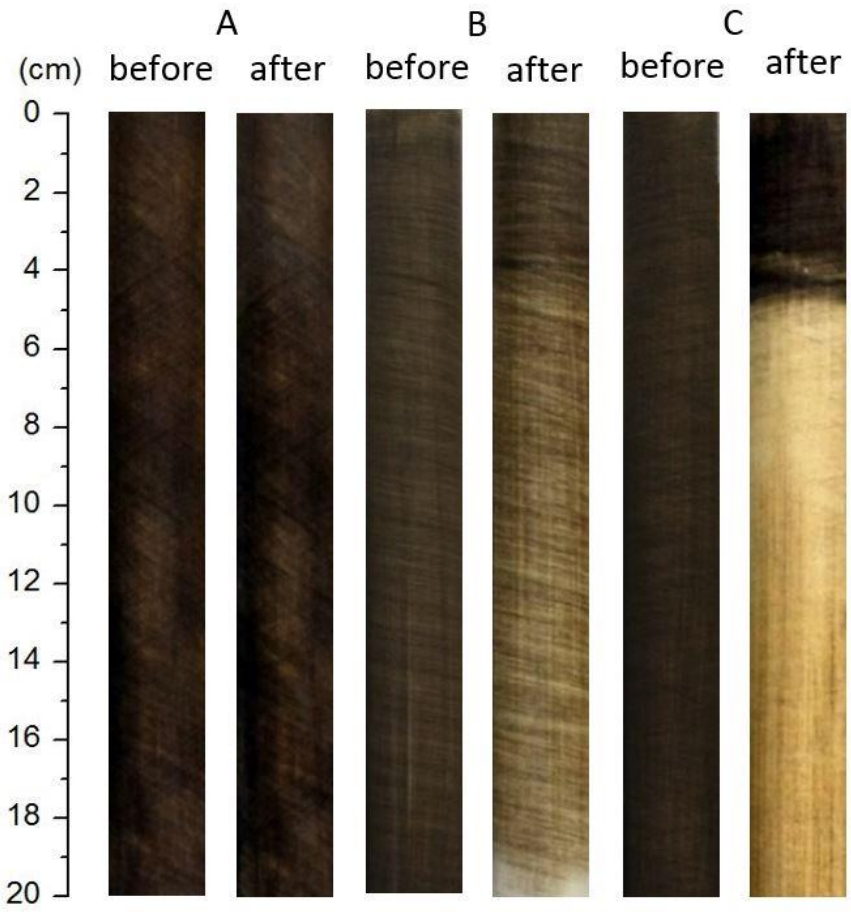

Figure 3.3 Manganese-oxide-coated redox bars before microcosm experiment and after 8 d of incubation under oxidizing (~450 mV) (A), weakly reducing (~175 mV) (B), and moderately reducing (~80 mV) (C) conditions. The height of the water table in the glass vessel was evident for both experiments run in the absence of O2 and separated the bars into those that were not depleted and those that were partly depleted (at 4 cm benchmark scale) (B and C).

The removal of Fe-oxide coating after the second week was twice that in the first week, with 18.4% above and 59.8% below the WT after the second week, and increased progressively to 31.3% above and 71.2% below the WT after the fourth week. Overall, the percentage removal of Mn-oxide coating exceeded that of Fe-oxide coating. These results are in accordance with the stability of the applied minerals. Due to the capillary rise, pores were water-filled in the upper part of the soil column; this prevented O_2 diffusion significantly. Oxygen diffusion coefficients vary between 10^{-2} cm^2 s^{-1} for dry aggregates and 10^{-6} cm^2 s^{-1} for water-filled pores (Smith, 1980). Hence, water-filled pores reduce the O_2 transport by four orders of magnitude, which supports the reductive dissolution of Mn-oxides in the upper part of the soil column. The lower removal of Fe-oxides reflected the fact that reducing conditions were not sufficient to reductively dissolve ferrihydrite and goethite in this part of the soil column.

Table 3.1 Cumulative removal of Mn- and Fe-oxide coatings from PVC bars and their rate of depletion during the course of four weeks. The bars were inserted into a soil column of 200-mm length having a water table set at 100 mm.

	Mn				**Fe**			
	Above†		Below‡		Above†		Below‡	
	Surface area	Rate of depletion	Surface area	Rate of depletion	Surface area	Rate of depletion	Surface area	Rate of depletion
	[%]	[$mm^2\ d^{-1}$]	[%]	[$mm^2\ d^{-1}$]	[%]	[$mm^2\ d^{-1}$]	[%]	[$mm^2\ d^{-1}$]
First week	55.5	515	54.6	507	6.1	57	30.8	286
Second week	94.4	443	99.5	462	18.4	85	59.8	277
Third week	95.6	295	99.0	306	22.4	69	64.0	198
Fourth week	96.3	223	98.1	227	31.3	72	71.2	165

† indicates the upper 100 mm of the bars above the water table
‡ indicates the lower 100 mm of the bars below the water table

Like Mn reduction, the reductive dissolution of Fe-oxides is microbially mediated and may be expressed as:

$$CH_3COO^- + 8Fe(OH)_3 \rightarrow 8Fe^{2+} + 2HCO_3^- + 15OH^- + 5H_2O \quad [2]$$

where acetate represents the electron donor. However, Mn reduction is thermodynamically favorable (free energy yield is 94.5 kJ mol^{-1} for Mn reduction vs. 24.3 kJ mol^{-1} for Fe reduction per mol of organic matter when CH_2O is the electron donator), and soil bacteria show an enzymatic preference for $Mn^{III,IV}$ compared with Fe^{III} (Lovley, 1991; Zehnder and Stumm, 1988). Hence, there is little overlap between the zone of Mn reduction and that of Fe, which was also shown in a field study (Mansfeldt, 2004).

Jenkinson and Franzmeier (2006) introduced the parameter "rate of depletion" to quantify and compare the oxide removal along IRIS tubes. The depletion of the oxide coating (mm^2) is divided by the surface area of the PVC bar in contact with the soil (mm^2) and multiplied by 100. This quotient is divided by the number of days the bar has been installed. The rate of depletion after 4 wk under the ambient conditions totaled 225 mm^2 d^{-1} for Mn-oxide- and 118 mm^2 d^{-1} for Fe-oxide-coated bars.

Field Application

Figure 3.4 illustrates the redox bars used during the field monitoring. The mean WT depth for the dry plot was –70.7 cm below the soil surface ("–" indicates below and "+" above the soil surface), with values varying between –76.9 and –64.6 cm (Fig. 3.5). These extrapolated values are in consistent with observations made during the monitoring because no groundwater was visible in the hole when the redox bars were retrieved. Consequently, the bars were not affected by groundwater during the study period, which is consistent with the appearance of the bars (Fig. 3.4A). No differences could be observed along the Mn-oxide- and Fe-oxide-coated bars from either abrasion due to inserting the bars in the soil or reductive dissolution. Consequently, we assume that the redox bars were in an oxidizing environment during the study. When assessing the suitability of Mn-oxide-coated redox bars for the identification of reducing conditions in soils, it is important to note that, besides the E_H, the pH also controls the solubility of Mn and Fe in soils. Manganese is more soluble under moderately acidic conditions between pH 5 and 6 than Fe (Gotoh and Patrick, 1972; Gotoh and Patrick, 1974). This is exactly the pH range of the site under investigation (Mansfeldt and Overesch, 2013). Lack of any dissolution patterns of the Mn-oxide coating indicates, however, that there was no proton-induced dissolution of the Mn-oxides during the 4 wk of insertion. Whether Mn-oxide-coated bars can be used in environments that are more acidic remains unanswered.

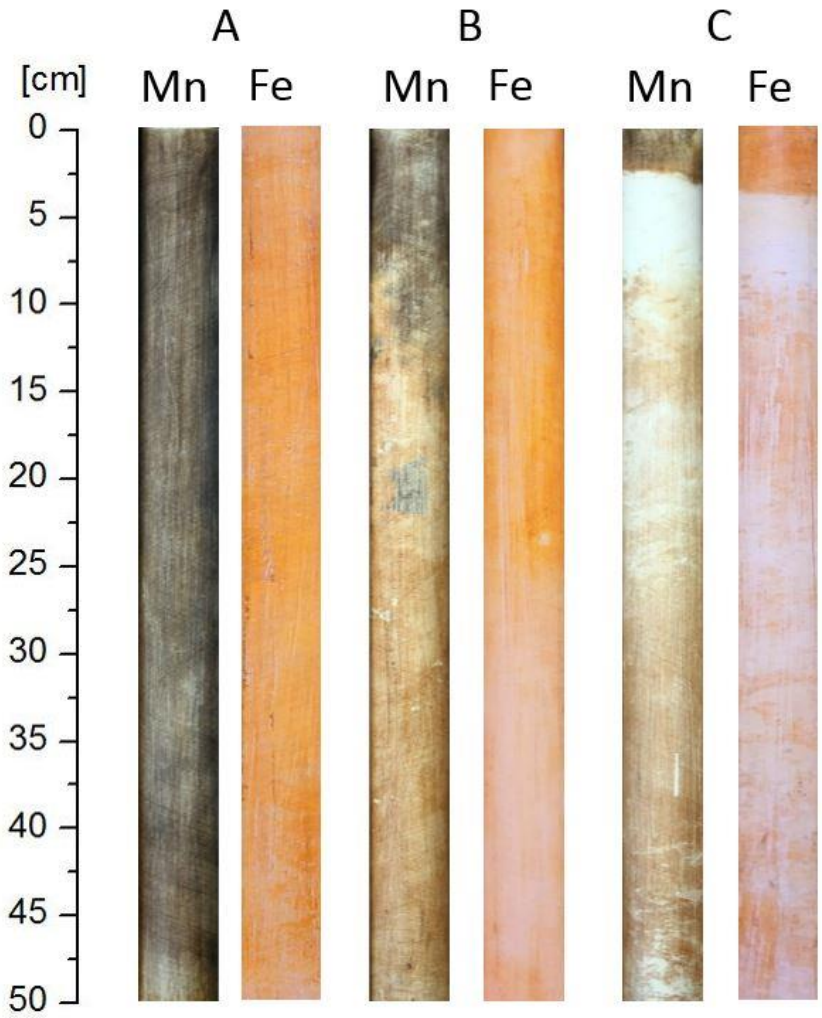

Figure 3.4 Field application of Mn- and Fe-oxide–coated redox bars inserted in a dry (A), an intermediate (B), and a periodically flooded (C) soil environment.

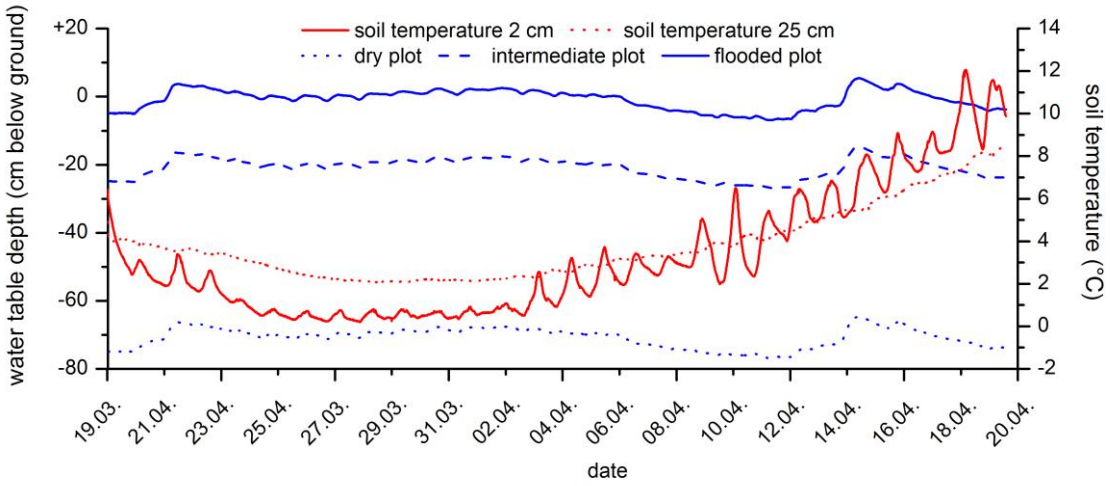

Figure 3.5 Soil temperature at 2 and 20 cm depth and water table depth for a dry (dry), an intermediate (wet), and a periodically flooded (flooded) soil environment. Water table depths for the dry and flooded plots were extrapolated.

The depletion patterns along the Mn-oxide-coated bar in the intermediate plot were consistent with the level of the WT (Fig. 3.4B). During the course of the study, the mean WT was –20.7 cm (range, –26.9 to –14.6 cm) (Fig. 3.5). The depletion patterns started at 7.5 cm (Fig. 3.4B; see benchmark), which is slightly higher than the WT. Elevated soil water contents in the capillary fringe presumably minimized the O_2 diffusion and enhanced the reductive dissolution of Mn-oxides. At first sight, we expected that the light brown coatings below 7.5 cm would be partially depleted Mn-oxides showing the white PVC surface underneath. However, treatment of the lower part of the bar with AAH solution did not cause any observed dissolution of the coating. To validate whether the coating consisted of Fe-oxides, we scraped 10 cm^2 of oxide coatings off the PVC bar shown in Fig. 3.4B (Mn) and treated the plastic chips with DCB. The solution was measured for Mn and Fe using inductively coupled plasma–mass spectrometry. We extracted 0.57 mg of DCB-soluble Fe but only 0.011 mg of Mn, which indicated the presence of Fe-oxide coatings. What could be the reason for the accumulation of the Fe-oxides? As outlined by Mansfeldt et al. (2012), Fe^{2+} is abundant in the shallow groundwater at this site and is relocated upward in the soil profile by capillary rise. An oxidation of Fe^{2+} by O_2 and subsequent formation of Fe-oxides could be possible on the near-surface part of the bars. Another reaction, especially in the lower part of the bars, could be:

$$MnO_2 + 2Fe^{2+} + 4H_2O \rightarrow Mn^{2+} + 2Fe(OH)_3 + 2H^+ \quad [3]$$

In this reaction, Fe^{2+} is the reductant and is oxidized to Fe^{3+}, which hydrolyzes and forms Fe-oxides along the Mn-oxide coating. In turn, the birnessite is dissolved and releases water-soluble Mn^{2+} from the PVC surface. Golden et al. (1986) confirmed this process in laboratory experiments. The Fe-oxide coating in the intermediate plot showed little transparency below 25 cm (Fig. 3.4B), which is related to the mean WT depth and indicates the occurrence of Fe^{III} reduction and hence moderately reducing conditions. Because Fe^{III} reduction occurs only in the absence of O_2, the presence of Fe-oxide coatings in the adjacent Mn-oxide-coated bar (5 cm, Fig. 3.4B) can only be explained by Eq. [3]; that is, by an abiotic process as outlined above.

The mean WT depth of the flooded plot was –0.7 cm (range, –6.9 to +5.4 cm) (Fig. 3.5). Neither Mn- nor Fe-oxide removal was visible at the top of the bar (0–2 cm for Mn and 0–4 cm for Fe), which can be attributed to poor soil contact or elevated O_2 content (Fig. 3.4C). From 2 to 10 cm and from 4 to 10 cm, respectively, complete removal of the Mn-oxide coating and nearly complete removal of the Fe-oxide coating occurred. We associated this with the high amount of organic C present there and with it a potentially high microbial activity. In general, because the reduction of Fe^{III} and $Mn^{III,IV}$ is associated with microbial activity, an increase in temperature will increase the reduction rate (Vaughan et al., 2009).

Whether the complete oxide removal was associated with increased soil temperatures at the end of the study period is speculative (Fig. 3.5). Below 10 cm, light brown coatings on the Mn-oxide-coated bar appeared. As shown by AAH and DCB extraction, the coatings on the Mn-oxide-coated redox bars consisted mainly of Fe-oxides, and we assume that the same abiotic process happened here.

Conclusions

Identification of reducing conditions in soils by Mn-oxide-coated redox bars is possible. The described procedure is easy to perform, and the coatings are homogenous and durable. Furthermore, the $Mn^{III,IV}$ of the coatings is bioavailable and acts as an electron acceptor, resulting in a dissimilatory reductive dissolution of the coatings. Because Mn-oxides are reduced at higher E_H compared with Fe-oxides, we recommend the use of Mn-oxide-coated redox bars (i) for short-term monitoring (e.g., on a weekly basis) or (ii) in soil environments where reducing conditions are too short or where only weakly reducing conditions are achieved and hence are not sufficient to remove the Fe-oxide coatings from the bar's surface. Such settings include soils having perched WTs. Overall, identification of the temporal and spatial distribution of reducing conditions and differentiation between weakly and moderately reducing conditions in soils can be improved by using Mn-oxide-coated redox bars together with the established IRIS technique. However, care must be taken in the interpretation of the process responsible for Mn reduction (i.e., enzymatic vs. nonenzymatic reduction) when reductants like Fe^{2+} are present.

Acknowledgements

The authors thank Karin Greef and Michael Eickmeier, both at the University of Cologne, for support with the field and laboratory analyses and the Duke of Croy and Thomas Seine, who enabled the field measurements. Reiner Dohrmann, Bundesanstalt für Geowissenschaften und Rohstoffe/Landesamt für Bergbau, Energie und Geologie, Hannover, Germany, performed the XRD analysis. The authors thank the anonymous reviewers for their comments and suggestions.

Supplemental Material

The supplemental material presents a XRD pattern of the synthesized birnessite before and after incubation at 180 °C for 24 h. An E_H–pH diagram of the microcosm experiment is shown. A video clip is presented explaining the preparation of birnessite and the coating of the redox bars.

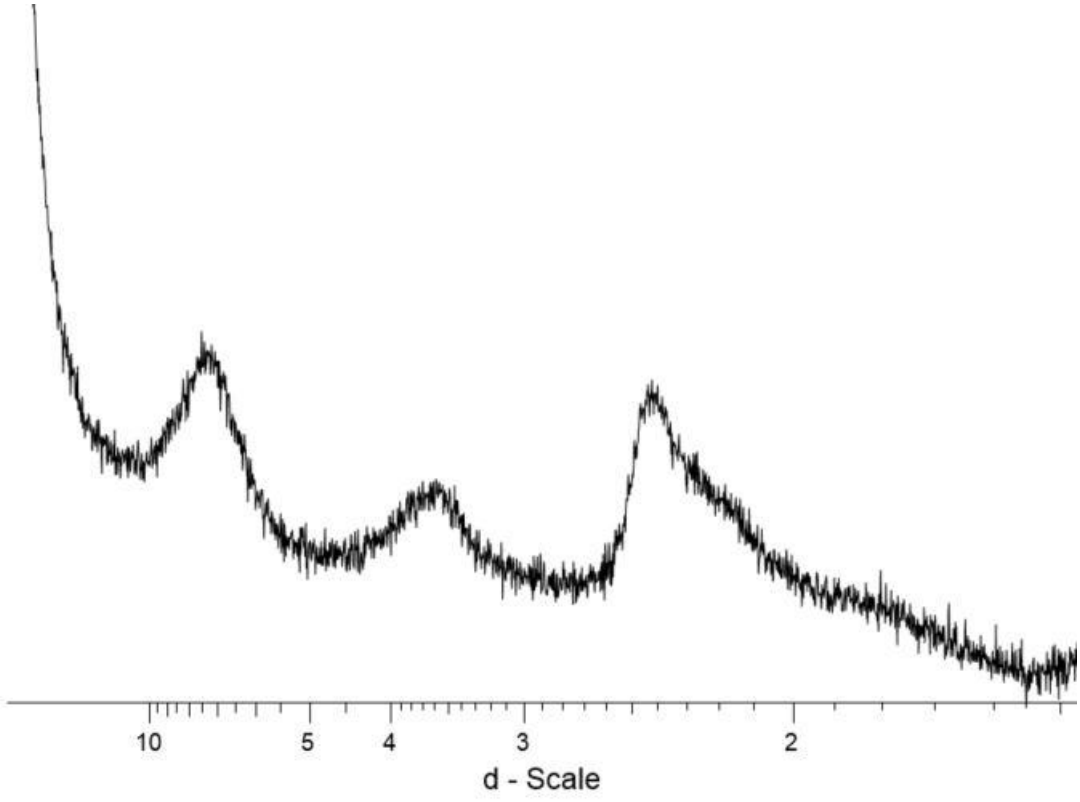

Figure 3.S1 XRD random powder pattern of birnessite showing typical broad basal plane peaks at around 7.4 Å and 3.6 Å (Co radiation) as well as the non-basal plane peak at around 2.4 Å indicating turbostratic disorder (Manceau et al., 2013, Villalobos et al., 2006).

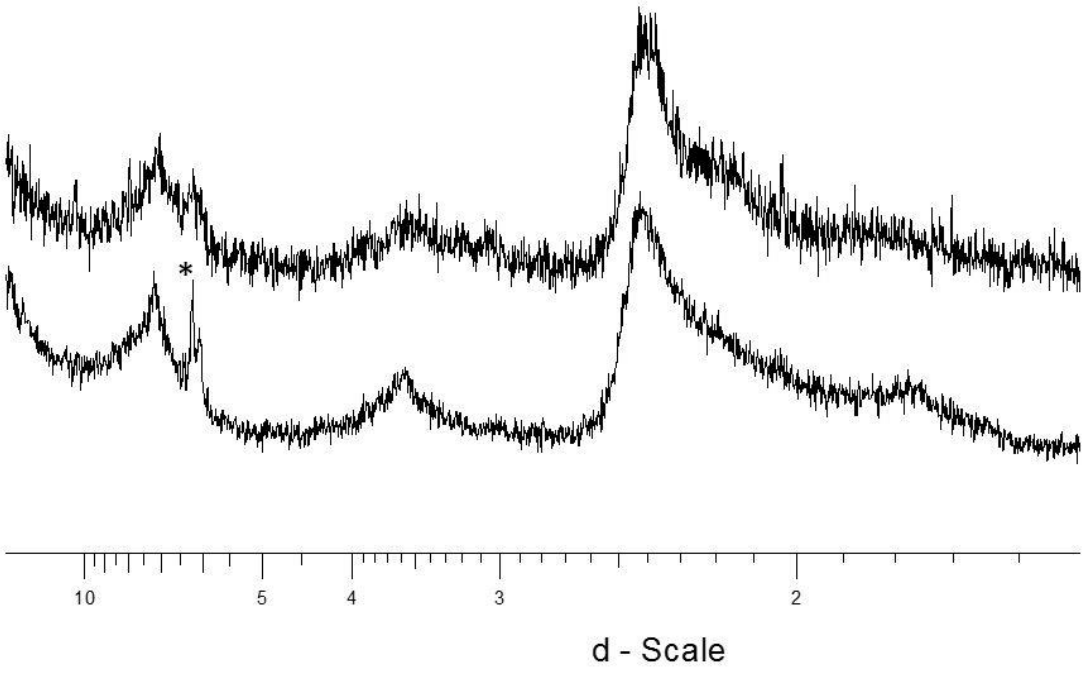

Figure 3.S2 XRD random powder pattern of birnessite incubated at 180 °C for 24 h (upper diffractogram) and at room temperature (lower diffractogram) showing typical broad basal plane peaks at around 7.4 Å and 3.6 Å (Co radiation) as well as the non-basal plane peak at around 2.4 Å indicating turbostratic disorder (Manceau et al., 2013; Villalobos et al., 2006). No mineralogical transformation caused by temperature can be assessed. *impurity caused by sample preparation

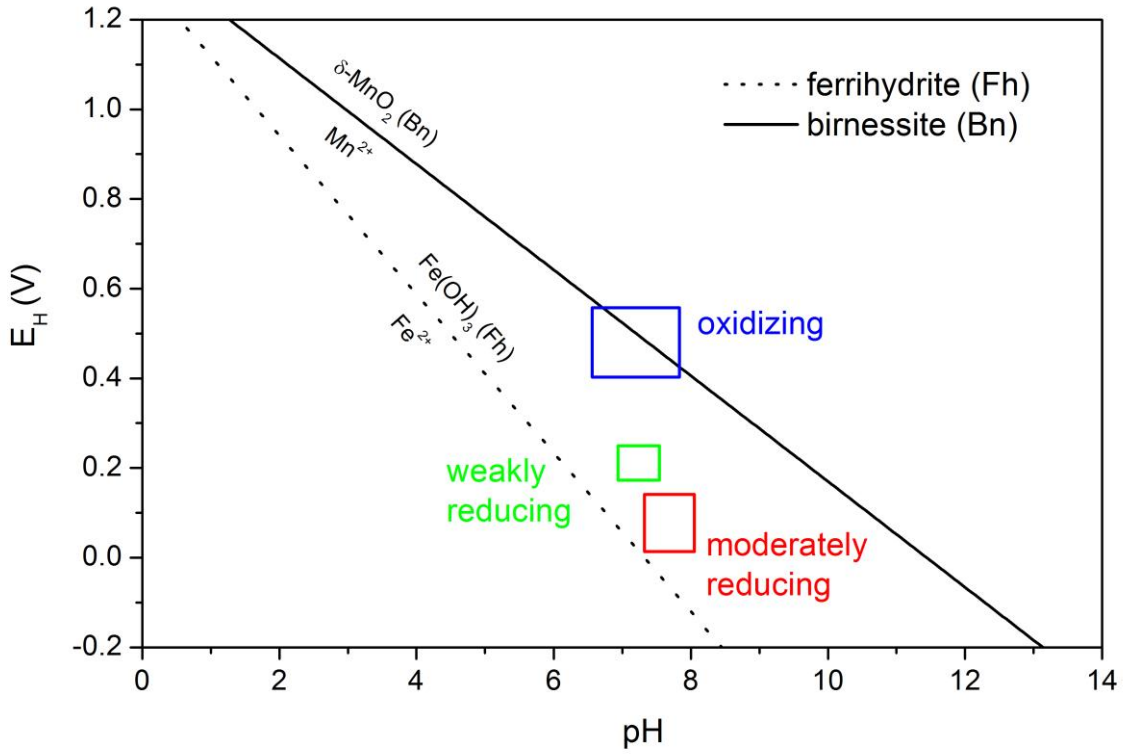

Figure 3.S3 E_H-pH diagram including the thermodynamic stability line for birnessite* (MnO_2/Mn^{2+}-system; $E_H = 1.23 - 0.03 \cdot \log 10^{-4}\ [Mn^{2+}] - 0.118 \cdot pH$) and ferrihydrite** ($Fe(OH)_3/Fe^{2+}$-system; $E_H = 1.06 - 0.06 \cdot \log 10^{-4}\ [Fe^{2+}] - 0.177 \cdot pH$) at 298.15 K, 0.101 MPa and 10^{-4} M ion activity (Brümmer, 1974). The data from the microcosm experiments under oxidizing, weakly reducing and moderately reducing soil conditions are plotted as boxes into the diagram. Care must be taken in the interpretation of the diagram, because reaction rates and kinetic pathways are not considered and the assumption of chemical equilibrium is not attained under natural conditions.

References

Ad-hoc-AG Boden. 2005. Bodenkundliche Kartieranleitung. 5th ed. Schweizerbart'sche Verlagsbuchhandlung. Hannover, Germany.

Bowell, R.J. 1994. Sorption of arsenic by iron oxides and oxyhydroxides in soils. Appl. Geochem. 9:279–286. doi:10.1016/0883-2927(94)90038-8

Castenson, K.L., and M.C. Rabenhorst. 2006. Indicator of reduction in soil (IRIS): Evaluation of a new approach for assessing reduced conditions in soil. Soil Sci. Soc. Am. J. 70:1222–1226. doi:10.2136/sssaj2005.0130

Chao, T.T. 1972. Selective dissolution of manganese oxides from soils and sediments with acidified hydroxylamine hydrochloride. Soil Sci. Soc. Am. Proc. 36:764–768. doi:10.2136/sssaj1972.03615995003600050024x

Childs, C.W. 1981. Field-tests for ferrous iron and ferric-organic complexes (on exchange sites or in water soluble forms) in soils. Aust. J. Soil Res. 19:175–180. doi:10.1071/SR9810175

Ching, S., D.J. Petrovay, M.L. Jorgensen, and S.L. Suib. 1997. Sol-gel synthesis of layered birnessite-type manganese oxides. Inorg. Chem. 36:883–890. doi:10.1021/ic961088d

Crowther, D.L., J.G. Dillard, and J.W. Murray. 1983. The mechanisms of Co(II) oxidation on synthetic birnessite. Geochim. Cosmochim. Acta 47:1399–1403. doi:10.1016/0016-7037(83)90298-3

Fakih, M., M. Davranche, A. Dia, B. Nowack, P. Petitjean, X. Chatellier, and G. Gruau. 2008. A new tool for in situ monitoring of Fe-mobilization in soils. Appl. Geochem. 23:3372–3383. doi:10.1016/j.apgeochem.2008.07.016

Fiedler, S., M.J. Vepraskas, and J.L. Richardson. 2007. Soil redox potential: Importance, field measurements, and observations. Adv. Agron. 94:1–54. doi:10.1016/S0065-2113(06)94001-2

Gao, S., K.K. Tanji, S.C. Scardaci, and A.T. Chow. 2002. Comparison of redox indicators in a paddy soil during rice-growing season. Soil Sci. Soc. Am. J. 66:805–817. doi:10.2136/sssaj2002.8050

Golden, D.C., J.B. Dixon, and C.C. Chen. 1986. Ion exchange, thermal transformations, and oxidizing properties of birnessite. Clays Clay Miner. 34:511–520. doi:10.1346/CCMN.1986.0340503

Gotoh, S., and W.H. Patrick. 1972. Transformation of manganese in a waterlogged soil as affected by redox potential and pH. Soil Sci. Soc. Am. Proc. 36:738–742. doi:10.2136/sssaj1972.03615995003600050018x

Gotoh, S., and W.H. Patrick. 1974. Transformation of iron in a waterlogged soil as influenced by redox potential and pH. Soil Sci. Soc. Am. Proc. 38:66–71. doi:10.2136/sssaj1974.03615995003800010024x

Händel, M., T. Rennert, and K.U. Totsche. 2013. A simple method to synthesize birnessite at ambient pressure and temperature. Geoderma 193–194:117–121. doi:10.1016/j.geoderma.2012.09.002

Isbell, R.F. 2002. The Australian soil classification. Revised ed. CSIRO Publishing, Melbourne, Australia. IUSS Working Group. 2006. World reference base for soil resources 2006. 2nd ed. World Soil Resources Rep. 103. FAO, Rome.

Jenkinson, B.J. 2002. Hydrology of sandy soils in northwest Indiana and iron oxide indicators to identify hydric soils. Ph.D. diss., Purdue Univ., West Lafayette, IN.

Jenkinson, B.J., and D.P. Franzmeier. 2006. Development and evaluation of iron-coated tubes that indicate reduction in soils. Soil Sci. Soc. Am. J. 70:183–191. doi:10.2136/sssaj2004.0323

Kay, J.T., M.H. Conklin, C.C. Fuller, and P.A. O'Day. 2001. Processes of nickel and cobalt uptake by a manganese oxide forming sediment in Pinal Creek, Globe Mining District, Arizona. Environ. Sci. Technol. 35:4719–4725. doi:10.1021/es010514d

Lovley, D.R. 1991. Dissimilatory Fe(III) and Mn(IV) reduction. Microbiol. Rev. 55:259–287.

Ma, Y., J. Luo, and S.L. Suib. 1999. Syntheses of birnessites using alcohols as reducing reagents: Effects of synthesis parameters on the formation of birnessites. Chem. Mater. 11:1972–1979. doi:10.1021/cm980399e

Manceau, A., B. Lanson, and V.A. Drits. 2002. Structure of heavy metal sorbed birnessite. Part III: Results from powder and polarized extended X-ray absorption fine structure spectroscopy. Geochim. Cosmochim. Acta 66:2639–2663. doi:10.1016/S0016-7037(02)00869-4

Mansfeldt, T. 2004. Redox potential of bulk soil and soil solution concentration of nitrate, manganese, iron, and sulfate in two Gleysols. J. Plant Nutr. Soil Sci. 167:7–16. doi:10.1002/jpln.200321204

Mansfeldt, T., and M. Overesch. 2013. Arsenic mobility and speciation in a Gleysol with petrogleyic properties: A field and laboratory approach. J. Environ. Qual. 42:1130–1141. doi:10.2134/jeq2012.0225

Mansfeldt, T., S. Schuth, W. Häusler, F. Wagner, S. Kaufhold, and M. Overesch. 2012. Iron oxide mineralogy and stable iron isotope composition in a Gleysol with petrogleyic properties. J. Soils Sediments 12:97–114. doi:10.1007/s11368-011-0402-z

McKenzie, R.M. 1971. The synthesis of birnessite, cryptomelane, and some other oxides and hydroxides of manganese. Mineral. Mag. 38:493–502. doi:10.1180/minmag.1971.038.296.12

Mehra, O.P., and M.L. Jackson. 1960. Iron oxide removal from soils and clays by a dithionite-citrate system buffered with sodium bicarbonate. Clays Clay Miner. 7:317–327. doi:10.1346/CCMN.1958.0070122

National Technical Committee for Hydric Soils. 2007. Technical note 11: Technical standards for hydric soils. http://www.nrcs.usda.gov/wps/portal/nrcs/detail/soils/home/?cid=nrcs142p2 _053973 (accessed 13 Feb. 2014).

Ottow, J.C.G. 2011. Microbiology of soils. (In German.) Springer, Heidelberg, Germany.

Patrick, W.H., R.P. Gambrell, and S.P. Faulkner. 1996. Redox measurements of soils. In: D.L. Sparks, editor, Methods of soil analysis. Part 3. Chemical methods. SSSA and ASA, Madison, WI. p. 677.

Patrick, W.H., B.G. Williams, and J.T. Moraghan. 1973. A simple system for controlling redox potential and pH in soil suspensions. Soil Sci. Soc. Am. J. 37:331–332. doi:10.2136/sssaj1973.03615995003700020048x

Peretyazhko, T., and G. Sposito. 2005. Iron(III) reduction and phosphorus solubilization in humid tropical forest soils. Geochim. Cosmochim. Acta 69:3643–3652. doi:10.1016/j.gca.2005.03.045

Ponnamperuma, F.N. 1972. The chemistry of submerged soils. Adv. Agron. 24:29–96. doi:10.1016/S0065-2113(08)60633-1

Rabenhorst, M.C. 2010. Visual assessment of IRIS tubes in field testing for soil reduction. Wetlands 30:847–852. doi:10.1007/s13157-010-0098-7

Rabenhorst, M.C., and S.N. Burch. 2006. Synthetic iron oxides as an indicator of reduction in soils (IRIS). Soil Sci. Soc. Am. J. 70:1227–1236. doi:10.2136/sssaj2005.0354

Reddy, K.R., and R.D. DeLaune. 2008. Biogeochemistry of wetlands: Science and applications. CRC Press, Boca Raton, FL.

Schwertmann, U. 1964. The differentiation of iron oxide in soils by a photochemical extraction with acid ammonium oxalate (in German). Z. Pflanzenernaehr. Dueng. Bodenkd. 105:194–202. doi:10.1002/jpln.3591050303

Smith, K.A. 1980. A model of the extent of anaerobic zones in aggregated soils, and its potential application to estimates of denitrification. J. Soil Sci. 31:263–277. doi:10.1111/j.1365-2389.1980.tb02080.x

Soil Survey Staff. 2010. Keys to soil taxonomy. 11th ed. USDA–NRCS, Washington, DC.

Stiles, C.A., E.T. Dunkinson, C.L. Ping, and J. Kidd. 2010. Initial field installation of manganese indicators of reduction in soils, Brooks Range, Alaska. Soil Surv. Horiz. 51:102–107.

Vaughan, K.L., M.C. Rabenhorst, and B.A. Needelman. 2009. Saturation and temperature effects on the development of reducing conditions in soils. Soil Sci. Soc. Am. J. 73:663–667. doi:10.2136/sssaj2007.0346

Yu, K.W., and W.H. Patrick. 2004. Redox window with minimum global warming potential contribution from rice soils. Soil Sci. Soc. Am. J. 68:2086–2091. doi:10.2136/sssaj2004.2086

Zehnder, A.J.B., and W. Stumm. 1988. Geochemistry and biogeochemistry of anaerobic habitats. In: A.J.B. Zehnder, editor, Biology of anaerobic microorganisms. John Wiley & Sons, New York. p. 1–38.

Zhang, X., X. Chang, N. Chen, K. Wang, L. Kang, and Z.-H. Liu. 2012. Synthesis and capacitive property of delta-MnO(2) with large surface area. J. Mater. Sci. 47:999–1003. doi:10.1007/s10853-011-5879-8

Chapter 4 Comparison of manganese and iron oxide-coated redox bars for characterization of the redox status in wetland soils

WETLANDS (2016) 36: 133–141

Co-authors: Michael Eickmeier and Tim Mansfeldt

Formatting and orthography of the manuscript is adapted to the dissertation style.

Abstract

Characterization of the soil redox status is important for pedogenesis but simple field methods for monitoring are limited. Recently, we introduced manganese ($Mn^{III,IV}$) oxide-coated redox bars as an indicator for reducing conditions in soils. In this study, we compared these redox bars with well-established iron (Fe^{III}) oxide-coated bars. For a 5-month monitoring period, we quantified the monthly oxide removal along three wetland plots with different variations in water table. Preferential dissolution of the Mn oxide coating exceeded the Fe oxide removal by two to five times that is coherent with the thermodynamic stability of the minerals. Enhanced removal of Mn oxide coatings in the capillary fringe compared to minor depletion of Fe oxides enables to differentiate weakly (300 to 100 mV, range of $Mn^{III,IV}$ reduction) and moderately (100 to −100 mV, range of Fe^{III} reduction) reducing conditions. Processes that occur under weakly reducing soil conditions, e.g. denitrification and trace metal mobilization associated with the reductive dissolution of Mn oxides, can be identified when Mn oxide removal along redox bars occurs but the Fe oxide coating remains stable. Simultaneous use of Mn and Fe redox bars results in a better temporal and spatial characterization of the soil redox status.

Keywords: Redox bars, Iron oxide, Manganese oxide, Monitoring, Soil reducing conditions, Microsites

Abbreviations: E_H = redox potential, WT = water table, CWB = climatic water balance

Introduction

The characterization of the temporal and spatial extent of reducing conditions in soils is a challenge for scientists worldwide. The intensity of soil reducing conditions, expressed as the redox potential (E_H), is a geochemical master variable and affects the mobility of nutrients and pollutants, the release of potent greenhouse gases and alters soil formation. Soil reducing conditions are induced when the microbial and root mediated oxygen (O_2) consumption exceeds the O_2 supply via diffusion from the atmosphere. Under these conditions, the soil milieu is termed anaerobic. The replenishment of O_2 is highest when the soil pores are filled with air and is negatively correlated with increasing soil water content (Smith 1980). Consequently, the onset of soil reducing conditions is related to soils affected by groundwater, soils having water logging due to perched water tables and soils influenced by flooding and irrigation events (Ponnamperuma 1972). Currently, 32 reference soil groups are established by the IUSS Working Group (IUSS Working Group WRB 2006). Four of these soil groups are identified due to the presence of reducing conditions, which include Gleysols, Planosols, Plinthosols and Stagnosols. In total, 1.085 billion ha, which make up 7.75% of the Earth's land surface, are covered with soils showing distinct redoximorphic features (IUSS Working Group WRB 2006; Kirk 2004; Reddy and DeLaune 2008). This illustrates the importance and all-round distribution of reduction in soils, and consequently, the need to easily quantify and monitor reducing conditions.

The prevalence of reducing soil conditions stimulates facultative and obligate anaerobe microorganisms to utilize selectively the following electron acceptors according to their free energy yields (ΔG^0; in kJ per mol organic matter when formaldehyde (CH_2O) represents the electron donor): oxygen (O_2; −125 kJ mol^{-1}), pentavalent nitrogen in nitrate (NO_3^-, −119 kJ mol^{-1}), manganese oxides (e.g., MnO_2, −94.5 kJ mol^{-1}), iron oxides (e.g. FeOOH, −24.3 kJ mol^{-1}), sulfate (SO_4^{2-}, −18 kJ mol^{-1}), and carbon dioxide (CO_2, −17.4 kJ mol^{-1}) (Schlesinger and Emily 2013). According to the electron acceptor in use, different redox zones or classes can be classified into oxidizing (E_H > 300 mV; O_2 and NO_3^- are consumed), weakly reducing (E_H ranges from 300 to 100 mV; Mn oxides are consumed), moderately reducing (E_H ranges from 100 to −100 mV; Fe oxides are consumed), and strongly reducing soil conditions (E_H < −100 mV; SO_4^{2-} and CO_2 are consumed) (Reddy and DeLaune 2008). This sequence is a stepwise one and known as the sequential reduction sequence (Ottow 2011).

Manganese and Fe are abundant in the soils environment and play a major role as soil constituents. In their oxidized form, manganic Mn ($Mn^{III,IV}$) and ferric Fe (Fe^{III}) are not water soluble, immobile and, due to their pigmenting power, easy to identify in oximorphic soil

horizons. However, under the absence of O_2 the minerals participate in reversible electron transfer reactions and may be liberated into soil solution under weakly reducing soil conditions as manganous Mn (Mn^{2+}) and under moderately reducing soil conditions as ferrous Fe (Fe^{2+}). Translocation and lack of both oxides characterize soil horizons as reductomorphic. The Mn and Fe chemistry of Gleysols (gleyic color pattern) is affected by water saturation due to the presence of groundwater, whereas Planosols, Plinthosols and Stagnosols show Mn and Fe reduction because of temporary waterlogging (stagnic color pattern) due to stagnant water. Methods to infer the redox status of the soil contain the use of (i) platinum (Pt) electrodes (Fiedler et al. 2007; Patrick et al. 1996), (ii) dyes (Childs 1981; Ringrose-Voase and Humphreys 1993), (iii) the terminal electron-accepting processes approach (Chapelle et al. 1995) (TEAPs), (iv) the concept of oxidative capacity (Scott and Morgan 1990), (v) striated polymer plates (Fakih et al. 2008) and (vi) iron metal rods (Owens et al. 2008). One has to keep in mind that each method contains various advantages and disadvantages and that the detection of soil reducing conditions cannot exclusively be attributed to one method. Considerations should be made if field monitoring is required (i, v, vi), avoidance of laboratory analysis (i, ii,vi), expensive (i) or low priced (ii, v, vi) equipment, if the focus of interest is in a larger hydrological (iii) or smaller pedological scale (i, ii, v, vi), if self-manufacturing is possible (v, vi) and differentiation of redox zones is desired (i, iii, iv). Jenkinson and Franzmeier (2006) introduced Fe oxide-coated tubes for assessing the redox status of a soil. Synthesized Fe oxides, consisting of ferrihydrite and goethite, are coated onto white polyvinyl chloride (PVC) tubes and installed into the soil. After a distinct time the tubes are removed from the soil and the depletion patterns are digitally analyzed or visually assessed. The reductive dissolution of the oxide coating approximates the *in situ* soil redox status and can be quantitatively interpreted for monitoring issues. In 2010, Mn oxide-coated tubes to further investigate reducing soil conditions were introduced (Stiles et al. 2010). However, the synthesis of Mn oxides and the manufacturing of the tubes were tedious, and documentation for manufacturing was missing, thus restricting this method as a diagnostic tool for reducing soil conditions. Dorau and Mansfeldt (2015) documented a useable method to apply Mn oxides to PVC bars to assess less strongly reducing soil conditions. The differentiation between redox zones seems reasonable, because Mn oxides are preferential and at higher E_H reduced compared to Fe oxides, as confirmed in laboratory experiments (Dorau and Mansfeldt 2015). The application of Mn oxide-coated redox bars together with Fe oxide-coated redox bars (henceforth, named Mn and Fe redox bars or redox bars in general) might bridge the gap to differentiate between weakly reducing (Mn reduction takes place) and moderately reducing (Fe reduction takes place) conditions in the field to better assess certain redox zones.

To improve the understanding of the temporal and spatial extent of reducing conditions in soils, Mn and Fe redox bars were tested in an intermittent wetland. The objectives of this research paper are (i) to monitor and discuss the Mn and Fe oxide removal along redox bars at a groundwater-influenced study site and (ii) examine the conditions that lead to different dissolution patterns along Mn redox bars.

Materials and Methods

Study Site

The monitoring site is within the Münsterland Cretaceous Basin in the district of Recklinghausen, North Rhine-Westphalia, Germany (51°48′59″ N, 7°12′59″ E). Shallow water table depths (< 1 m) prevail along the grassland site, and glaciofluvial processes resulted in a micro-relief (47.6 to 49.0 m asl). The relief favors the separation into elevated dry sites and flooded sites in lower terrain where water is periodically ponding. Hence, variations in the soil hydrologic regime and soil properties render this site very suitable for investigations using Mn and Fe redox bars. The soil types can be classified according to WRB as Haplic Gleysol (Petrogleyic) for the elevated and predominantly aerobic plot (named plot A), Haplic Gleysol (Hyperhumic) for the intermediate plot (B) and Mollic Gleysol for the flooded plot (C) (Table 4.1). The distance between the sites was approximately 100 m, and the dominant plant species at all plots was velvet grass (Holcus lanatus), which is an indicator plant for hydric soils and adapted to frequent phases of water saturation. However, more specialized plants were found at plot A (e.g. field meadow foxtail (Alopecurus pratensis)), B (blue rush (Juncus inflexus)), and C (common sedge (Carex nigra)).

Table 4.1 Selected soil properties of the predominantly aerobic (A), intermediate (B), and flooded (C) plot

plot	Depth	pH ($CaCl_2$)	Soil texture	CEC[a] ($mmol_c\ kg^{-1}$)	BS[b] (%)	C_{org}[c]	N	S ($g\ kg^{-1}$)	Fe	Mn
A	0 to 20	4.6	Silt loam	73.5	90	46.1	3.82	0.72	97.0	1.27
	20 to 50	4.9	Loamy sand	50.9	95	7.11	0.47	0.27	73.5	1.11
B	0 to 50	4.9	Loamy sand	83.0	82	72.6	4.53	1.47	12.3	0.05
C	0 to 15	4.4	Silt loam	234	78	146	10.8	3.74	21.1	0.16
	15 to 50	4.4	Silt loam	181	84	95.6	4.56	2.27	23.6	0.30

[a] effective cation exchange capacity
[b] base saturation
[c] organic carbon

Soil Characterization

We took disturbed soil samples from an excavation pit for diagnostic horizons for plots A, B, and C. The samples were oven dried at 40 °C, sieved < 2 mm, and subsamples were pulverized in a mixer mill (MM400, Retsch, Haan, Germany) to determine total element

concentrations. The soil pH was measured potentiometrically using a glass electrode in a 0.01 mol L^{-1} $CaCl_2$ solution mixed 5:1 with soil (v/v). Organic carbon (C_{org}), nitrogen (N), and sulphur (S) were measured by dry combustion with a CNS analyzer (vario EL cube, Elementar, Hanau, Germany). Cation exchange capacity (CEC) was determined by percolating 2.5 g of soil sample using 1 M NH_4Cl solution, and bases were measured in the percolate using flame atomic absorption spectroscopy (F-AAS) (iCE 3000 series, Thermo Scientific, Waltham, USA).

Field Monitoring

The manufacturing of redox bars is presented in detail for Mn redox bars in Dorau and Mansfeldt (2015), and for Fe redox bars in Jenkinson and Franzmeier (2006) and Rabenhorst and Castenson (2005). Redox bars were 60 cm in length (50 cm coated surface, Ø 21 mm) and we installed three Mn and three Fe redox bars per month and per plot at the predominant aerobic, the intermediate and the flooded plot. The dimension of the plots was 1 · 1 m. Installation and removal of the redox bars was on a monthly basis from March to July 2013. Water table (WT) depth was measured in a groundwater well (PDLR 70, EcoTech, Bonn, Germany) at the intermediate plot. Data was extrapolated to the aerobic and the flooded plot using a digital elevation model derived by airborne laser scanning (±10 mm data accuracy in height, GEOBASIS NRW). Soil temperature was recorded at the intermediate plot as well and assumed to be the same at all plots (temperature lance with RS 485 interface, UIT, Dresden, Germany). Precipitation and air temperature data were taken from a free access weather station, 6 km east of the study site in the city of Dülmen (51°49′04″ N, 07°18′40″ E). We determined the climatic water balance as the difference between precipitation and calculated potential evapotranspiration (PET) on a monthly basis. To calculate PET we used the Haude formula (PET_{Haude}) with monthly coefficients for grass, which is suitable for the estimation of monthly sums but inaccurate for daily values (Bormann et al. 1996).

Digital Analysis of Redox Bars

We quantified the oxide removal of Mn and Fe redox bars for the upper (0 to 25 cm) and the lower (25 to 50 cm) part using digital image analysis. The analysis procedure contained the following steps: (i) we obtained four images of 90° sections of each redox bar, (ii) cropped the distorted images together, and (iii) created a binary image by means of a user-defined threshold (GIMP v.2.8.4). The threshold was adjusted to correlate best with visual depletion patterns. Only minor difficulties to quantify the oxide removal along Fe redox bars into depleted and non-depleted areas arose (Rabenhorst 2010). We had to adapt the

quantification of the oxide removal along Mn redox bars, since Fe precipitates mimic partially depleted Mn oxides, but actually indicate that no Mn remained. An efficient way to verify if Fe precipitated without chemical analysis is to hold a portable XRF analyzer with small observation spot (2 mm diameter, 40 s runtime with small, medium, and large filter; Niton XL3, Thermo Scientific, Waltham, USA) along the Mn redox bars' surface. When the XRF signal indicated Fe, no Mn (or in negligible traces) remained at the PVC surface. This was confirmed by inductively coupled plasma mass spectrometry (ICP-MS) (XSeries 2, Thermo Scientific, Waltham, USA) measurements for various Mn redox bars used in the monitoring campaign (e.g. a XRF signal of 6.3 g kg^{-1} Fe equaled 0.57 mg DCB-soluble Fe and only 0.011 mg Mn for a 10 cm^2 oxide coating area). Exclusively for Mn redox bars, using coloring as a hint and XRF for verification, areas and boundaries of Fe precipitation were sketched and managed as total Mn oxide removal. Because the color of *in situ* precipitated Fe oxides differed remarkably compared to the remaining Mn oxide coatings, digital analysis enables to differentiate areas of Mn oxides and Fe precipitates. X-ray fluorescence is therefore not an essential methodology to quantify the oxide removal.

Results and Discussion

Climatic Water Balance, Water Table Depth and Soil Temperature

Figure 4.1a shows the monthly sums of precipitation, potential evapotranspiration (PET_{Haude}) and the climatic water balance (CWB) and Fig. 4.1b, the dynamics of the WT depth for the aerobic (A), intermediate (B) and flooded (C) plot on an hourly basis as well as the development of soil temperature as monthly mean. The PET_{Haude} steadily increased from 20.9 mm in March to 76.2 mm in July as the water demand of the atmosphere rises (Fig. 4.1a). When the intake of precipitation was low, the climatic water balance became negative in March, April, May and July. The water balance turned positive in June when 100 mm of precipitation fell. This month was untypically wet with 65% more rainfall compared to the period from 2005 to 2012. The groundwater level varied from −77 ("−" indicates below soil surface) to −23 cm (mean − 56 cm) for the aerobic plot, −52 to +1 cm (−32 cm) for the intermediate, and −34 to +19 cm (−13.9 cm) for the flooded plot (Fig. 4.1b). Diurnal WT fluctuations of 6 cm become apparent by mid-May because of the enhanced root water uptake by daytime. The development of the WT responded rapidly to the precipitation event on 01.06.2013 with 48.7 mm, which was about 50% of the monthly sum.

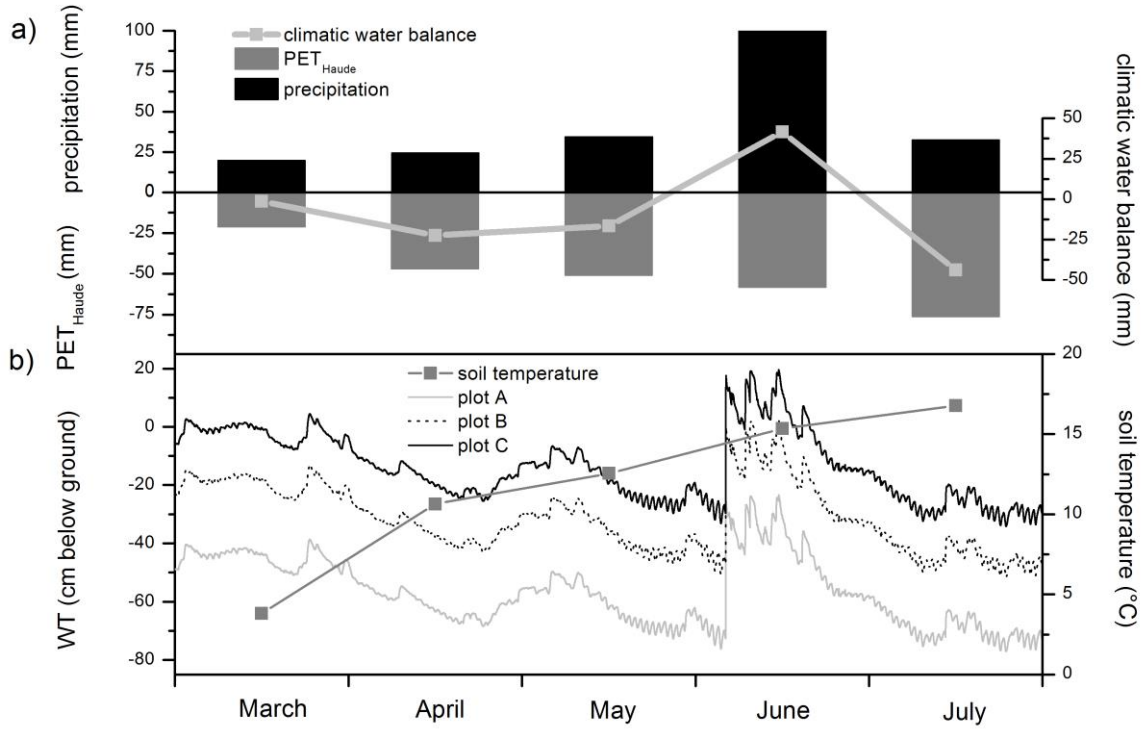

Figure 4.1 Monthly sums of precipitation, evapotranspiration and calculated climatic water balance (a) and development of soil temperature and water table depth for a predominantly aerobic (A, grey solid), an intermediate (B, black dotted), and a periodically flooded (C, black solid) soil environment (b) from March to July 2013. Water table depth was measured at plot B and extrapolated to plots A and C using a digital elevation model, and soil temperature was measured at plot B and assumed to be the same for the other plots.

At the beginning of the study period, soil temperatures were low in 25 cm depth (3.8 °C) and steadily increased by the end of the study period in July (16.8 °C) with a mean soil temperature of 12.0 °C during the course of the study (Fig. 4.1b).

Oxide Removal along Redox Bars

Table 4.2 displays the oxide removal along Mn and Fe redox bars from 0 to 25 cm and 25 to 50 cm respectively. Due to the low WT at plot A (Fig. 4.1b), aerobic conditions prevailed in this soil, which is expressed by the marginal Mn and Fe oxide removal along the redox bars throughout the study period (Table 4.2). The Mn oxide removal ranged from 0 to 50% for the upper part and 0 to 10% for the lower part, and 0 to 15% and 0 to 3% for Fe redox bars, respectively. At the intermediate plot, near-surface groundwater intensified the reductive dissolution of the Mn and Fe oxide coating with variations from 6 to 73% and 83 to 100% for the top and bottom of Mn redox bars. Corresponding values were 2 to 30% and 22 to 86% for the Fe redox bars. The WT at the flooded plot was constantly above 25 cm below ground. Hence, the depleted area exceeded the oxide removal of the aerobic plots

significantly. Values for Mn redox bars ranged from 32 to 95% and complete removal, and for Fe redox bars ranged from 8 to 63% and 10 to 96%.

In general, depletion of the coating was more intense in the subsoil because capillary rise from shallow groundwater favored elevated water contents, and hence the onset of anaerobiosis. This pattern was reversed in the higher elevation plot (A) in June. Then, the depletion of the oxide coating along Mn (Fe) redox bars was 5% (3%) at the bottom, significantly lower compared to 50% (15%) at the top, respectively. High precipitation, which favored elevated water contents in the topsoil, and elevated soil temperatures and C_{org} contents in the topsoil, might be responsible for this reversal (Table 4.1). These results are similar with data from Rabenhorst and Castenson (2005). When the soil was water saturated, they found greater Fe oxide removal along IRIS tubes in surface horizons with higher amounts of C at temperatures between 8 and 20 °C compared to 2 and 8 °C. Beyond these findings, oxide removal along Mn redox bars was favorable by the factor of 2 to 5 compared to Fe redox bars throughout the study period and across all plots. This is in accordance with the thermodynamic stability of the applied minerals as outlined by Dorau and Mansfeldt (2015).

Table 4.2 Mean oxide removal for the upper (0 to 25 cm) and lower (25 to 50 cm) part of Mn and Fe oxide-coated redox bars installed in triplicate at a predominantly aerobic (A), intermediate (B) and periodically flooded (C) soil environment with the corresponding standard deviation.

Redox bar	Plot	depth	March	April	May	June	July
			oxide removal (%)				
Mn	A	0 to 25	0.1 ±0.1%	1.7 ±2.1%	2.4 ±1.3%	50.5 ±14%	0.6 ±1.7%
		25 to 50	0.1 ±2.0%	3.4 ±4.7%	2.1 ±1.2%	5.3 ±4.8%	10.7 ±1.0%
	B	0 to 25	44.6 ±4.2%	6.5 ±1.1%	12.9 ±5.0%	73.0 ±10%	10.1 ±2.7%
		25 to 50	98.4 ±0.2%	93.0 ±0.3%	95.4 ±0.4%	100.0 ±0.1%	83.2 ±0.5%
	C	0 to 25	93.6 ±3.1%	93.7 ±2.5%	55.6 ±8.7%	95.1 ±2.1%	32.4 ±4.8%
		25 to 50	100.0 ±2.0%	100.0 ±0.5%	100.0 ±0.4%	100.0 ±0.3%	100.0 ±0.1%
Fe	A	0 to 25	0.1 ±0.1%	0.5 ±1.1%	0.2 ±0.1%	15.7 ±5.3%	2.6 ±0.1%
		25 to 50	0.1 ±0.1%	0.2 ±0.1%	3.6 ±0.1%	3.4 ±1.9%	2.0 ±1.0%
	B	0 to 25	18.1 ±0.1%	14.2 ±1.1%	2.0 ±1.5%	30.6 ±8.9%	7.5 ±0.1%
		25 to 50	86.0 ±2.4%	78.3 ±1.3%	28.3 ±3.7%	22.8 ±4.0%	51.4 ±3.2%
	C	0 to 25	63.1 ±3.2%	40.3 ±2.5%	8.0 ±5.0%	58.6 ±4.7%	22.6 ±2.9%
		25 to 50	96.9 ±3.1%	66.0 ±2.3%	44.1 ±4.3%	10.2 ±1.0%	80.3 ±3.6%

Interestingly, the Fe oxide removal steadily declined for plots B and C from March to June (Table 4.2). Jenkinson and Franzmeier (2006) found similar results, and attributed this to a nutrient decrease for microbes, which limited microbial activity, and hence, conditions to sufficiently reduce trivalent Fe along the coating. The data of the decreasing Fe oxide removal supports this assumption and highlights the importance of C_{org} turnover when delineating the temporal and spatial distribution of soil reducing conditions. Manganese redox bars did not reflect this turnover related decline. The complete removal of the Mn oxide

coating at the flooded plot (Table 4.2) indicated that the installation time of 30 days does not yield the desired spatial resolution to delineate reducing conditions at study sites with high C_{org} content (Table 4.1) and permanent water saturation. Elevated soil water contents and temperatures in the topsoil favored a more pronounced standard deviation in June, indicating that hotspots of reduction were distributed heterogeneously in the soil profile. However, as the standard deviation was below 5% (Table 4.2) for most of the time during the study period, the delineation of soil reducing conditions using redox bars in triplicate is possible.

Environmental Conditions Favoring Oxide Removal

The impact of environmental conditions, which induce the oxide removal along redox bars, is difficult to distinguish for various reasons. Time-independent parameters affecting the onset of reducing conditions and, therefore, depletion patterns of the oxide coating, include soil pH, texture and C_{org} inventory, whereas time-dependent boundary conditions include soil water content, WT depth, soil temperature, C_{org} flux and microbial activity. On the one hand, the O_2 diffusion coefficient can be defined as a steady-state condition because the replenishment is primarily driven by the texture, the pore sizes and the connectivity of the pores. On the other hand, this variable is in a transient state because it is affected by the time-variable parameters of soil water content and microbial activity. Figure 4.2 shows the relationship between the period of water saturation and the oxide removal of Mn and Fe redox bars used in the monitoring campaign, whereby water saturation is defined as the period when the WT was within 0 to 25 cm for the topsoil and 25 to 50 cm for the subsoil. Both regression lines indicate that longer periods of water saturation favor higher rates of oxide removal. When water saturation prevails for 15 days of the installation time, Mn oxide removal (45%) is favorable by four times compared to Fe oxide removal (11%) (Table 4.2).

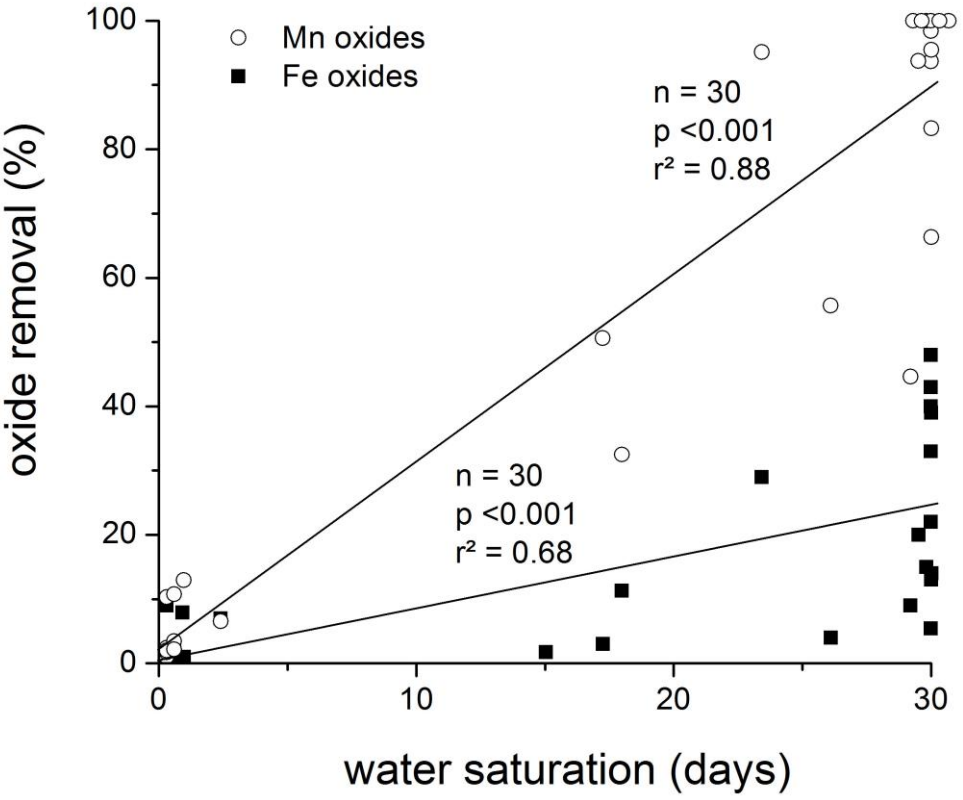

Figure 4.2 Relationship between the period of water saturation and the oxide removal of Mn (○) and Fe (■) oxide-coated redox bars. Period of water saturation is defined as the time when the water table was in contact with the upper part (0 to 25 cm) and the lower part (25 to 50 cm) of the redox bar, and correlated with the corresponding oxide removal for Mn and Fe redox bars installed during the 5-month monitoring period.

Jenkinson and Franzmeier (2006) proposed the term Upper Depletion Depth (UDD) to delineate where reduction increased significantly along Fe redox bars. According to our data, there was good agreement between the UDD and the maximum rise of the WT for Mn redox bars (Fig. 4.3a), whereas the UDD along Fe redox bars corresponds with the mean WT (Fig. 4.3b). Hence, the onset of weakly reducing soil conditions in the capillary fringe, where soil pores are not fully water saturated but soil water contents are close to saturation, plays an important role and is assessable using Mn redox bars. The differentiation between weakly and moderately reducing soil conditions in these settings is therefore possible using Mn and Fe redox bars simultaneously rather than using one sole type of redox bar. Because the oxide removal of Mn oxide was rapid and favorable, especially at plots B and C, we recommend the usage of Mn redox bars on a weekly or biweekly basis (Dorau and Mansfeldt 2015). Further research should focus on relating the percentage Mn oxide removal during field application with E_H measurements. For instance, Castenson and Rabenhorst (2006) evaluated the Fe oxide removal along Fe redox bars and found that the soil was reducing with respect to the thermodynamic stability line of Fe when 30% of Fe oxide loss occurred.

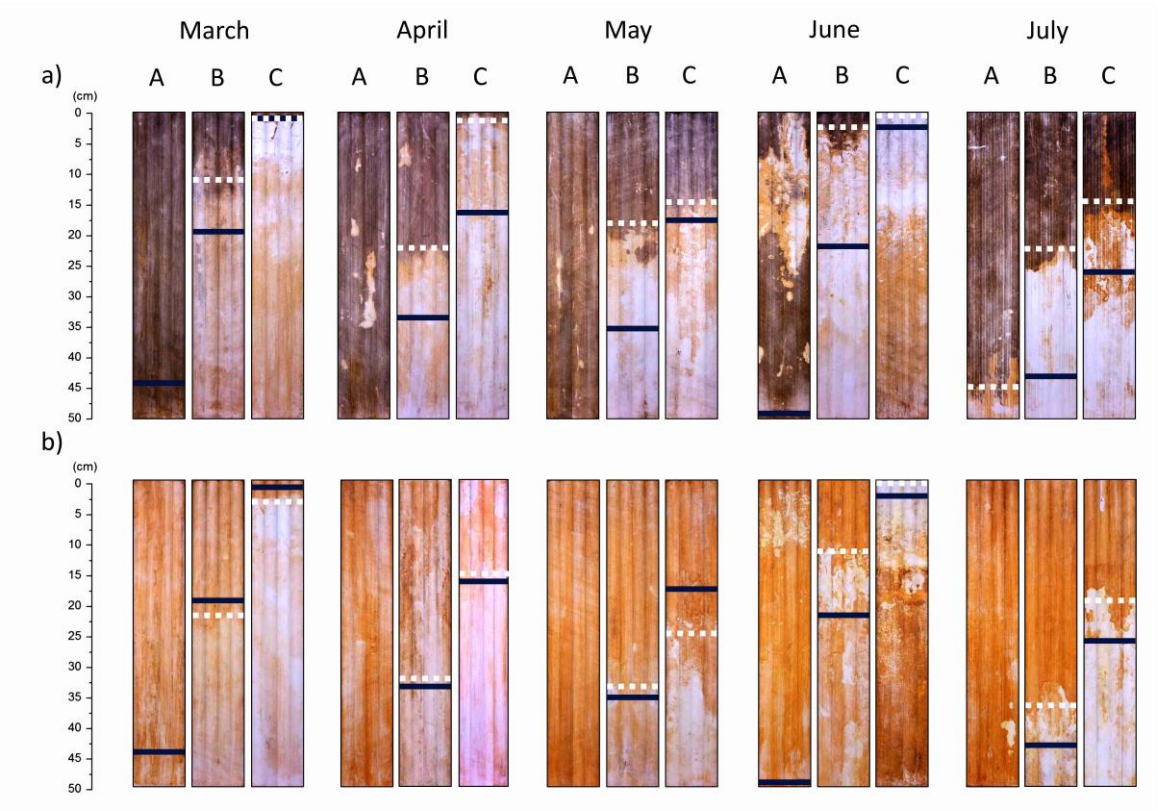

Figure 4.3 Examples of Mn (a) and Fe (b) oxide-coated redox bars installed at a predominantly aerobic (A), intermediate (B) and periodically flooded (C) soil environment from March to July 2013. The blue line indicates the mean water table depth during the installation time of 30 days and the dotted white line the upper depletion depth. Where there is no line, the water table was below the redox bar or the upper depletion depth was not apparent.

Typical depletion patterns along redox bars

Figure 4.4 summarizes important characteristics observed along Mn redox bars removed after one month of installation. Differences in the color indicate the presence of the original Mn oxide coating (solid black box) beside freshly formed Fe oxides (dashed black box) and spots where the white PVC (dotted black box) is visible at very short scale, i.e. < 1 cm (Fig. 4.4a). The *in situ* precipitated Fe oxides along the PVC surface of the Mn redox bar originate from ferrous Fe^{2+} in soil solution, which is abundant in the shallow groundwater at the study site (Mansfeldt and Overesch 2013), and further reacts with the Mn oxide coating according to $MnO_2 + 2Fe^{2+} + 4H_2O \rightarrow Mn^{2+} + 2Fe(OH)_3 + 2H^+$ [1]. From the edge to the center of a depletion spot, a gradient of oxidizing (E_H > 300 mV; Mn oxides remain stable), weakly reducing (E_H 300 to 100 mV; Mn oxides are reduced and Fe oxides remain stable), and moderately reducing soil conditions (E_H 100 to −100 mV; Fe oxides are reduced) can be derived. These patterns highlight that E_H must vary significantly at short distances by at least three redox ranges under field conditions. Quantification of zones where Mn oxide reduction occurs but Fe oxides remain stable are relevant to delineate hot

spots of nitrous oxide emission (Yu and Patrick 2004) and assess the risk of trace metal mobilization potentially bound to the surface of Mn oxides due to the reductive dissolution of the sorbent (Della Puppa et al. 2013) under weakly reducing soil conditions.

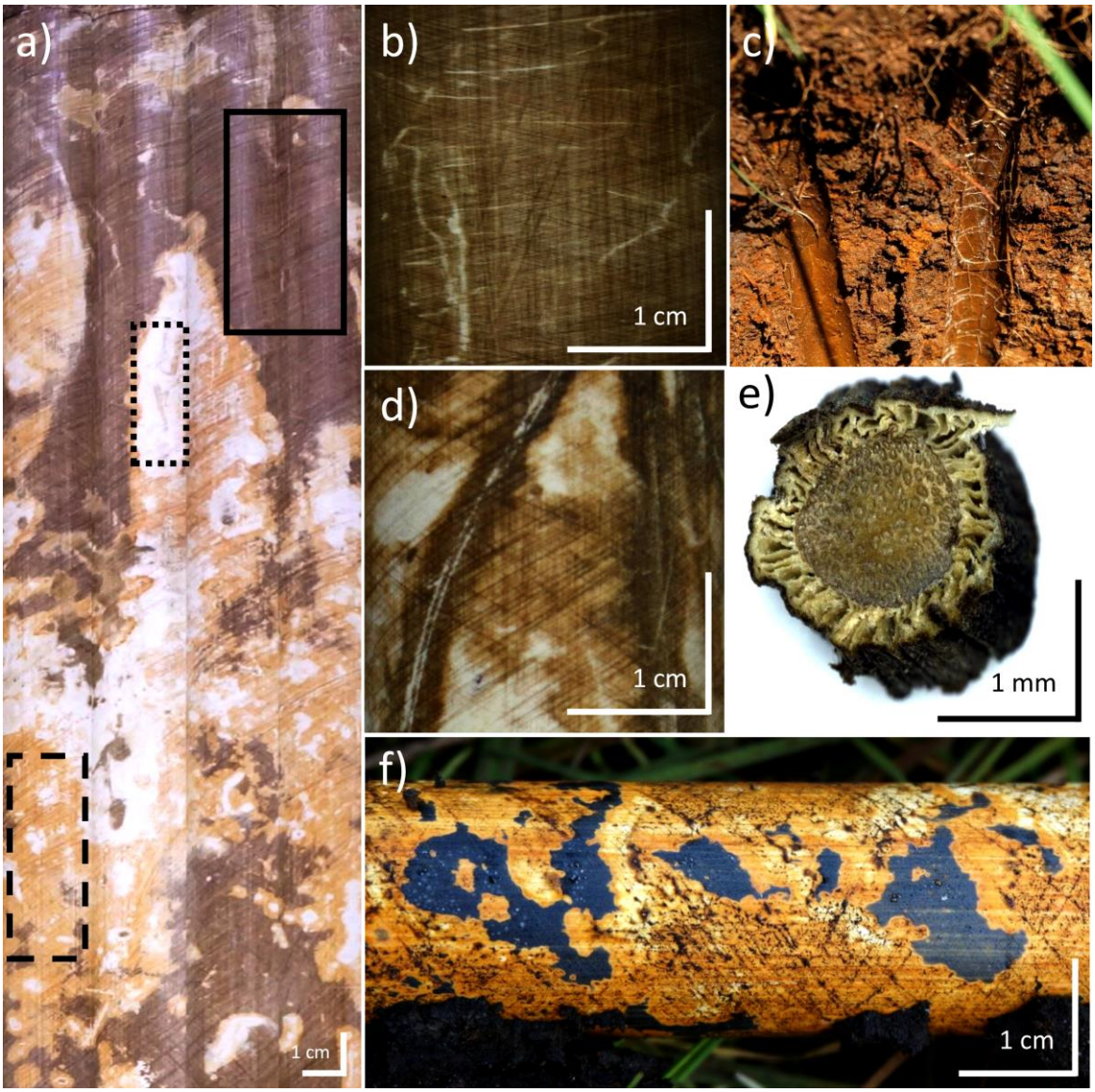

Figure 4.4 Examples of depletion patterns observed at Mn and Fe redox bars during the monitoring campaign: a) Coexistence of areas with complete oxide removal (white, dotted box), Fe oxide precipitation (light brown, dashed box) and Mn oxide persistence (dark brown, solid box) along 0 to 25 cm at one Mn redox bar installed in June, b) linear depletion patterns of Mn oxide removal caused by root exudates, c) borehole photo where a Fe (left) and a Mn redox bar (right) were installed at plot A in June, d) linear patterns of Mn oxide coatings in an anaerobic soil environment, e) cross-section of aerenchyma (*Carex nigra*), f) formation of FeS along Fe redox bars at plot C in July.

Jenkinson and Franzmeier (2006) assessed linear depletion patterns along Fe oxide-coated tubes caused by roots as organic matter source. We observed a mesh of linear Mn oxide depletion (Fig. 4.4b) on a redox bar placed in a borehole with a network of fine roots

(Fig. 4.4c, right borehole). Like Fe, Mn is a micronutrient for plants but far less abundant in the soil of plot A with 1.27 g Mn and 97.0 g Fe kg^{-1} soil (Table 4.1). Higher densities of fine roots in the Mn bar borehole (Fig. 4.4c, right) compared to the Fe bar borehole (Fig. 4.4c, left) indicate that fine root growth was favored because of the supplemental micronutrient in form of the Mn oxide coating.

Phytosiderophores (PS) are metal chelating compounds released by plant roots to selectively mobilize Fe and other micronutrients from the soil when plant stress due to nutrient deficiency occurs (Römheld 1991). This was shown in a laboratory experiment using calcareous soil material, where root exudates barely increased the amounts of Cu < Fe < Zn < Mn in the designated order by a factor of 20 (Treeby et al. 1989). However, as indicated by the depletion pattern along Mn redox bars (Fig. 4.4b) and the absence of patterns along Fe redox bars, we assume that PS are responsible for selective Mn mobilization also under acid soil conditions present at the study site (pH 4.6, Table 4.1). In addition to this, it is known that plant roots radiate O_2 from the atmosphere towards the growing plant roots to oxygenate the immediate surroundings. The O_2 rich zones vary up to ~1 mm (Bezbaruah and Zhang 2004). Figure 4.4d gives an example of a Mn redox bar installed at plot B in June. We collected roots from the distinct depth and analyzed cross-sections of it (VHX-5000, Keyence, Osaka, Japan). Aerenchyma inside the plant roots (Fig. 4.4e; *Carex nigra*) promote the transfer of O_2 from the atmosphere, e.g. to detoxify the rhizosphere by oxidation of Mn^{2+} or other phytotoxins (Wheeler et al. 1985). The linear Mn oxide coatings clearly follow the root path, whereas reducing conditions and lack of O_2 facilitated complete or partial dissolution of the Mn oxide coating in the surroundings. The pattern is contrary to the described E_H gradient in Fig. 4.4a with decreasing O_2 contents and intensified reduction in the center of the spot. Overall, the formation of dissolution patterns of the Mn oxide coating caused by plant roots is possible and reported previously for Fe redox bars (Jenkinson and Franzmeier 2006).

Dark pigments along Fe redox bars indicate that SO_4^{2-} must have been reduced to S^{2-} to form iron monosulfide (FeS) coatings (Fig. 4.4f). Rabenhorst et al. (2010) discussed this process and demonstrated that the use of Fe oxide-coated tubes enables quantitative estimation of S^{2-} concentrations in marsh pore waters. We assume that the formation of dark coatings occurred from the reaction of gaseous hydrogen sulfide (H_2S) with the Fe hydroxide surface according to $2Fe(OH)_3(s) + 3H_2S(g) \rightarrow 2FeS(s) + 1/8S_8(s) + 6H_2O$ [2] (Davydov et al. 1998) rather than precipitation of S^{2-} from soil solution. This assumption is reasonable because (i) the FeS coatings in Fig. 4.4f (5 to 15 cm) were above the mean WT (–25 cm) in July at plot C and at points where no soil material adhered and the coating did not have contact with the soil directly. Furthermore, (ii) water droplets were found at the

Fe redox bar that might originate from water condensation above the WT and simultaneous precipitation of H_2S along the Fe oxide coating. Finally, (iii) organoleptic assessment of the Fe redox bar directly after retrieval revealed the unique H_2S smell. The soil pH of 4.4 at plot C (Table 4.1) would certainly push the species from S^{2-} to HS^- (pK_a 12.9) and further to H_2S (pK_a 7.0).

Conclusions

Characterization of the spatial and temporal distribution of soil reducing conditions is challenging but possible using $Mn^{III,IV}$ and Fe^{III} oxide-coated redox bars. In environments where soil hydrologic properties vary at field scale and water table fluctuations are present, Mn redox bars showed two to five times enhanced oxide removal compared to Fe redox bars, in accordance with the thermodynamic stability of the applied minerals. Especially in the capillary fringe, Mn reduction was favorable compared to only minor depletion patterns along Fe redox bars. The spatial variability of E_H in soils from oxidizing to strongly reducing soil conditions at very short scale (< 1 cm) was apparent as Fe^{III} oxide precipitation coincided with regions of Mn oxide reduction, indicating weakly reducing conditions persisted under ambient field conditions. Areas of Fe precipitates differed remarkably because of differences in color, and were closely related to parts along the bar where the Mn oxide coating remained, and parts where neither Mn nor Fe oxide remained. Hence, differentiation between the redox ranges of weakly ($Mn^{III,IV}$ oxide reduction) and moderately (Fe^{III} oxide reduction) reducing soil conditions is possible, but care must be taken when reductants like Fe^{2+} are abundant in soil solution. To delineate the soil redox status, the use of each of three Mn and Fe redox bars yielded good results, as evidenced by a low standard deviation of the percentage oxide removal (< 5%). However, when soil temperatures are high and changes of soil water content rapidly a surplus of up to five redox bars seems reasonable.

Acknowledgments

This study was financially supported by *Verein der Freunde und Förderer der Universität zu Köln*. Additionally, we are grateful to the Duke of Croy and Thomas Seine, who enabled the field measurements along the study site.

References

Bezbaruah AN, Zhang TC (2004) pH, redox, and oxygen microprofiles in rhizosphere of bulrush (Scirpus validus) in a constructed wetland treating municipal wastewater. Biotechnol and Bioeng 88:60–70. doi: 10.1002/bit.20208

Bormann H, Diekkrüger B, Richter O (1996) Effects of data availability on estimation of evapotranspiration. Phys Chem Earth 21:171–175. doi: 10.1016/S0079-1946(97)85580-2

Castenson KL, Rabenhorst MC (2006) Indicator of reduction in soil (IRIS): evaluation of a new approach for assessing reduced conditions in soil. Soil Sci Soc Am J 70:1222–1226. doi: 10.2136/sssaj2005.0130

Chapelle FH, McMahon PB, Dubrovsky NM, Fujii RF, Oaksford ET, Vroblesky DA (1995) Deducing the distribution of terminal electron-accepting processes in hydrologically diverse groundwater systems. Water Resour Res 31:359–371. doi: 10.1029/94WR02525

Childs CW (1981) Field-tests for ferrous iron and ferric-organic complexes (on exchange sites or in water soluble forms) in soils. Aust J Soil Res 19:175–180. doi: 10.1071/SR9810175

Davydov A, Chuang KT, Sanger AR (1998) Mechanism of H_2S oxidation by ferric oxide and hydroxide surfaces. The Journal of Physical Chemistry 102:4745–4752 doi: 10.1021/jp980361p

Dorau K, Mansfeldt T (2015) Manganese-oxide–coated redox bars as an indicator of reducing conditions in soils. J Environ Qual 44:696–703. doi:10.2134/jeq2014.03.0140

Della Puppa K, Momarek M, Bordas F, Bollinger JC, Joussein E (2013) Adsorption of copper, cadmium, lead and zinc onto a synthetic manganese oxide. J Colloid Interface Sci 399:99–106. doi: 10.1016/j.jcis.2013.02.029

Fakih M, Davranche M, Dia A, Nowack B, Petitjean P, Chatellier X, Gruau G (2008) A new tool for in situ monitoring of Fe-mobilization in soils. Appl Geoch 23:3372–3383. doi: 10.1016/j.apgeochem.2008.07.016

Fiedler S, Vepraskas MJ, Richardson JL (2007) Soil redox potential: importance, field measurements, and observations. In: Sparks DL (ed) Advances in Agronomy. Elsevier Academic Press Inc, San Diego, pp 1-54

IUSS Working Group WRB, 2006. World reference base for soil resources. World Soil Resources Reports No. 103, FAO, Rome.

Jenkinson BJ, Franzmeier DP (2006) Development and evaluation of iron-coated tubes that indicate reduction in soils. Soil Sci Soc Am J 70:183–191. doi: 10.2136/sssaj2004.0323

Kirk G (2004) The biogeochemistry of submerged soils. John Wiley & Sons, Hoboken

Mansfeldt T, Overesch M (2013) Arsenic mobility and speciation in a Gleysol with petrogleyic properties: a field and laboratory approach. J Environ Qual 42:1130–1141. doi: 10.2134/jeq2012.0225

Ottow JCG (2011) Microbiology of soils. Springer, Heidelberg

Owens PR, Wilding LP, Miller WM, Griffin RW (2008) Using iron metal rods to infer oxygen status in seasonally saturated soils. Catena 73:197–203. doi: 10.1016/j.catena.2007.07.009

Patrick WH, Gambrell RZ, Faulkner SP (1996) Redox measurements of soils. In: Sparks DL et al. (eds) Methods of soil analysis: chemical methods part 3. Soil Science Society of America and American Society of Agronomy, Madison, pp 1255–1273

Ponnamperuma FN (1972) The Chemistry of Submerged Soils. Adv Agron 24:29–96. doi:10.1016/S0065-2113(08)60633-1

Rabenhorst MC, Castenson KL (2005) Temperature effects on iron reduction in a hydric soil. Soil Sci 170:734–742. doi: 10.1097/01.ss.0000185908.26083.53

Rabenhorst MC (2010) Visual assessment of IRIS tubes in field testing for soil reduction. Wetlands 30:847–852. doi: 10.1007/s13157-010-0098-7

Rabenhorst MC, Megonigal JP, Keller J (2010) Synthetic iron oxides for documenting sulfide in marsh pore water. Soil Sci Soc Am J 74:1383–1388. doi:10.2136/sssaj2009.0435

Reddy KR, DeLaune RD (2008) Biogeochemistry of wetlands: science and applications. CRC Press, Boca Raton

Ringrose-Voase AJ, Humphreys GS (1993) Soil micromorphology: studies in management and genesis. Developments in Soil Science, 22. Elsevier, Amsterdam

Römheld V (1991) The role of phytosiderophores in acquisition of iron and other micronutrients in graminaceous species: an ecological approach. Plant Soil 130:127–134 doi: 10.1007/BF00011867

Schlesinger WH, Emily SB (2013) Biogeochemistry: an analysis of global change. 3rd edn. Academic Press, Amsterdam

Scott MJ, Morgan JJ (1990) Energetics and conservative properties of redox systems. In: American Chemical Society (ed) Chemical modeling of aqueous systems II. ACS Symposium Series, pp 368–378.

Smith KA (1980) A model of the extent of anaerobic zones in aggregated soils, and its potential application to estimates of denitrification. J Soil Sci 31:263–277. doi: WOS:A1980KB99200008

Stiles CA, Dunkinson ET, Ping CL, Kidd J (2010) Initial field installation of manganese indicators of reduction in soils, Brooks Range, Alaska. Soil Survey Horizons 51:102–107.

Treeby M, Marschner H, Römheld V (1989) Mobilization of iron and other micronutrient cations from a calcareous soil by plant-borne, microbial, and synthetic metal chelators. Plant Soil 114:217–226 doi: 10.1007/BF02220801

Wheeler BD, Al-Farraj MM, Cook RED (1985) Iron toxicity to plants in base-rich wetlands: comparative effect on the distribution and growth of Epilobium Hirsutum L. and Juncus Subnodulosus Schrank. New Phytologist 100:653–669. doi:10.1111/ j.1469-8137.1985.tb02810.x

Yu K, Patrick WH (2004) Redox window with minimum global warming potential contribution from rice soils. Soil Sci Soc Am J 68:2086–2091. doi: 10.2136/sssaj2004.2086

Chapter 5 Manganese and iron oxide-coated redox bars as a tool to in situ study the element sorption in wet soils

Journal of Soils and Sediments (2016) 16(3): 976–986

Co-author: Tim Mansfeldt

Formatting and orthography of the manuscript is adapted to the dissertation style.

Abstract

Purpose When studying redox conditions in soils with manganese (Mn) and iron (Fe) oxide-coated redox bars, we observed the formation of Fe oxides along the Mn oxide coating and assumed sorption of other elements from soil solution to oxide surface. The objective of this study was to investigate the formation of Fe oxides along Mn redox bars and to analyze element sorption from soil solution to either Mn or Fe oxide along redox bar coatings.

Materials and methods We protruded Mn redox bars into solutions with defined Fe^{2+} concentrations and removed the bars at distinct time intervals. The Mn oxide coating and potential Fe oxides were extracted using dithionite-citrate-bicarbonate (DCB). To investigate *in situ* element sorption behavior, we used previously field-installed redox bars, protruding these Mn redox bars into acidified hydroxylamine hydrochloride (AAH) to selectively extract Mn oxide and afterwards into DCB to dissolve the remaining Fe oxide coating. This two-step extraction procedure enabled the differentiation of elements bonded to either Mn or Fe oxide. Additionally, we analyzed the redox bar coatings at a very small scale (< 1 mm^2) via energy-dispersive X-ray spectroscopy (EDX).

Results and discussion Iron oxides precipitated along the Mn oxide coating at low concentrations of 0.05 mg Fe^{2+} L^{-1}, but did not trigger a color change. Although a change in color did occur instantaneously at 500 mg Fe^{2+} L^{-1}, it is expected that Fe^{2+} concentrations are significantly lower under field conditions because ferrous Fe auto-oxidized within the artificial setup. Whereas Mn oxide sorbed cationic elements from the soil solution in the order Cu > Pb > Zn, Fe oxide preferentially sorbed oxyanions with As > P > Mo > V, respectively. “Field”-Fe oxides precipitating along the Mn redox bars sorbed elevated levels of As and P compared with the action of synthesized “lab”-Fe oxides along Fe redox bars, a finding which we attribute to short-range-ordered Fe phases with elevated sorption capacity.

Conclusions Besides providing information regarding the monitoring of soil redox status, the developed sequential two-step extraction procedure enables the differentiation of the selective sorption of elements in the soil solution to the coating of Mn and Fe redox bars. The collection of Fe oxides formed naturally along the Mn redox bar coatings further enables the investigation of temporally and spatially diverse Fe oxide-forming processes.

Keywords Ferrous iron, Iron oxide, Manganese oxide, Metal element sorption, Redox conditions

Introduction

The characterization of soil redox status is of great importance because different pedogenetic responses are triggered under oxidizing or reducing soil conditions. In soil environments in which oxygen (O_2) is scarce (e.g., due to groundwater or perched water tables), manganese ($Mn^{III,IV}$) and iron (Fe^{III}) oxides are important soil constituents because both minerals participate in reversible electron transfer reactions and are able to take up electrons released by the microbially mediated oxidation of reduced carbon (C) occurring in the soil organic matter pool (Ottow 2011). Whereas the transformation of $Mn^{III,IV}$ oxide to Mn^{2+} takes place at redox potentials (E_H) as high as 500 mV at pH 5 (Gotoh and Patrick 1972), critical E_H values for Fe^{III} reduction have been recorded at 300 mV (Gotoh and Patrick 1974). Overall, a lowering of E_H will result in enhanced Mn and Fe reduction rates (Atta et al. 1996) and furthermore, to the potential mobilization of trace elements bonded to the oxide surface.

One tool developed to test whether a soil is in a reduced state is the Indicator of Reduction in Soils (IRIS) (Jenkinson and Franzmeier 2006), in which synthesized Fe oxides consisting of ferrihydrite and goethite are coated on polyvinyl chloride (PVC) bars and installed in the soil for a defined period. In the absence of O_2, the coating reductively dissolves, with the depletion patterns visually assessed to delineate soil reducing conditions. Dorau and Mansfeldt (2015) adapted this method, coating PVC bars with synthesized Mn oxide consisting of birnessite (hereafter referred to as Mn and Fe redox bars or redox bars in general). Field monitoring of soil redox status was performed at a study site characterized by elevated concentrations of Fe and arsenic (As) in the groundwater, originating from the weathering of fossil bog Fe (Mansfeldt and Overesch 2013). The manganese redox bars proved their better suitability for the identification of reducing soil conditions, with oxide removal two to five times greater than that achieved using Fe redox bars (Dorau et al. 2015). Furthermore, sections of the Mn redox bar surfaces differed remarkably in color from the original dark brown Mn oxide coating. Chemical extraction using dithionite-citrate-bicarbonate(DCB) (Mehra and Jackson 1960) combined with elemental analysis of a previously installed bar revealed precipitated Fe to be the cause for this change in color. The presence of Fe^{2+} in soil solution mediates a non-enzymatic redox reaction that favors the dissolution of the Mn oxide coating. According to the reaction

$$MnO_2 + 2Fe^{2+} + 4H_2O \rightarrow Mn^{2+} + 2Fe(OH)_3 + 2H^+ \quad [1]$$

Fe^{2+} acts as a reductant that is oxidized to Fe^{3+} and hydrolyzes along the Mn oxide coating. In turn, Mn^{2+} is released from the surface, with *in situ* formed Fe oxides remaining as a durable coating (Dorau and Mansfeldt 2015). Along with the precipitated Fe oxides, we

also hypothesized that As and other elements would be detectable in the extracts. Thus far, no study has investigated the sorption behavior of distinct elements to either the Mn or Fe oxide coating on redox bars.

In aerobic soil environments, $Mn^{III,IV}$ and Fe^{III} (hydr)oxides are known to sorb and minimize the solubility of a variety of elements, for example, As (Manning and Goldberg 1997; Nesbitt et al. 1998), chromium (Cr) (Ajouyed et al. 2010; Bradl 2004; Rai et al. 1989; Zachara et al. 1987), copper (Cu) (Abd-Elfattah and Wada 1981), molybdenum (Mo) (Hooda 2010), nickel (Ni) (Arai 2008), phosphorus (P) (Peretyazhko and Sposito 2005), lead (Pb) (Abd-Elfattah and Wada 1981; Hooda 2010), vanadium (V) (Hooda 2010), and zinc (Zn) (Roberts et al. 2002; Scheinost et al. 2002). Variations in the mineral structure of birnessite (a common Mn oxide in soils), as well as ferrihydrite and goethite (prominent Fe oxides in soils), cause bonding mechanisms to differ between less reversible inner-sphere surface complexes and rather weakly bonded outer sphere surface complexes, with soil pH altering the element-specific pH adsorption edge (Bradl 2004). The linkage between the liberation of distinct trace metals into the soil solution under weakly reducing ($Mn^{III,IV}$ reduction; E_H 400 to 200 mV at pH 7) and moderately reducing soil conditions (Fe^{III} reduction; E_H 200 to −100 mV at pH 7) was recently shown in microcosm experiments (Hindersmann and Mansfeldt 2014). These findings also highlighted that Mn and Fe oxides selectively sorb distinct trace metals from soil solution. However, it should be noted that (i) the E_H controls the speciation of some trace elements via electron transfer reactions (e.g., As) (Smedley and Kinniburgh 2002; Mansfeldt and Overesch 2013), (ii) dissolved organic matter (DOM) is able to sequester certain trace metals (e.g., Pb) (Adriano 2001), and (iii) sulfide (S^{2-}) in soil solution forms sparingly soluble trace metal-sulfide phases (e.g., CdS, PbS, and ZnS) (Morse and Luther 1999). Hence, various soil processes and properties alter the mobilization of trace metals and a universal concept is impossible to apply. Moreover, information regarding the *in situ* soil-surface chemistry of Mn and Fe oxides is difficult to obtain because major restrictions prevail when separating pure oxides from bulk soil. Rennert et al. (2013) developed a device with which to collect freshly precipitated Fe oxides without producing physical or chemical artifacts during sampling. Issues related to soil-mineral formation, e.g., redox-induced Fe oxide aging (Thompson et al. 2006) or interactions between Fe oxides and DOM, can be studied by applying microscopic and spectroscopic techniques (Rennert et al. 2013).

The objectives of this article were (i) to improve the understanding of Fe precipitation and the formation of Fe oxide along Mn redox bars, (ii) to investigate the sorption of various elements from the soil solution to either Mn or Fe oxide along the redox bar coating, using

a selective chemical extraction procedure, and (iii) to analyze the Mn and Fe oxide coatings at a very small scale via energy-dispersive X-ray spectroscopy (EDX).

Materials and Methods

Study site

The monitoring site is in the district of Recklinghausen, North Rhine-Westphalia, Germany (51° 48′ 59″ N, 7° 12′ 59″ E). Water table (WT) depths across the study site range from ponding surface water to 1 m below ground at small scale, reflecting the action of glaciofluvial processes that produced a micro-relief (47.6 to 49.0 m asl) segregating elevated dry sites from flooded sites in lower terrain.

Field monitoring

The manufacturing process for the Mn redox bars is presented in detail in Dorau and Mansfeldt (2015) and that for the Fe redox bars in Jenkinson and Franzmeier (2006) and Castenson and Rabenhorst (2006). Three Mn and three Fe redox bars 60 cm in length and with the lower 50 cm coated, were installed in a flooded plot in lower terrain where water was periodically ponding. At this site, Fe oxide formation was favorable because Fe^{2+} was abundant in the soil solution (plot C in Dorau and Mansfeldt 2015); we also assumed that the potential sorption of distinct elements to the oxide coating would be detectable by the selected analytical methods. We removed the redox bars on a monthly basis from March to July 2013. Environmental monitoring comprised measurement of WT depths (PDLR 70, EcoTech, Bonn, Germany); soil temperature (temperature lance with RS 485 interface, UIT, Dresden, Germany); and oxide removal along redox bars. A detailed description of soil properties and site specific characteristics is presented in Mansfeldt et al. (2012).

Elemental analysis

Disturbed soil samples were taken from an excavation pit at the designated plot from 0 to 25 cm and from 25 to 50 cm depth. Soil sampling was not carried out genetically based on soil horizons but followed the analytical procedure of elements bonded to the upper (0 to 25 cm) and lower (25 to 50 cm) sections of redox bar coatings. The obtained soil samples were oven dried at 40 °C, sieved < 2 mm, and homogenized, with subsamples then pulverized in a mixer mill (MM400, Retsch, Haan, Germany) to determine total element concentrations. Pseudo-total concentrations of As, Cr, Cu, Mo, Ni, Pb, V, and Zn were measured via inductively coupled plasma mass spectrometry (ICP-MS) (XSeries 2, Thermo Scientific, Waltham, USA), and those of Fe, Mn, and P via optical emission spectroscopy (ICP-OES) (ULTIMA 2, Horiba Scientific, Unterhaching, Germany) in an inverse aqua regia

digestion solution (2 mL concentrated HCl and 6 mL concentrated HNO_3, 200 mg sample weight).

Fe precipitation along Mn redox bars

As outlined in Dorau and Mansfeldt (2015), the presence of Fe^{2+} in the soil solution is responsible for the non-enzymatic reductive dissolution of the Mn oxide coating. To prove the reaction kinetics of this abiotic process and to investigate possible color changes, we protruded three Mn redox bars of 8 cm length into 20-mL solutions containing 0.05, 5, and 500 mg Fe^{2+} L^{-1}, removing one bar from each solution after 1, 15, and 30 days. The concentration of 5 mg Fe^{2+} L^{-1} approximates the upper limit of divalent Fe found in the soil solution at the study site (Mansfeldt and Overesch 2013), while the 30-day limit is equal to the installation time of redox bars during monitoring. Additionally, we performed a run with 100 mg Fe^{2+} L^{-1} at shorter intervals of 1, 2, 4, 8, 16, and 24 h. After removing the redox bars from the solutions and prior to their dry storage, we rinsed the bars with deionized water to remove any adhering solution containing Fe^{2+}. As the pH of the $FeCl_2$ solution varied depending on the Fe^{2+} concentration, all solutions were standardized to the pH conditions found at the study site (pH 4.5), with sodium hydroxide (0.1 M NaOH) and nitric acid (0.1 M HNO_3) used to increase and decrease solutions to the desired pH, respectively. After removing the redox bars, the pH of the solution was measured again. To establish whether Fe precipitated along the Mn oxide coating, we protruded the bars into 50 mL vials and performed a DCB extraction (Mehra and Jackson 1960). This extracting agent simultaneously dissolves both Mn and Fe oxides in soils. Afterwards the solution was analyzed for total Mn and Fe concentrations via flame atomic absorption spectroscopy (F-AAS) (iCE 3000 series, Thermo Scientific,Waltham, USA). The experiment was performed in duplicate repetition.

Sorption characteristics of redox bars for various elements

We performed a two-step extraction procedure to differentiate elements sorbed to either Mn or Fe oxide along the redox bar surface. In this analysis, we first cut two Mn and two Fe redox bars (the 50-cm coated surface) per month into 8.33-cm PVC sections. We investigated the elemental composition of the redox bar coating for both the topsoil (0 to 25 cm; upper three sections) and subsoil (25 to 50 cm; lower three sections), along with soil characterization. For this purpose, redox bar sections were protruded for 10 min into 50-mL vials 10 cm in height (2.5 cm Ø) and containing 25 mL of extracting agent; the complete surface of each section was in contact with the solution. To investigate elements bonded to Mn oxide, we used acidified hydroxylamine hydrochloride solution (AAH; 0.1 M $HONH_2 \cdot HCl$ in 0.01 M HNO_3, pH 2), which selectively extracts Mn oxides in soils (Chao

1972) and dissolves the Mn oxide coating within minutes (Dorau and Mansfeldt 2015). The residual Fe oxide coating and elements bonded to it were extracted using DCB (Mehra and Jackson 1960). Manganese redox bars were thus sequentially treated with AAH and DCB, and Fe redox bars only with DCB. Total concentrations of As, Cr, Cu, Mo, Ni, Pb, V, and Zn were determined via ICP-MS, and those of Fe, Mn, and P via ICP-OES; these values were then converted to extractable element contents. To characterize the sorption behavior of elements bonded to either Mn or Fe oxide, we calculated the quotient between the mean AAH-extractable (assumed to bond to Mn oxide) and DCB-extractable element contents (assumed to bond to Fe oxide) exclusively for Mn redox bars. The final dataset also included two replicates each for the top and bottom of the Mn redox bars for the 5-month period (n = 20).

EDX analysis of redox bars

We used a scanning electron microscope (SEM) (NEON 40, Zeiss, Jena, Germany) at 15 keV accelerating voltage equipped with an EDX detector (Dry Cool, Oxford instruments, Abingdon, UK) to analyze the element contents of redox bar coatings at a very small scale (~1 mm^2). This approach was employed in order to address a scaling problem, because chemical extraction integrated the elemental content of 16,493 mm^2, equal to 25 cm of coated PVC surface, according to the employed methodological setup. In contrast, for SEM investigations, smaller sample dimensions are required and thus the bars were prepared in the following way: Each previously field-installed Mn and Fe redox bar served as an example, and was first cut lengthwise into 1-cm sections and then crosswise to obtain plastic chips ~4 mm in height. We also analyzed an uncoated PVC chip as a reference in order to exclude any elements incorporated into the plastic material. For SEM investigations, sample surfaces must be electrically conductive and hence the plastic chips were coated with a 15-nm-thick layer of C prior to analysis (K950X, EMITECH, Ashford, UK).

Results and Discussion

Fe precipitation along Mn redox bars

Figure 5.1 shows the DCB-extractable Fe contents recorded along Mn redox bars protruded into solutions of different Fe^{2+} concentration (a) and the corresponding pH values of these solutions (b) at distinct time intervals, and Fig. 5.2 illustrates the corresponding color of the Mn oxide coatings after removing the Mn redox bars from the Fe^{2+}-containing solutions. A steady increase in DCB-extractable Fe content was observed in the experiment with the 100 mg Fe^{2+} L^{-1} solution, which reached a steady state and stagnated after 24 h of reaction. These findings indicate the fast reaction kinetics of Fe^{2+} (reductant) with

the Mn oxide coating (oxidant), and are coherent with data published by Golden et al. (1986). The latter authors reported increased Mn^{2+} concentrations in the solution phase resulting from the reduction of $Mn^{III,IV}$ oxides in the presence of Fe^{2+}, also proposing that Fe^{2+} oxidized to Fe^{3+} in turn hydrolyzes in a further step to form Fe^{III} oxides according to Eq. (1).

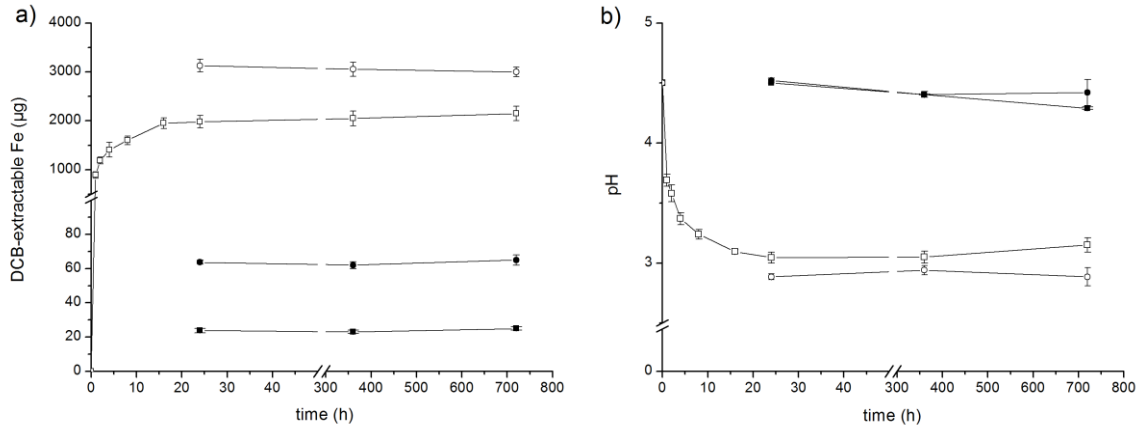

Figure 5.1 Dithionite-citrate-bicarbonate (DCB) extractable Fe content of Mn redox bars in duplicate protruded into $FeCl_2$-solution containing 0.05 (black squares), 5 (*black circles*), 100 (*white squares*), and 500 (*white circles*) mg Fe^{2+} L^{-1} at defined time intervals (a), and pH of the corresponding solutions after bar removal (b). *Error bars* represent the standard deviation.

Presumably, the pseudomorphic Fe precipitates are composed of ferrihydrite or feroxyhite, which progressively transform into goethite (Golden et al. 1986). As the oxidation of ferrous Fe is a proton-producing process, pH values at 100 and 500 mg Fe^{2+} L^{-1} fell rapidly from pH 4.5 at the beginning of the experiment to pH 3.1 and 2.9, respectively, at the end of the experiment (Fig. 5.1b). The release of H^+ due to the adsorption of Fe^{2+} and Fe^{3+} is also partly responsible for the pH drop. No decrease and only an insignificant pH decline occurred at 0.05 and 5 mg Fe^{2+} L^{-1}, respectively. Although according to *Le Chatelier's* principle, low pH values in a system tend to push the reaction to the left side of Eq. (1), with the formation of Fe oxides along Mn redox bars thus more favorable at sites with neutral soil, this was not the case in the present study. Elevated concentrations of Fe^{2+} in a solution resulted in enhanced Fe oxide formation along the Mn oxide coating, with 23, 63, 2000, and 3100 µg DCB-extractable Fe recorded at 0.05, 5, 100, and 500 mg Fe^{2+} L^{-1}, respectively (Fig. 5.1a). At 5 mg Fe^{2+} L^{-1}, which approximates concentrations found in the soil solution at the study site (Mansfeldt and Overesch 2013), oxidation and hydrolysis of Fe along the Mn oxide coating obviously occurred (63 µg Fe could be extracted by DCB) but without favoring a change in coating color (Fig. 5.2).

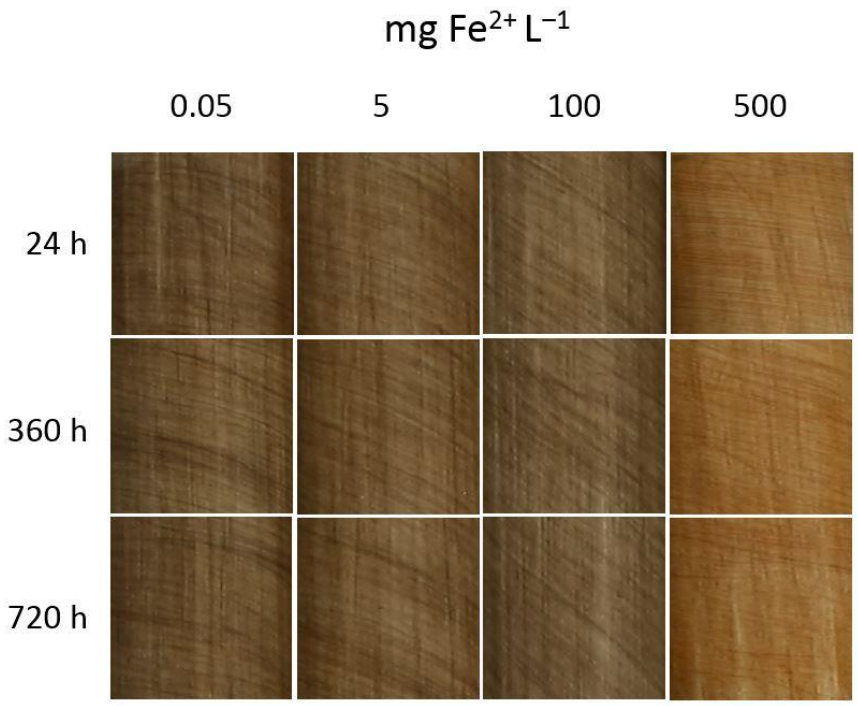

Figure 5.2 Images of Mn redox bars protruded into $FeCl_2$-solutions of varying Fe^{2+} concentration after defined time intervals.

Indeed, concentrations of at least 500 mg Fe^{2+} L^{-1} were necessary to obtain a significant change in the color of the original dark brown Mn oxide coating to a light orange Fe oxide coating (Fig. 5.2). After a protruding time of 30 days in the 500 mg Fe^{2+} L^{-1} solution, only a minor Mn content of 73 µg remained along the 8-cm long redox bar, a figure which is significantly lower than the average of 740 µg Mn present directly after bar manufacture. Due to the non-uniform application procedure, Mn contents ranged from 500 to 2200 µg Mn. Assuming 500 µg Mn to be the upper and 2200 µg Mn to be the lower limit, Fe^{2+} contents of 1020 to 4470 µg Fe^{2+} (according to Eq. (1)) would have been required to completely dissolve the Mn oxide coating, which corresponds to 51 to 224 mg Fe^{2+} L^{-1}. According to the stoichiometric calculation, a change of color should have occurred below 500 mg Fe^{2+} L^{-1}; indeed, field observations highlighted that Fe oxides formed at significantly lower concentrations (see Fig. 5.3).

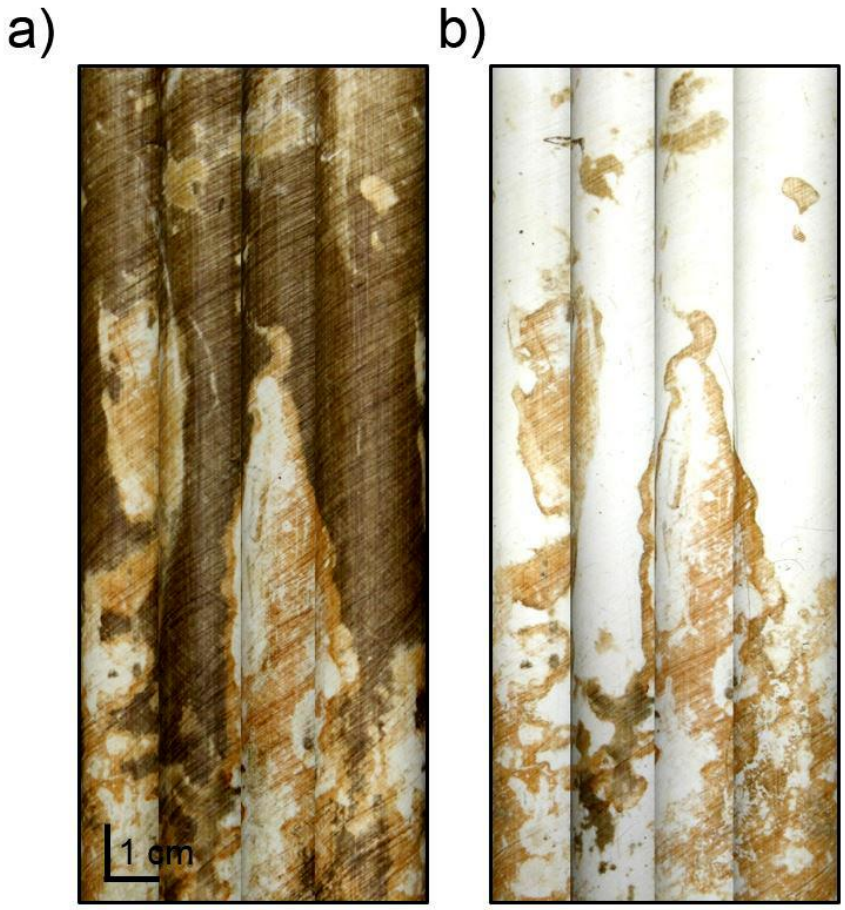

Figure 5.3 Image of a Mn redox bar before (a) and after (b) protrusion into acidified hydroxylamine hydrochloride (AAH) solution for 10 min

What might be the reason for this discrepancy? Under natural conditions, the capillary rise of Fe^{2+}-rich shallow groundwater ensured a constant supply of the reductant into the top-soil for a period of 30 days, considerably different from the artificial setup in the laboratory, in which Fe^{2+} concentrations in the solution were presumably auto-oxidized (by O_2) within 24 h. This pH-dependent step has been reported to take place from < 1 min to hours (Kosman 2013) and provides the most suitable explanation of the observed incongruity.

Another important observation made during the experiment was that tri- and tetravalent manganese as an oxidant for Fe^{2+} is an essential precursor to the formation of a durable Fe oxide coating along the PVC surface. This assumption is interesting, because we neither observed Fe precipitates along uncoated PVC bars protruded into solutions of various Fe^{2+} concentrations, nor along uncoated PVC bars installed during the monitoring campaign.

Extractable element contents along redox bars

Figure 5.3 shows an Mn redox bar before and after protrusion into AAH solution for 10 min. The original dark brown Mn oxide coating (Fig. 5.3a) dissolved instantaneously, showing the white PVC surface underneath (Fig. 5.3b). Boundaries of the remaining Fe oxides were easy to identify. Hence, it is possible to differentiate and analyze elements potentially bonded to either Mn or Fe oxide along the Mn redox bar surface using a selective chemical extraction procedure.

Figure 5.4 illustrates the mean contents of various elements bonded to synthesized Mn oxides (AAH-extractable; Fig. 5.4a), to Fe oxides naturally precipitated along Mn redox bars (DCB-extractable; Fig. 5.4b), and elements bonded to synthesized Fe oxides along Fe redox bars (DCB-extractable; Fig. 5.4c). For reasons of simplicity and further discussion, *in situ* formed Fe oxides are termed “field”-Fe oxides, and those used for the manufacture of Fe redox bars as “lab”-Fe oxides. Along Mn redox bars, Mn was the major AAH-extractable element, at 1.84 µM. In accordance with the percentage oxide removal determined via digital analysis (Dorau et al. 2015), the highest levels of Mn were found in July (10.38 µM) when the WT was low, favoring aerobic conditions and no reductive dissolution of the coating, and lowest in June (0.02 µM) when reducing conditions were intensified. Iron was the main adsorbate for Mn oxide, followed by elements in the following order: Zn > P > Cr > Cu > As > V > Pb > Ni > Mo (Fig. 5.4a). A positive and highly significant relationship between Mn and element content was found for Pb (r = 0.751***), V (r = 0.730***), and Mo (r = 0.682***), while a weaker relationship was found for Zn (r = 0.401*); no statistically significant relationship was present for the other elements (Table 5.1).

Table 5.1 Spearman correlation coefficient (r) (n = 20) between various elements and both acidified hydroxylamine hydrochloride (AHH) extractable Mn and dithionite-citrate-bicarbonate (DCB) extractable Fe content along Mn and Fe redox bars.

Redox bars				As	Cr	Cu	Mo	Ni	P	Pb	V	Zn
Mn	AAH	Mn	r	-0.143	0.060	0.190	0.682	0.283	-0.027	0.751	0.730	0.401
			p	0.548	0.801	0.421	<0.001	0.227	0.910	<0.001	<0.001	0.080
	DCB	Fe	r	0.941	-0.046	0.056	-0.138	0.361	0.789	0.179	-0.174	0.117
			p	<0.001	0.845	0.814	0.560	0.117	<0.001	0.450	0.462	0.622
Fe	DCB	Fe	r	0.678	0.309	-0.215	0.523	0.920	0.819	0.218	0.749	0.663
			p	<0.001	0.183	0.361	0.017	<0.001	<0.001	0.356	<0.001	<0.001

The sink function of Mn oxides has been reported for Pb (McKenzie 1980), Mo (Barling and Anbar 2004), Zn (Komárek et al. 2013), and V (Takematsu et al. 1985; Yin et al. 2015). Matern and Mansfeldt (2015) demonstrated the strong effect of molybdate (MoO_4^{2-}) adsorption onto the surface of a synthetic birnessite. The synthesis of birnessite in this latter

study is equivalent to the procedure employed here for the manufacture of the Mn redox bars, with the correlation indicating the coherence between laboratory batch experiments (Matern and Mansfeldt 2015) and the present field experiments. Manganese oxides have been also identified as the most efficient stabilizing agent for Cu, Co, Cd, and Zn (Komárek et al. 2013). However, concurrency of sorption sites along the Mn oxide coating and the presence of DOM are only two possible factors that could result in weak correlation with Cu and Zn (Table 5.1). Han et al. (2006) confirmed the presence of competitive adsorption and found a decrease in Cu adsorption in the presence of Pb ions. When retrieving the redox bars from the soil, organoleptic assessment revealed the unique smell of H_2S; metal precipitation with S^{2-} is therefore an additional process that may cause inconsistent sorption of elements from the soil solution to the redox bar coatings. However, the stronger correlation between Mn oxide and Pb compared to that between Mn oxide and Cu (Table 5.1) indicates a stronger affinity for Pb sorption onto Mn oxide surfaces. These results are in agreement with data by Feng et al. (2007).

Visual assessment of Mn redox bars revealed zones of field-Fe oxides along the PVC surface, an observation in agreement with the content of the DCB extracts. Indeed, Fe was the main DCB-extractable element, at 4.97 µM (Fig. 5.4b). The content of adsorbate bonded to Fe oxide followed the order P > As > Mn > Zn > V > Cr > Ni > Pb > Mo > Cu (Fig. 4b). Among these elements, As (r = 0.941***) and P (r = 0.789***) exhibited a strong relationship with extractable Fe (Table 5.1), with both elements showing very strong sorption characteristics probably forming an inner-sphere bidentate binuclear complex (Manning and Goldberg 1997) with the Fe^{III} oxide surface. The DCB-extractable element composition of lab-Fe oxides (Fig. 5.4c) revealed similar sorption behavior to that of field-Fe oxides (Fig. 5.4b). Nevertheless, the iron content of 5.90 µM was slightly higher than the 4.97 µM Fe found along Mn redox bars, with minor differences also occurring in the order of adsorbate content: P > As > Zn > V > Mn > Cr > Ni > Mo > Pb > Cu (Fig. 5.4c). Nickel (r = 0.920***), P (r = 0.819***), V (r = 0.749***), As (r = 0.678***), and Zn (r = 0.663***) were strongly correlated, Mo (r = 0.523*) was slightly less correlated, and no statistically significant correlation was recorded for Cr, Cu, and Pb with Fe content along Fe redox bars (Table 5.1). The adsorption of Ni, Zn (Brümmer et al. 1988), V (Peacock and Sherman 2004), P (Strauss et al. 1997), As (Giménez et al. 2007), and Mo (Goldberg et al. 2009) to the surface of goethite minerals has been reported previously. The consistency of the applied Fe oxide minerals in the suspension used for Fe redox bar manufacture might explain the stronger correlation between many elements and lab-Fe oxides compared to field-Fe oxides. We characterized the initial Fe oxide suspension using both an oxalate (Fe_o) and a DCB (Fe_d) extraction. Whereas the former selectively extracts short-range-ordered and

nano-crystalline Fe phases (e.g., ferrihydrite, but also nano-goethite), the latter extracts all Fe oxides from soils. The Fe oxide suspension possessed a Fe_o/Fe_d ratio of 0.76, indicating that 76% was ferrihydrite and 24% goethite that remained stable when applied to the PVC bars (Rabenhorst et al. 2008). The defined goethite and ferrihydrite content of lab-Fe oxides is therefore a unique characteristic. Whereas the synthesis of Fe oxides is widespread and commonly adapted in the laboratory, the mechanisms involved in their formation under natural conditions are complex and diverse, leading to a broad range of *in situ* formed Fe oxides (Jolivet et al. 2004).

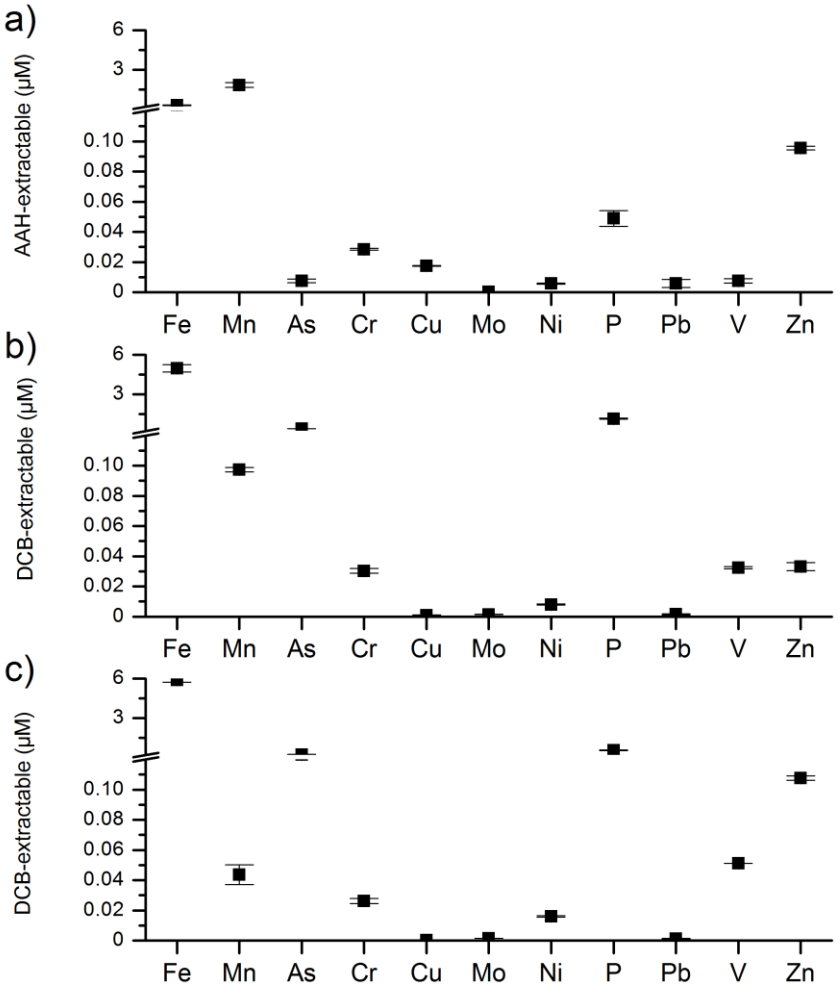

Figure 5.4 Acidified hydroxylamine hydrochloride (AAH) and dithionite-citrate-bicarbonate (DCB) extractable mean content of elements bonded to Mn oxide along Mn redox bars (a), to Fe oxides along Mn redox bars (b), and to Fe oxides along Fe redox bars (c). The averaged element contents include data covering the period from March to July for the top and bottom of Mn and Fe redox bars in duplicate (n = 20). Error bars represent the standard deviation.

At the study site, most of the *in situ* formed Fe^{III} oxides were composed of ferrihydrite (Mansfeldt et al. 2012). The key factor altering oxide form and crystallinity is the rate of

Fe^{2+} contribution to the initial nuclei and the rate of Fe^{2+} oxidation (Cornell and Schwertmann 2003; Wang et al. 2013a). Boundary conditions leading to characteristic pathways of Fe oxide formation include pH, concentration of Fe^{3+}, and temperature. Due to the presence of variable WT depths and water content changes in the capillary fringe, the hydraulic gradient varies and the supply of Fe^{2+} into the topsoil is not constant. Hence, the formation of Fe^{III} via redox reaction with the Mn oxide coating will also vary. Furthermore, soil temperature at the study site increased from 3.8 °C in March to 16.8 °C in July at 25-cm depth (Dorau and Mansfeldt 2015). It thus seems reasonable that variations in the mineral structure and further in the sorption capacity of field-Fe oxides resulted in the observed reduction in statistical correlation compared with the constant conditions experienced by lab-Fe oxides along Fe redox bars (Table 5.1).

Preference for element sorption to Mn or Fe oxides

We categorized quotients of mean AAH- to DCB-extractable element contents above 1.5 as indicating element preference for bonding to Mn oxide, values between 1.5 and 0.5 as indicating similar sorption behavior toward Mn and Fe oxides, and values below 0.5 as indicating a preference for bonding to Fe oxides (Table 5.2).

Table 5.2 Quotient between AAH-extractable and DCB-extractable element contents indicating element preference for sorption to Mn or "field"-Fe oxides along Mn redox bars. The averaged contents on a molar basis include data covering the period from March to July for the top and bottom of Mn redox bars in duplicate (*n = 20*), with the corresponding standard deviation.

As	Cr	Cu	Mo	Ni	P	Pb	V	Zn
0.02	0.94	19.7	0.16	0.72	0.04	3.6	0.23	2.9
±0.02	±0.87	±30.4	±0.16	±0.26	±0.09	±5.42	±0.30	±2.74

Manganese oxide was found to sorb 19.7 times more Cu and was associated with slightly elevated Pb (3.6) and Zn (2.9) content compared to field-Fe oxides, a result in agreement with numerous studies in the literature (reviewed by Komárek et al. 2013). Whereas chromium (0.94) and Ni (0.72) sorbed equally to Mn and Fe oxide surfaces, preferential sorption to Fe oxides was evident in the following order: As (0.02), P (0.04), Mo (0.16), and V (0.23). The latter elements occur as oxyanions in the soil solution under the assumed E_H-pH conditions of 400 mV (Mn and Fe oxides remain stable and play the role of adsorbents) and pH 4.5 (the soil pH at the study site). The high point of zero charge (PZC) of ferrihydrite (pH 7.9) and goethite (pH 9.7) favors functional group protonation under the acidic soil conditions present at the study site, in contrast to birnessite (pH 2.6). This enables oxyanions in the soil solution to be electrostatically bonded, e.g., to positively charged OH groups (Cornell and Schwertmann 2003; Bradl 2004). Although only a limited number of studies

have dealt with the role of Mn oxides as stabilizing amendments, successful element immobilization has been reported for Cu, Pb, and Zn (Della Puppa et al. 2013; Komárek et al. 2013), a finding that we can verify here in the sorption behavior of these predominantly cationic elements. Our results suggest that differences in the characteristics of the Mn and Fe oxide coatings (e.g., PZC, cation exchange capacity, and specific surface area) lead to selective sorption behavior for dissolved elements present in the soil solution to the redox bar coatings under field conditions.

Sorption capacities: field-Fe oxides versus lab-Fe oxides

The crystallinity of Fe oxides in soil varies widely from short-range-ordered to long-range-ordered phases due to changes in geochemical conditions in an open system, a process that is especially relevant for soils with changing redox conditions. This phenomenon was previously shown via an artificial setup in which biweekly soil redox oscillations from 200 to 700 mV led to an increase in Fe oxide crystallinity (Thompson et al. 2006). As these oxides are important interfaces for the sorption of dissolved elements in the soil solution, sorption capacity is also a function of crystallinity (Wang et al. 2013b).

Assuming ferrihydrite ($Fe_5HO_8 \cdot 4H_2O$) with a corresponding specific surface area of 200 $m^2\ g^{-1}$ (Cornell and Schwertmann 2003) to be the major Fe oxide along the Mn redox bar coating, the recorded DCB-extractable Fe contents of 1.97 to 17.05 µM Fe are equal to a total surface area of 0.19 to 1.64 m^2. Exclusively for Fe redox bars, the goethite (FeOOH) content of 24% in the initial Fe oxide suspension is considered to have a total surface area of 50 $m^2\ g^{-1}$ (Cornell and Schwertmann 2003), with the remaining 74% being ferrihydrite. This assumption yields total surface areas for lab-Fe oxides along Fe redox bars in the range of 0.12 to 0.90 m^2. Figure 5.5 shows the development of element loading for As (Fig. 5.5a) and P (Fig. 5.5b) on a hypothetical Fe oxide surface from March to July along Mn and Fe redox bars. These two elements are known to strongly sorb onto Fe oxides, and here were associated with the strongest correlation between DCB extractable field- and lab-Fe oxides (Table 5.1); hence, the two are suitable for the comparison of element loading between naturally formed and synthesized Fe oxides. Element loading under natural conditions can be considered “actual” sorption (AS). In contrast to this, potential sorption (PS) can be derived from laboratory batch experiments and is equivalent to the sorption capacity of a distinct mineral for an adsorbent. The AS values of As and P with respect to the Fe oxide surface varied throughout the study period, but were, in general, lower at the top than at the bottom of redox bars (Fig. 5.5a, b), a finding which we attribute to elevated As and P concentrations in the capillary fringe (Mansfeldt and Overesch 2013). Increased levels of As and P in the topsoil (Table 5.3) seem to play a minor role regarding sorption to the redox bar coating. Besides this, the top and bottom of

field-Fe oxides sorbed on average 0.69 µM As m^{-2} and 2.29 µM P m^{-2}, levels significantly higher than the 0.38 and 1.04 µM As and P m^{-2}, respectively, sorbed by lab-Fe oxides (Fig. 5.5a, b). Since goethite has lower sorption capacities for $H_2AsO_4^-$ and $H_2PO_4^-$ m^{-2} oxide surface (1.33 and 2.5 µM) compared to ferrihydrite (15.5 and 3.1 µM) (Borggaard 1983; Strauss et al. 1997; Raven et al. 1998; Giménez et al. 2007), we assume that *in situ*-formed Fe oxide phases are solely short-range-ordered. Considering the AS values recorded at the top and bottom of redox bars, field-Fe oxides sorbed on average 1.8 times more As and 2.2 times more P compared to lab-Fe oxides.

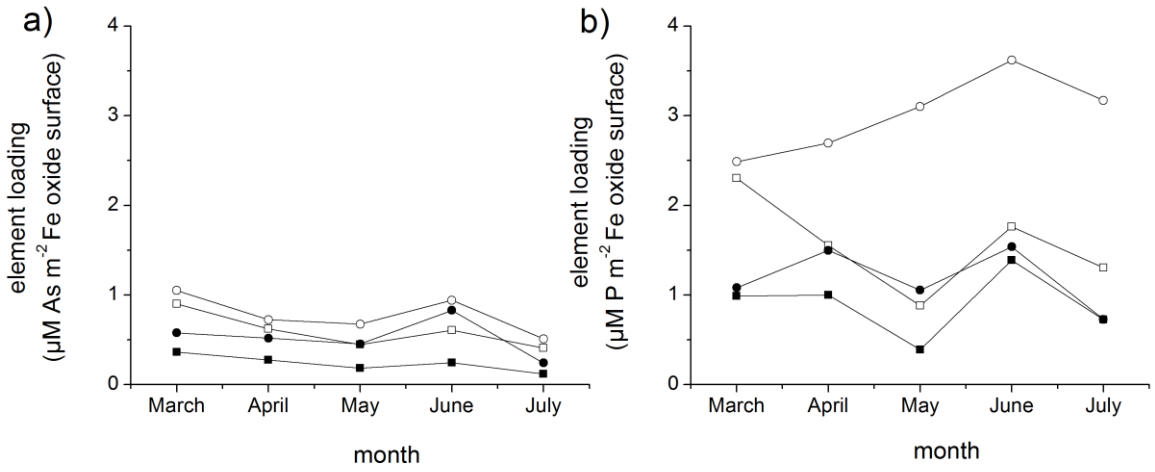

Figure 5.5 Element loading of field-Fe oxides along Mn redox bars (*open symbols*) and of lab-Fe oxides along Fe redox bars (solid symbols) with As (a) and P (b) for the top (*white squares*, *black squares*) and bottom (*white circles, black circles*) sections of previously installed redox bars, for the period from March to July. Dithionite-citrate-bicarbonate (DCB) extractable Fe contents were transformed to Fe oxide surfaces by assuming a ferrihydrite-(FH) formula of $Fe_5HO_8 \cdot 4H_2O$ and a goethite-(GT) formula of FeOOH with a corresponding surface area of 200 (50) m^2 g^{-1} FH (GT). We assume that field-Fe oxides are solely composed of FH while lab-Fe oxides are composed of 76% FH and 24% GT. The corresponding As and P contents are transformed to molarities.

It should be noted that the development of monthly element loading onto field- and lab-Fe oxides varied in magnitude, likely due to variations in As and P concentrations in the soil solution (Fig. 5.5). Mansfeldt et al. (2012) previously found high δ^{57}Fe values in the topsoil at the study site, caused by the rapid precipitation of ferrihydrite when Fe^{2+} was exposed to O_2. These findings underline the previous assumption and also that the goethite content of lab-Fe oxides seems to be responsible for the lower AS. Finally, a number of discrepancies were observed because the AS of field-Fe oxides with P (Fig. 5.5b) generally exceeded that with As (Fig. 5.5a). This contradicts the PS data reported in the literature, in which the adsorption capacity of ferrihydrite for As (Raven et al. 1998) is reported to exceed that for P (Borggaard 1983). Hence, differences are apparent between the PS results derived in laboratory batch experiments using synthesized minerals and those obtained in

the present study via the use of naturally formed minerals. Nevertheless, the AS values of field- and lab-Fe oxides are below the PS values reported in the literature, which supports the validity of studying the *in situ* sorption behavior of elements in wet soils using redox bars.

Table 5.3 Selected element content of the soil profile in which the redox bars were installed.

Depth	Fe	Mn	As	Cr	Cu	Mo	Ni	P	Pb	V	Zn
cm	($g\ kg^{-1}$)					($mg\ kg^{-1}$)					
0 to 25	47	160	111	52	159	0.7	14.0	1,184	78	115	159
25 to 50	23	300	30	19	29	0.3	7.3	619	3.9	45	29

Energy-dispersive X-ray spectroscopy of redox bars

Figure 5.6 shows typical color patterns observed on redox bars of the original Mn oxide coating (A), Fe precipitates (B), and complete oxide removal (C) along Mn redox bars (a), as well as of the partial depletion of Fe oxides (D), and the original Fe oxide coating (E) on Fe redox bars (b). The former color pattern displays an E_H gradient ranging from oxidizing soil conditions ($Mn^{III,IV}$ oxides remain stable, A) at the edge to strongly reducing soil conditions ($Mn^{III,IV}$ and Fe^{III} oxides are reduced, C) in the center. The partial depletion of Fe oxides (D) was often observed in combination with pale yellow zones reflecting the preferential dissolution of ferrihydrite over goethite (Rabenhorst et al. 2008). Energy-dispersive X-ray spectroscopy of the uncoated PVC chip revealed 11% O, 81% Cl, and no incorporation of Mn and Fe within the plastic material (Table 5.4). As Cl is the major component of the polymer material and the penetration depth of the emitted electrons is approximately 15 µm, we analyzed the Cl content of samples A to E, with background values ranging from 35 to 71%.

Table 5.4 Spectrum of selected elements along Mn and Fe redox bars analyzed via EDX. Sample letters A to E refer to the rectangles in Figure 5.6.

sample	O	Cl	Mn	Fe
		(%)		
Blank	11	81	0	0
A	33	54	10	3
B	37	47	1	15
C	27	71	0	2
D	37	53	0	8
E	39	35	0	26

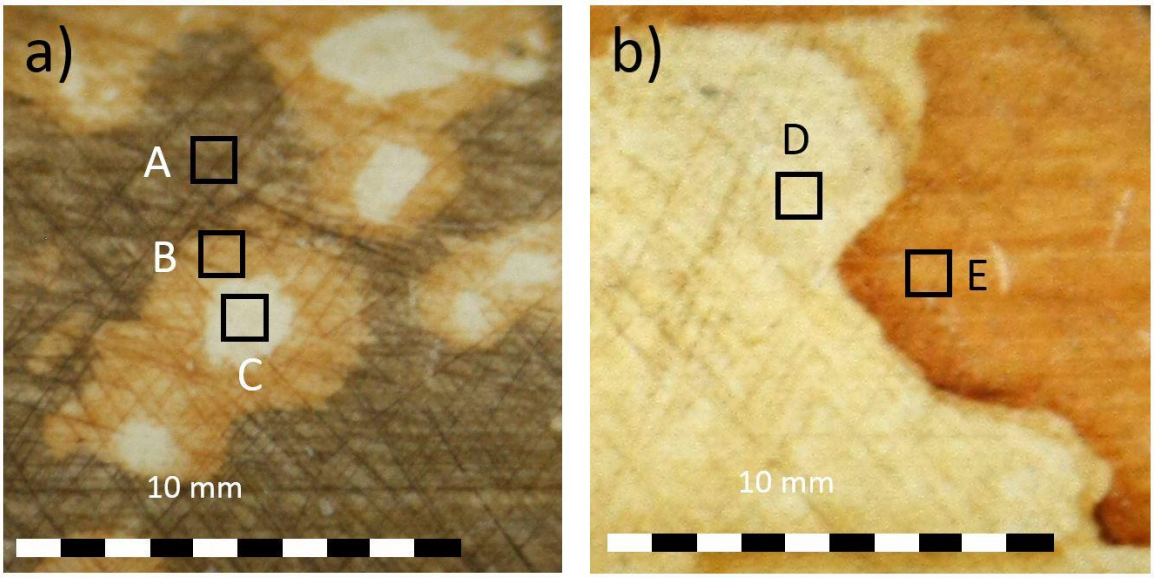

Figure 5.6 Detailed image of a Mn (a) and Fe (b) redox bar previously installed in June. The *rectangles* (*A* to *E*) denote areas used for EDX point measurements

Hence, the oxide coating clearly attenuated the Cl signal. Chemical extraction already revealed that Fe oxides are precipitated along the Mn oxide coating without triggering a change in color, a finding further confirmed at spot A (Fig. 5.6a) with 3% Fe and 10% Mn. The higher Fe content at spot B (15% Fe) favored a change in color accompanied by complete dissolution of remaining Mn oxides (Table 5.4). To the center of the depletion spot, Fe content further decreased to 2%. Soil-reducing conditions intensified reductive dissolution of the Fe oxide coating at spot D with only 8% Fe, compared to 26% Fe at spot E, where oxidizing conditions prevailed. Hence, EDX enabled the determination of element distribution along the Mn and Fe redox bars at very small scale (< 1 mm^2).

Conclusions

The presented selective chemical extraction procedure enables the study of the *in situ* sorption behavior of elements to either Mn or Fe oxide-coated redox bars. Both the laboratory experiments and field observations highlight the importance of Mn oxide as a precursor favoring the likelihood of oxidizing ferrous Fe from the soil solution. Whereas the Mn oxide coating showed preferential sorption behavior for cationic elements (Cu, Zn, and Pb), the Fe oxide coating was enriched in As, P, Mo, and V. The latter elements occur as oxyanions in the soil solution and show a bonding preference for positively charged Fe oxide surfaces as favored at the study site (pH 4.5). Arsenic as a pollutant and P as a nutrient exhibited strong correlation with DCB-extractable Fe oxides along redox bars. Field-Fe oxides precipitated along Mn redox bars sorbed 1.8 (2.2) times more As (P) than did synthesized lab-Fe oxides along Fe redox bars, indicating that naturally precipitated

oxides have a higher sorption capacity due to their lower crystallinity. In general, various elements showed distinct affinities for bonding to either Mn or Fe oxides, with EDX spectroscopy enabling the analysis of the oxide coating at a very small scale (< 1 mm^2). Besides the characterization of soil redox status, Mn and Fe redox bars can be an additional tool with which to study and monitor the element sorption behavior of nutrients and pollutants in wet soils.

Acknowledgments

This study was financially supported by Verein der Freunde und Förderer der Universität zu Köln. We would like to thank Karin Greef (University of Cologne) and Gerd Welp and Addi Kiener (University of Bonn) for analyzing the extracts, and Ruth Bruker and Stefan Roitsch (University of Cologne) for EDX analysis. Additionally, we are grateful to the Duke of Croy and Thomas Seine, who enabled the field measurements.

References

Abd-Elfattah ALY, Wada K (1981) Adsorption of lead, copper, zinc, cobalt, and cadmium by soils that differ in cation-exchange materials. J Soil Sci 32:271–283

Adriano DC (2001) Trace elements in terrestrial environments: biogeochemistry, bioavailability, and risks of metals, 2nd edn. Springer, Heidelberg

Ajouyed O, Hurel C, Ammari M, Allal LB, Marmier N (2010) Sorption of Cr(VI) onto natural iron and aluminum (oxy)hydroxides: effects of pH, ionic strength and initial concentration. J Hazard Mater 174: 616–622

Arai Y (2008) Spectroscopic evidence for Ni(II) surface speciation at the iron oxyhydroxides−water interface. Environ Sci Technol 42:1151–1156

Atta SK, Mohammed SA, Van Cleemput O, Zayed A (1996) Transformations of iron and manganese under controlled E_H, E_H-pH conditions and addition of organic matter. Soil Technol 9:223–237

Barling J, Anbar AD (2004) Molybdenum isotope fractionation during adsorption bymanganese oxides. Earth Planet Sci Lett 217:315–329 Borggaard OK (1983) Effects of surface area and mineralogy of iron oxides on their surface charge and anion-adsorption properties. Clay Clay Miner 31:230–232

Bradl HB (2004) Adsorption of heavy metal ions on soils and soils constituents. J Colloid Interface Sci 277:1–18

Brümmer GW, Gerth J, Tiller KG (1988) Reaction kinetics of the adsorption and desorption of nickel, zinc and cadmium by goethite. I. adsorption and diffusion of metals. J Soil Sci 39:37–52

Castenson KL, Rabenhorst MC (2006) Indicator of reduction in soil (IRIS): evaluation of a new approach for assessing reduced conditions in soil. Soil Sci Soc Am J 70:1222–1226

Chao TT (1972) Selective dissolution of manganese oxides fromsoils and sediments with acidified hydroxylamine hydrochloride. Soil Sci Soc Am J 36:764–768

Cornell RM, Schwertmann U (2003) The iron oxides: structure, properties, reactions, occurences, and uses, 2nd edn. Wiley-VCH, Weinheim

Della Puppa L, Komárek M, Bordas F, Bollinger JC, Joussein E (2013) Adsorption of copper, cadmium, lead and zinc onto a synthetic manganese oxide. J Colloid Interface Sci 399:99–106

Dorau K, Mansfeldt T (2015) Manganese-oxide-coated redox bars as an indicator of reducing conditions in soils. J Environ Qual 44:696–703

Dorau K, Eickmeier M, Mansfeldt T (2015) Comparison of manganese and iron oxide-coated redox bars for characterization of the redox status in wetland soils. WETLANDS revised version under review

Feng XH, Zhai LM, Tan WF, Liu F, He JZ (2007) Adsorption and redox reactions of heavy metals on synthesized Mn oxide minerals. Environ Pollut 147:366–373

Giménez J, Martínez M, de Pablo J, Rovira M, Duro L (2007) Arsenic sorption onto natural hematite, magnetite, and goethite. J Hazard Mater 141:575–580

Goldberg T, Archer C, Vance D, Poulton SW (2009) Mo isotope fractionation during adsorption to Fe (oxyhydr)oxides. Geochim Cosmochim Acta 73:6502–6516

Golden DC, Dixon JB, Chen CC (1986) Ion exchange, thermal transformations, and oxidizing properties of birnessite. Clay Clay Miner 34: 511–520

Gotoh S, Patrick WH (1972) Transformation of manganese in a waterlogged soil as affected by redox potential and pH. Soil Sci Soc Am Proc 36:738–742

Gotoh S, Patrick WH (1974) Transformation of iron in a waterlogged soil as influenced by redox potential and pH. Soil Sci Soc Am Proc 38: 66–71

Han R, Zou W, Li H, Li Y, Shi J (2006) Copper(II) and lead(II) removal from aqueous solution in fixed-bed columns by manganese oxide coated zeolite. J Hazard Mater 137:934–942

Hindersmann I, Mansfeldt T (2014) Trace element solubility in a multimetal-contaminated soil as affected by redox conditions. Water Air Soil Pollut 225:1–20

Hooda PS (2010) Trace elements in soils, 1st edn. Wiley, West Sussex

Jenkinson BJ, Franzmeier DP (2006) Development and evaluation of iron-coated tubes that indicate reduction in soils. Soil Sci Soc Am J 70:183–191

Jolivet JP, Chanéac C, Tronc E (2004) Iron oxide chemistry. From molecular clusters to extended solid networks. Chem Commun 5:481–483

Komárek M, Vaněk A, Ettler V (2013) Chemical stabilization of metals and arsenic in contaminated soils using oxides – a review. Environ Pollut 172:9–22

Kosman DJ (2013) Iron metabolism in aerobes: managing ferric iron hydrolysis and ferrous iron autoxidation. Coord Chem Rev 257: 210–217

Manning BA, Goldberg S (1997) Arsenic(III) and arsenic(V) adsorption on three california soils. Soil Sci 162:886–895

Mansfeldt T, Overesch M (2013) Arsenic mobility and speciation in a Gleysol with petrogleyic properties: a field and laboratory approach. J Environ Qual 42:1130–1141

Mansfeldt T, Schuth S, Häusler W, Wagner F, Kaufhold S, Overesch M (2012) Iron oxide mineralogy and stable iron isotope composition in a Gleysol with petrogleyic properties. J Soils Sediments 12:97–114

Matern K, Mansfeldt T (2015) Molybdate adsorption by birnessite. Appl Clay Sci 108:78–83

McKenzie R (1980) The adsorption of lead and other heavy metals on oxides of manganese and iron. Aust J Soil Res 18:61–73

Mehra OP, Jackson ML (1960) Iron oxide removal from soils and clays by a dithionite-citrate system buffered with sodium bicarbonate. Clay Clay Miner 7:317–327

Morse JW, Luther GW (1999) Chemical influences on trace metal-sulfide interactions in anoxic sediments. Geochim Cosmochim Acta 63: 3373–3378

Nesbitt HW, Canning GW, Bancroft GM (1998) XPS study of reductive dissolution of 7Å-birnessite by H_3AsO_3, with constraints on reaction mechanism. Geochim Cosmochim Acta 62:2097–2110

Ottow JCG (2011) Microbiology of soils (In German), 1st edn. Springer, Heidelberg

Peacock CL, Sherman DM (2004) Vanadium(V) adsorption onto goethite (α-FeOOH) at pH 1.5 to 12: a surface complexation model based on ab initio molecular geometries and EXAFS spectroscopy. Geochim Cosmochim Acta 68:1723–1733

Peretyazhko T, Sposito G (2005) Iron(III) reduction and phosphorous solubilization in humid tropical forest soils. Geochim Cosmochim Acta 69:3643–3652

Rabenhorst MC, Ming DW, Morris RV, Golden DC (2008) Synthesized iron oxides used as a tool for documenting reducing conditions in soils. Soil Sci 173:417–423

Rai D, Eary LE, Zachara JM (1989) Environmental chemistry of chromium. Sci Total Environ 86:15–23

Raven KP, Jain A, Loeppert RH (1998) Arsenite and arsenate adsorption on ferrihydrite: kinetics, equilibrium, and adsorption envelopes. Environ Sci Technol 32:344–349

Rennert T, Mueller CW, Mansfeldt T, Lugmeier J (2013) Collecting in situ precipitated iron oxides in their natural soil environment. J Plant Nutr Soil Sci 176:497–499

Roberts DR, Scheinost AC, Sparks DL (2002) Zinc speciation in a smelter-contaminated soil profile using bulk and microspectroscopic techniques. Environ Sci Technol 36:1742–1750

Scheinost AC, Kretzschmar R, Pfister S, Roberts DR (2002) Combining selective sequential extractions, X-ray absorption spectroscopy, and principal component analysis for quantitative zinc speciation in soil. Environ Sci Technol 36:5021–5028

Smedley PL, Kinniburgh DG (2002) A review of the source, behavior and distribution of arsenic in natural waters. Appl Geochem 17:517–568

Strauss R, Brümmer GW, Barrow NJ (1997) Effects of crystallinity of goethite: II. Rates of sorption and desorption of phosphate. Euro J Soil Sci 48:101–114

Takematsu N, Sato Y, Okabe S, Nakayama E (1985) The partition of vanadium and molybdenum between manganese oxides and sea water. Geochim Cosmochim Acta 49:2395–2399

Thompson A, Chadwick OA, Rancourt DG, Chorover J (2006) Iron oxide crystallinity increases during soil redox oscillations. Geochim Cosmochim Acta 701710–1727

Wang X, Liu F, Tan W, Feng X, Koopal LK (2013a) Transformation of hydroxycarbonate green rust into crystalline iron (hydr)oxides: influences of reaction conditions and underlying mechanisms. Chem Geol 351:57–65

Wang X, Liu F, Tan W, Li W, Feng X, Sparks DL (2013b) Characteristics of phosphate adsorption-desorption onto ferrihydrite: comparison with well-crystalline Fe (hydr)oxides. Soil Sci 178:1–11

Yin H, Feng X, Tan W, Koopal LK, Hu T, Zhu M, Liu F (2015) Structure and properties of vanadium(V)-doped hexagonal turbostratic birnessite and its enhanced scavenging of Pb^{2+} from solutions. J Hazard Mater 288:80–88

Zachara JM, Girvin DC, Schmidt RL, Resch CT (1987) Chromate adsorption on amorphous iron oxyhydroxide in the presence of major groundwater ions. Environ Sci Technol 21:589–594

Chapter 6 Wetland restoration management under the aspect of climate change at a mesotrophic fen in Northern Germany

Ecological Engineering (2015) 48: 84–91

Co-authors: Henrik Gelhausen, Dirk Esplör and Tim Mansfeldt

Formatting and orthography of the manuscript is adapted to the dissertation style.

Highlights

- Wetland restoration management has to be validated under the aspect of climate change
- We studied 15 years of water table (WT) depth development at 46 monitoring wells
- 84% of WTs declined according to the trend line despite re-wetting measures
- Climate projection until 2100 indicates drier summers, which will intensify WT draw-down

Abstract

Wetland restoration management is an important tool for stakeholders and practitioners to mitigate climate change and preserve ecological functioning. Various approaches to modifying the water management of a catchment for restoration purposes exist and were performed in a preservation area in northwest Germany. To validate the effect of the re-wetting practice, a monitoring network of 46 wells was established and monthly readings were taken from 1997 onwards. A declining trend in water table depth was present at 39 wells and equaled on average a lowering of 20 cm during the study period from 1997 to 2012. So far, half of the trend lines are above 40 cm below ground, which is an indicator of an effective re-wetting practice, but they will decline below this threshold until 2032 according to linear regression analysis. The progress of water table depths might be accelerated by climate change. According to the meteorological forecast, air temperatures will rise and the annual precipitation pattern will change. Thus, the climatic water balance tends toward more negative values in the summer and positive values in the winter, favoring an earlier and more intense water table draw-down. Because root water extraction from shallow groundwater is limited to a certain depth, the forecast of water table depth development according to the recent trend depicts a worst-case scenario. Nevertheless, the results emphasize that restoration management should be validated and has to be adapted in certain ways when mitigating the impact of climate change.

Keywords: restoration management, wetlands, climate change, monitoring, shallow groundwater

Abbreviations: WT – water table; CWB – climatic water balance; RCP – representative concentration pathways

Graphical abstract

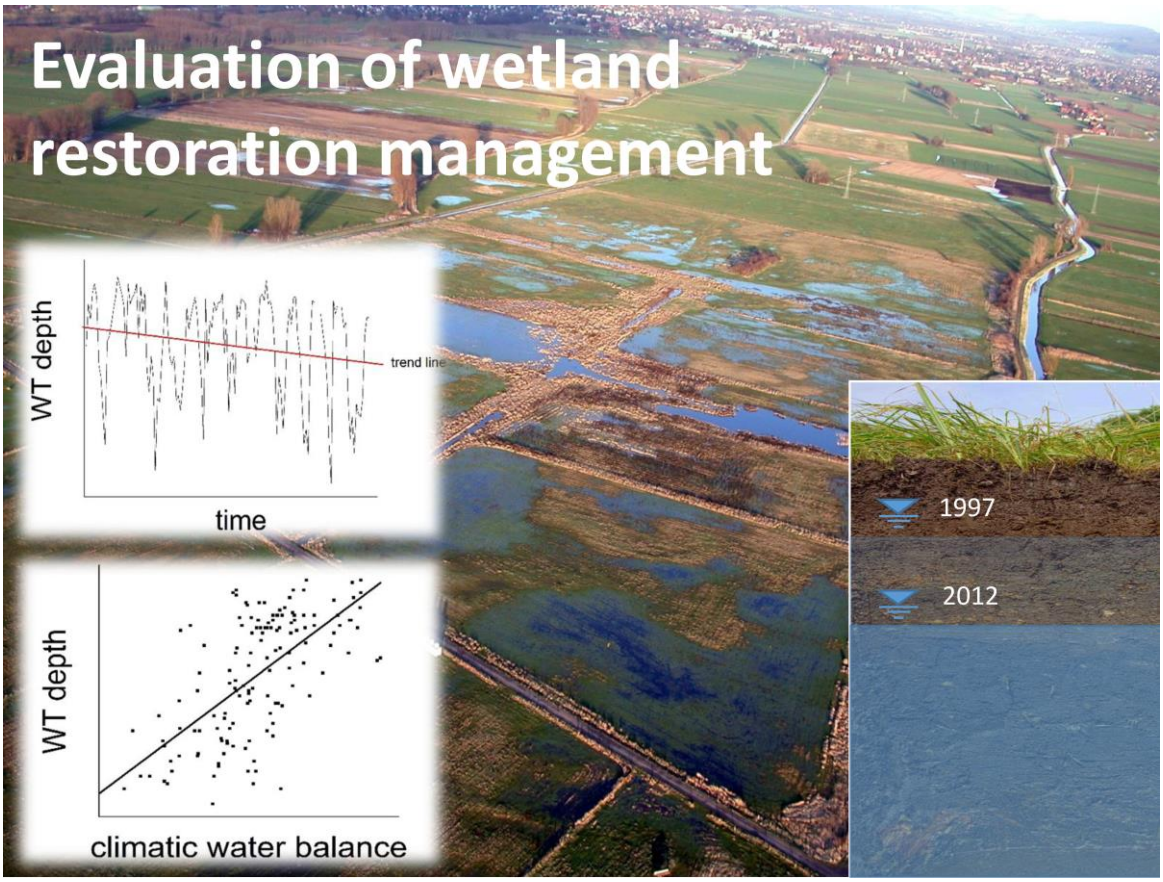

Introduction

Wetlands are important and complex ecosystems and globally account for 800 million ha, which is equal to 6% of the Earth's land surface (Reddy and DeLaune, 2008). They can serve as sinks, sources, or transformers of contaminants, filter nutrients from atmospheric deposition, contain mechanisms to regulate floods, and sustain and promote endangered species because of their biological productivity. The physical, chemical, and biological processes in wetlands control their functioning. Wetlands are usually located in landscapes with low elevation and shallow water tables (WTs). Hence, important characteristics are seasonal or permanent water saturation, which favors anaerobic soil conditions. In the absence of oxygen, many microbially mediated processes are slowed down. As a result, organic carbon (C_{org}) accumulates, which makes wetlands important terrestrial carbon pools. Different types of wetlands can be classified according to their position in the landscape and other characteristic features. Fens are one of the dominant wetland types worldwide with an extent of 148 million ha (21.8% of all wetlands) (Kirk, 2004). Together with bogs, the estimated carbon stocks account for 455 Pg, which is one third of the soil carbon pool (Laine et al., 1996).

Protection and restoration management

To protect and conserve wetlands around the world, the international treaty known as the Ramsar Convention was signed 1971 in Iran and currently has 168 contracting parties. Since then, numerous projects have evolved to stop the loss of wetlands in central Europe due to drainage and intensification of agriculture (Brülisauer and Klötzli, 1998). Price et al. (2003) summarize various approaches to modifying the water management of a catchment for restoration purposes. The general approaches include (i) blocking or refilling of ditches, (ii) minimizing surface-runoff using terraces or bunds, (iii) hydrological buffer-zones, (iv) re-modeling of the surface, and (v) minimizing water loss via evapotranspiration by microclimate modifications. To reduce the effects of drainage, measures to achieve ecological restoration have to be adapted. Besides the restoration measures, a network of wells to monitor the development of WT depths is essential to verify the success of the restoration strategy and re-wetting goals.

Impacts of wetlands on climate change

Drainage and aeration of formerly undisturbed wetlands contribute carbon fluxes to the atmosphere via oxidation of organic matter and gaseous loss of carbon dioxide (CO_2) (Maljanen et al., 2010). Further, the transformation into arable land leads to the emission of nitrous oxide (N_2O) from organic soils, which accounts for an estimated 25% of the

national anthropogenic N_2O emission in Finland (Kasimir-Klemedtsson et al., 1997). However, simultaneously enhanced activity of methane-oxidizing bacteria in the aerated part of the soil profile due to drainage and oxidation will reduce the emission of methane (CH_4) being released to the atmosphere. Carbon dioxide, N_2O, and CH_4 are by far the most important greenhouse gases (GHGs) and have a significant impact on the global warming potential (GWP) (Yu and Patrick, 2004). Because of complex feedback mechanisms on different time-scales, the source–sink function of the soil and atmosphere for the three GHGs is difficult to obtain. Freeman et al. (1992) measured fluxes of CO_2, CH_4, and N_2O from soil columns packed with peat monoliths while subsequently lowering the WT height. They found maximum increases in CO_2 and N_2O fluxes of 146% (646–1590 mg CO_2 m^{-2} d^{-1}) and 936% (0.11–1.14 mg N_2O m^{-2} d^{-1}), respectively, and a decrease in CH_4 of −80% (230–45 mg CH_4 m^{-2} d^{-1}). Moore and Knowles (1989) verified this process, where lowering of the WT height resulted in a linear increase of CO_2 production and a logarithmic decrease in CH_4 evolution.

Climate change

Recently, Koirala et al. (2014) demonstrated the important role of capillary flux from groundwater in the representation of land surface models. According to their results, global mean evapotranspiration increases by 9% when considering water flux to the atmosphere by capillary rise from shallow groundwater, with the largest impact occurring in the semi-arid regions during the dry season (25%) and minimal impact in humid and high-latitude regions. On the other hand, enhanced evapotranspiration rates due to climate change would alter the WT drawdown in the summer time (Laine et al., 1996; Manabe and Wetherald, 1986) because the atmospheric boundary condition, as well as the soil texture, determines the depth to which plant roots can extract water from the groundwater surface. Overall, long-term developments of WT depths are of interest because the boundary between aerobic and anaerobic zones within wetlands might shift toward oxidizing conditions in formerly water-saturated environments.

The primary aim of the study is to assess (i) the impact of wetland restoration and management on the WT depth development of a formerly drained meadow fen in western Germany. Restoration started in 1997 and WT depth monitoring was performed from 1997 onward on a monthly basis at 46 groundwater wells along the study site. Based on precipitation and reference evapotranspiration, we calculated the climatic water balance (CWB) to address (ii) the influence of the ambient meteorology on WT fluctuations. According to the trend line derived by linear regression of WT data for each monitoring well, increasing, constant, or decreasing WT depths under the recent hydrological situation were evaluated. We used a climate projection until 2100 to give an outlook of the future development of

WT depths and to discuss the (iii) impact and vulnerability to climate change when restoring formerly drained wetlands.

Materials and methods

Study site

The conservation area Bastauwiesen is a mesotrophic meadow fen which extends 10.5 km eastwards and 1.4–2.1 km southwards in the district of Minden-Luebbecke, North Rhine-Westphalia (latitude 52°18′ N, longitude 8°47′ E). The setting is within the glacial valley of the River Weser and the basement is composed of Pleistocene sandy to gravel deposits underlying Holocene glaciofluvial calcareous material showing loamy texture underlying peat of variable heights. A decrease of the peat occurs from 4 m thickness in the west to non-coverage in the east and to the edges of the conservation area, which is coherent with a decline of the relief from 50 m asl in the west to 45.3 m in the east (Fig. 6.1). Analogous to the relief is the main flow direction of the channelized River Bastau in the south of the conservation area and a smaller trench running parallel through the study site 100 m northwards. The channels collect interflow from the southwards-located Wiehengebirge and from numerous rectangular shaped ditches, constructed from 1958 to 1960 to intensify agriculture as a result of land consolidation acts. Before that, 90% of the area was managed as intensive grassland and the peat was exploited as fossil fuel. Mean annual precipitation and air temperatures of 688 mm and 9.3 °C characterize the climate as moderate sub-Atlantic with mild winters and relatively cool summers.

Restoration acts and WT depth monitoring

In 1988, the study site became a natural conservation area to protect several endangered flora and fauna species. Former agricultural land was bought by public authorities and changed into extensively managed grassland. Besides this, drain pipes in the fields were destroyed by deep plowing, artificial subsidence was performed by excavation and decommissioned ditches were refilled with the excavated material, numerous concrete weirs (Fig. 6.1) were established to alter the flow characteristics, and hardwood was cleared to facilitate a land cover of pasture and meadow with sedges. For management purposes, four plots were established (I–IV, Fig. 6.1) where WT depths were recorded on a monthly basis in 200-cm perforated polyvinyl chloride pipes (Ø 2.7 cm). Monitoring of WT depths started in December 1999 at plot II, in November 2000 at plot III, and in April 1997 at plot IV, in 10, 24, and 12 monitoring wells, respectively, using an acoustic water level indicator (Nordmeyer, Peine, Germany). So far, management plans for plot I exist but monitoring and restoration are not possible because public authorities have not been able to achieve

the acquisition of connected parcels. The restoration measures and the WT depth monitoring started simultaneously for plot II and IV but the restoration measures started with a delay of three years prior to the recording of WT depth for plot III.

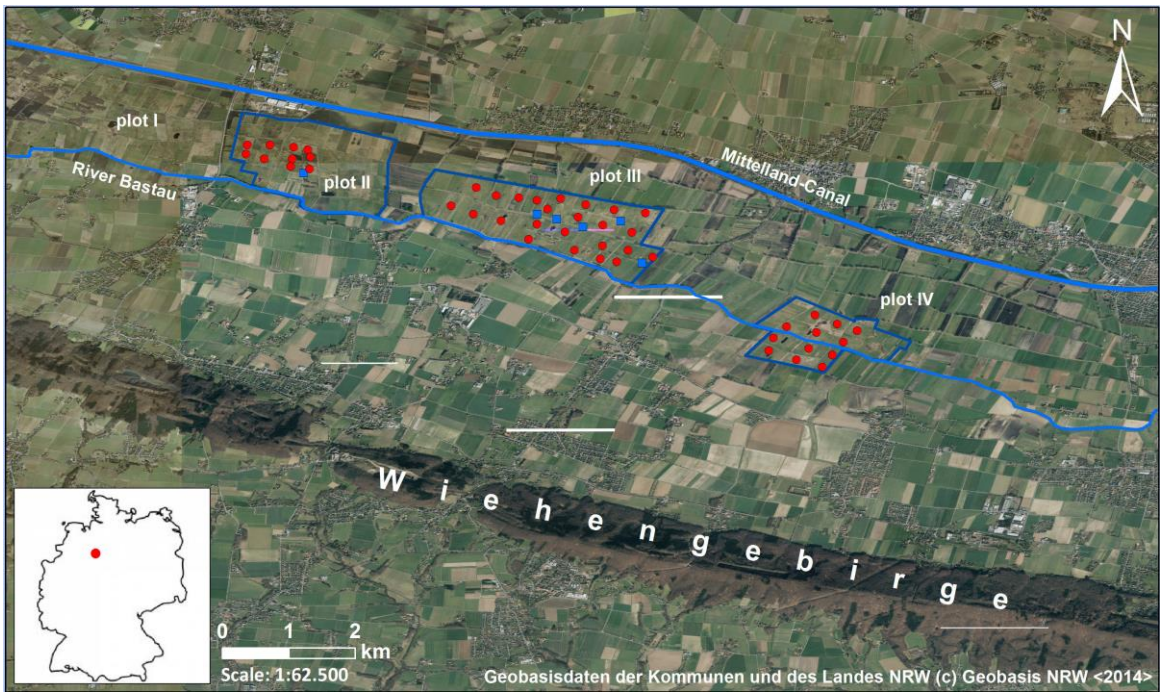

Figure 6.1 Map of the study site showing the boundaries of the plots (blue line), the locations of the groundwater monitoring wells (red dots), and concrete weir (blue dots).

Meteorological parameters

To relate the response and variations of WT depth to meteorological parameters, we calculated the climatic water balance (CWB) as the difference between precipitation and calculated potential evapotranspiration using the Haude formula (PET_{Haude})

$$PET_{Haude} = f \cdot e_s \cdot \left(1 - \frac{F}{100}\right) \quad \text{[Eq. 1].}$$

PET_{Haude} is the evapotranspiration after Haude (mm day^{-1}), f is the Haude factor for single months for a distinct vegetation (Table 6.1), F is the relative humidity (%) and e_s is the water vapor saturation deficit (hPa) for air at 14:00 CET. We used the Haude factor for grass (Löpmeier, 1994), which is most applicable to the study site because it approximates the predominantly occurring plant community, and data of air temperature (°C), relative humidity , and precipitation (mm) on an hourly basis were taken from a free access weather station in Rahden-Varl (Deutscher Wetterdienst, 2009). The vapor pressure deficit (e_s) was calculated using the mean air temperature (T) according to

$$e_s = 6.11 \cdot e^{\frac{(17.62 \cdot T)}{(243.12+T)}} \quad \text{[Eq. 2].}$$

Table 6.1 Haude factor for grass on monthly basis.

Jan	Feb	Mar	Apr	May	Jun	Jul	Aug	Sep	Oct	Nov	Dec
0.20	0.20	0.21	0.29	0.29	0.28	0.26	0.25	0.23	0.22	0.20	0.20

Statistical analysis

To analyze seasonal or long-term patterns of WT depths, we decomposed the time series of each monitoring well by applying the "Seasonal-Trend decomposition procedure based on Loess (STL)" within the statistical language R. The method consists of various smoothing operations and decomposes the time series into a trend, and a seasonal, and a residual component (Cleveland et al., 1990). The STL method uses the locally weighted regression (LOESS) technique and is specifically suitable to detect nonlinear patterns in long-term trends. We chose window widths of 7 for the seasonal component and a default value for the trend (Cleveland et al., 1990; Shamsudduha et al., 2009). Afterwards, we applied a linear fit for each smoothed STL trend line to assess whether the WT depths (i) declined, (ii) increased, or (iii) remained constant during the course of 13 years for plot II, 12 years for plot III, and 15 years for plot IV. The classification was done according to the slope of the linear regression model ($f(x) = mx + b$), whereas a slope of $m > 0.00025$ indicates an increase of WT depth and hence a successful restoration practice, $m \leq 0.00025$ to -0.00025 indicates a stable position of WT without any trend, and $m < -0.00025$ indicates a decrease of WT and hence a lack of success of re-wetting. We categorized these classes because a slope of 0.00025 to −0.00025 equals a WT increase/decrease of less than ±5 cm from 1997 to 2012 that is insignificant. Additionally, we analyzed the individual months within the time series of each well using the Mann–Kendall (MK) trend test within the Addinsoft software XLSTAT-time to make conclusions about the duration characteristics (hydroperiod) when the WT is underneath a certain depth. The MK trend test is a rank-based non-parametric test and has proven its reliability in detecting monotonic trends in many hydro-meteorological time-series (Yue et al., 2002). To accelerate a return of the previous hydrological conditions, it is necessary that the sphagnum moss recovers, and the WT should be > −40 cm below ground (Schouwenaars, 1988; Shantz and Price, 2006). Other authors suggest that the WT at the ditches surrounding the site of interest should be between 30 and 50 cm (Tiemeyer et al., 2006). We used > −40 cm below ground as a threshold to assess the potential for a successful recovery in terms of effective re-wetting practice. Additionally, we forecast the duration needed for each linear fit of the STL line by solving the slope equation for $f(x) = -40$ cm below ground. The result should emphasize the duration when the trend line is deeper than 40 cm below ground. Because the CWB is

one of the main drivers altering the development of WT depths, we determined the coefficient of correlation between each well as the dependent variable and CWB as the independent variable.

Forecast of climatic development

To assess the development of WT depths in the Bastauwiesen under the aspect of climate change, we used the forecasts of air temperature, precipitation, and CWB until 2100. Under financial promotion by the European Institute of Innovation and Technology (EIT), the project “Climate Impact Expert System” was introduced in 2012 by the Potsdam Institute for Climate Impact Research (PIK) and the WetterOnline Meteorologische Dienstleistung GmbH (Bonn, Germany). In this project, climate scenarios are presented to support discussions on how to mitigate climate change. The scenarios were calculated using the regional climate model STAR (DWD, 2009; Orlowsky et al., 2008; PIK, 2013) and account the Representative Concentration Pathways (RCPs) 2.6 and 8.5. Both scenarios describe future anthropogenic GHG emissions and the possible range of radiative forcing with 2.6 and 8.5 W m^{-2}, proposed by the Intergovernmental Panel on Climate Change (IPCC).

Results and discussion

Climatic water balance and water table depths

During the study period from 1997 to 2012, mean annual precipitation was 697 mm, air temperature was 10.1 °C, PET_{Haude} was 281 mm, and the CWB varied between 163 and 734 mm. Significant differences occurred between years, as indicated by the moist and relatively cool year in 2002 with 966 mm of precipitation and 231 mm of PET_{Haude} compared to the above-average warm and dry year of 2003 with 519 and 332 mm respectively. The CWB was positive 85% of the time (Fig. 6.2a), because precipitation exceeded PET_{Haude} on a monthly basis. The CWB became partly negative (white dots in Fig. 6.2a) only from April to September of each year, with the lowest value occurring in August 2003 (−53 mm).

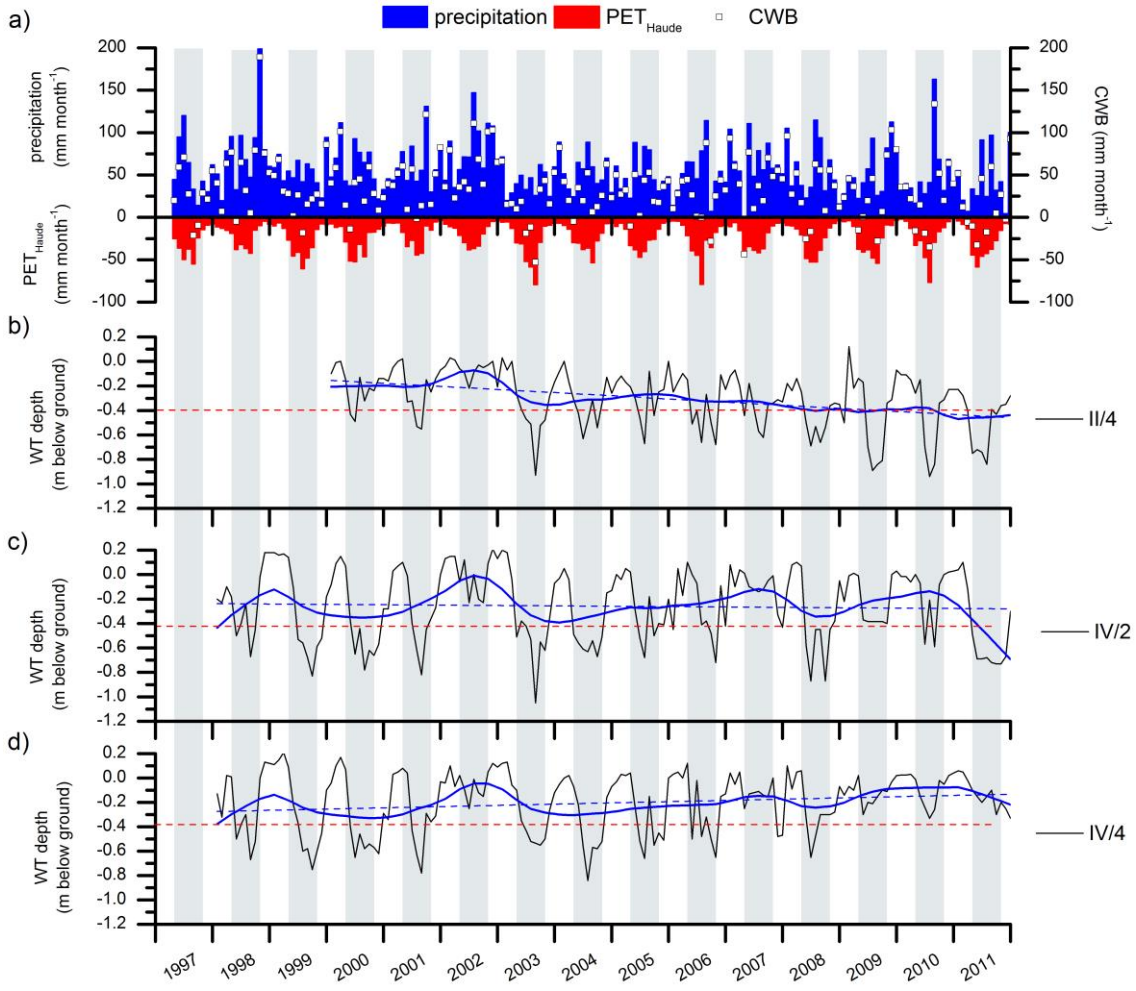

Figure 6.2 Precipitation, potential evapotranspiration (PET), and climatic water balance (CWB) (a) calculated as the difference between reference evapotranspiration according to Haude and precipitation on a monthly basis and examples of a declining (b), constant (c), and increasing (d) water table (WT) between 1997 and 2012. The solid blue line indicates the trend derived by STL analysis and the dashed blue line the linear fit of the corresponding STL trend. Roman letters indicate the plots while Arabic numerals indicate the wells of each plot. The red dashed line marks 40 cm below ground, which is an indicator of an effective re-wetting practice.

In general, increasing evapotranspiration from April to September of each year (light gray bars in the background of Fig. 6.2) promotes a decrease of the WT depth. Fig. 6.2b–d shows examples of the WT depth development for each plot. For all wells along the study site (n = 46), the WT depth varied between −1.2 m below ground in the summertime (light gray bars) and near surface groundwater or periodically ponding groundwater of maximum 0.2 m above ground (white bars) in the wintertime. Especially from April to August of each year, a major mechanism responsible for WT drawdown is root water uptake by plant roots from shallow groundwater (Price and Maloney, 1994). Due to the close connection between the phreatic and vadose zones (within 0.5 m below ground depending on the texture), water loss by evapotranspiration is primarily driven by extraction from groundwater

(Shah et al., 2007). The atmospheric boundary condition controlled by evapotranspiration influences the depth of WT drawdown in shallow and intermittent wetlands (Radcliffe and Simunek, 2010). Hence, distinct patterns of annual WT fluctuations with very shallow groundwater in 2002 and low WT depths in 2003 can be derived and arise for well II/4 and IV/2 (Fig. 6.2b and c).

Relationship between WT depths and climate forcing

To investigate the influence of climate change on groundwater resources and WT depth development it is essential to assess the dependency on atmospheric forcing. A simplified assumption can be derived by the water balance equation, where the gain of water by precipitation and run-off into the catchment equals the loss by evapotranspiration, run-off out of the catchment, and changes of the storage term. We correlated the CWB as the difference between precipitation and PET_{Haude} and the corresponding WT depth for each well on a monthly basis. We had to neglect the storage term and run-off into and out of the catchment because of lacking data. It is therefore not possible to compute the relative magnitude of these flows between plot II, III and IV, although these flows will bias the relationship between the CWB and WT depths. Fig. 6.3 shows two examples of moderate and weak correlation plots for wells II/9 (Fig. 6.3a) and IV/10 (Fig. 6.3b). As the CWB changes to positive values, the WT depths tend to increase, whereas negative values favor a decrease. For all wells along the study site, the correlation is statistically significant ($p < 0.001$). Hence, the risk of falsely rejecting the null hypothesis that a decrease of the CWB, which might be due to enhanced PET_{Haude} or reduced precipitation rates, will favor a decrease of WT depth is less than 0.1%. The coefficient of determination is better for wells along plot II having a mean r^2 of 0.58 with variations between 0.48 and 0.65. A decline is observable for plot III with $r^2 = 0.52$ and a range of 0.43 to 0.58 and for plot IV with $r^2 = 0.45$ and a range of 0.38 to 0.51.

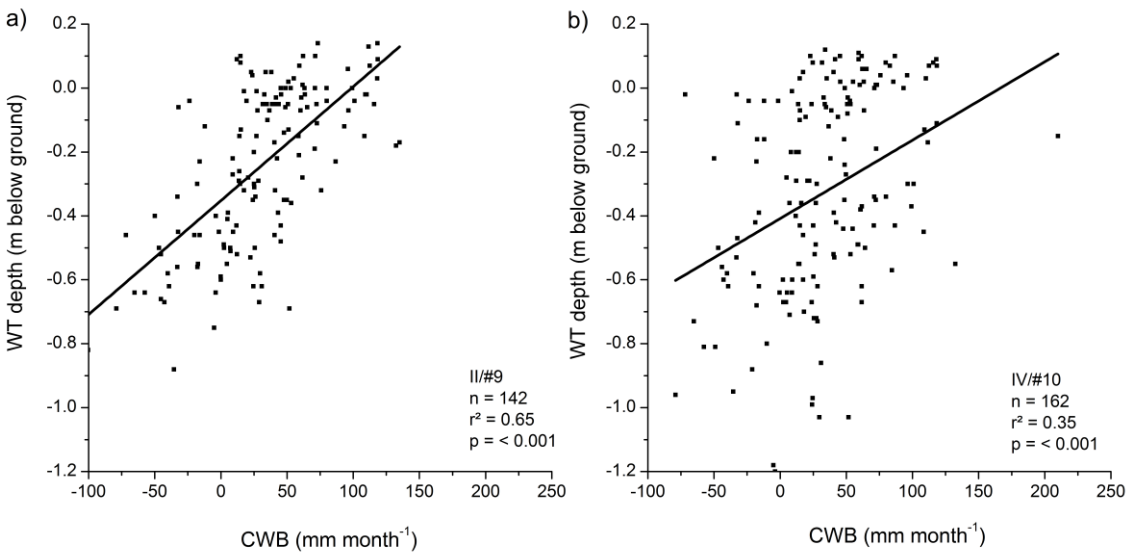

Figure 6.3 Correlation between water table (WT) depth and climatic water balance (CWB) for wells II/9 (a) and IV/10 (b) at the study site.

Hence, a decline occurs from the west to the east of the study site, which follows the decline of the relief and accompanies a decrease of the peat coverage. We assume that the specific yield (Sy), which is termed the 'water storage coefficient' (Price, 1996) and is equivalent to the gradient of the regression line of a change in water storage per unit area versus a change in WT (Price et al., 2003), is responsible for this pattern. The peat coverage in the west retains water after precipitation events whereas the lower Sy in the east, where peat excavation was intensified, leads to weaker statistical relationships. However, there is an uncertainty whether differences in the Sy or surface run-off is responsible for this pattern. Holden et al. (2011) measured WT and rainfall dynamics at 20 min intervals along an undisturbed, drained, and restored blanket peat and attributed differences (e.g., 1 mm of rainfall induces a X mm rise in WT) to the Sy. Water table fluctuations were reported to be more variable in the order drained > blocked > intact. Even though differences between the sites were evident, they stated that their conclusions about the Sy should be treated with caution, since they are not a direct measure. A differentiation for the Bastauwiesen is therefore not possible because of lacking data (surface run-off) or because of the temporal resolution of monthly WT depth readings (Sy).

Meteorological forecast

During the reference period from 1980 to 2010, mean annual air-temperature was 9.4 °C and annual precipitation was 694 mm. Air-temperatures will rise to 10.1 °C (12.6) for the RCP2.6 (RCP8.5) scenario for the period from 2070 to 2100 and will be accompanied with no change (decrease) in the amount of precipitation to 700 (605) mm. The precipitation pattern will also change with 5.4% (−13.3%) more (less) rainfall in the summer months

from April to September with a slight (moderate) decrease of −3.7% (−10.8%) in the winter months from October to March. The divergence between the two projections accounts especially for precipitation, since it varies more in space and time and the prediction is prone to error because of short-scale variations due to natural (volcanic and solar) forcing. Anthropogenic forcing, which is primarily responsible for the steady increase in air-temperature, is therefore easier to predict and less susceptible to variations. However, long-term data of precipitation is a useful indicator to assess the likelihood of changes in the hydrological cycle (Allen and Ingram, 2002). Besides these constraints, both RCP scenarios of the CWB indicate that the Bastauwiesen will become drier from April to August in the range of −29 (−42) to −65 (−85) mm compared with the reference period from 1980 to 2010. A decrease of the annual CWB by −25 mm would favor a lowering of the WT by −8.9 cm (Fig. 6.3a) or −6.2 cm (Fig. 6.3b). The influence of climate change becomes more evident when comparing characteristic days classified by the German Meteorological Service. The extremes between mild winters and warmer summers will be enhanced by a decrease of Frosttage (daily min. < 0 °C) from on average 64 days during the reference period from 1980 to 2010 to 55 (29) during the RCP2.6 (RCP8.5) scenario from 2070 to 2100. On the contrary, heiße Tage (daily max. ≥ 30 °C) will rise from 6 to 8 (20) and Sommertage (daily max. ≥ 25 °C) from 29 to 36 (67).

Forecast of WT depth development

At first sight, the restoration management seems to be successful because the trend line of WT depths at 7 out of 10 monitoring wells at plot II, 9 out of 24 wells at plot III, and 8 out of 12 wells at plot IV are above 40 cm below ground (Table 6.2). Taking into account the slope of the trend line, 9 out of 10 wells at plot II and nearly all of the monitoring wells at plot III indicate a decline of WT depths and hence a trend contrary to that desired since 1997 when restoration management started. Plot IV is the exception, with only 7 declining, 4 intermediate, and 1 increasing STL trend lines (Table 6.2).

All of the average WT depths will be 40 cm below ground according to the linear fit of the STL analysis until 2032 under the ambient meteorological forcing. The position of the trend line in 1997 and 2012 highlights this process and indicates a lowering of the average WT position along all wells at plot II from −0.12 to −0.32 cm and at plot III from −0.19 to −0.42 cm with no clear trend at plot IV (Fig. 6.4a and b).

Table 6.2 Selected statistical data for long-term water table depth monitoring of three designated plots along the study site.

Plot	Since	Total number of wells	WT_{trend}[a]	WT_{trend}[b]	WT_{slope}[c]	WT_{slope}[d]	WT_{slope}[e]
II	Dec 1999	10	7/10	3/10	9/10	1/10	0/10
III	Nov 2000	24	9/24	15/24	23/24	1/24	0/24
IV	Apr 1997	12	8/12	4/12	7/12	4/12	1/12

[a] Number of wells for which the linear fit of the STL line is above −40 cm below ground
[b] Number of wells for which the linear fit of the STL line is below −40 cm below ground
[c] Number of wells for which the slope of the STL line declines
[d] Number of wells for which the slope of the STL line is intermediate
[e] Number of wells for which the slope of the STL line increases

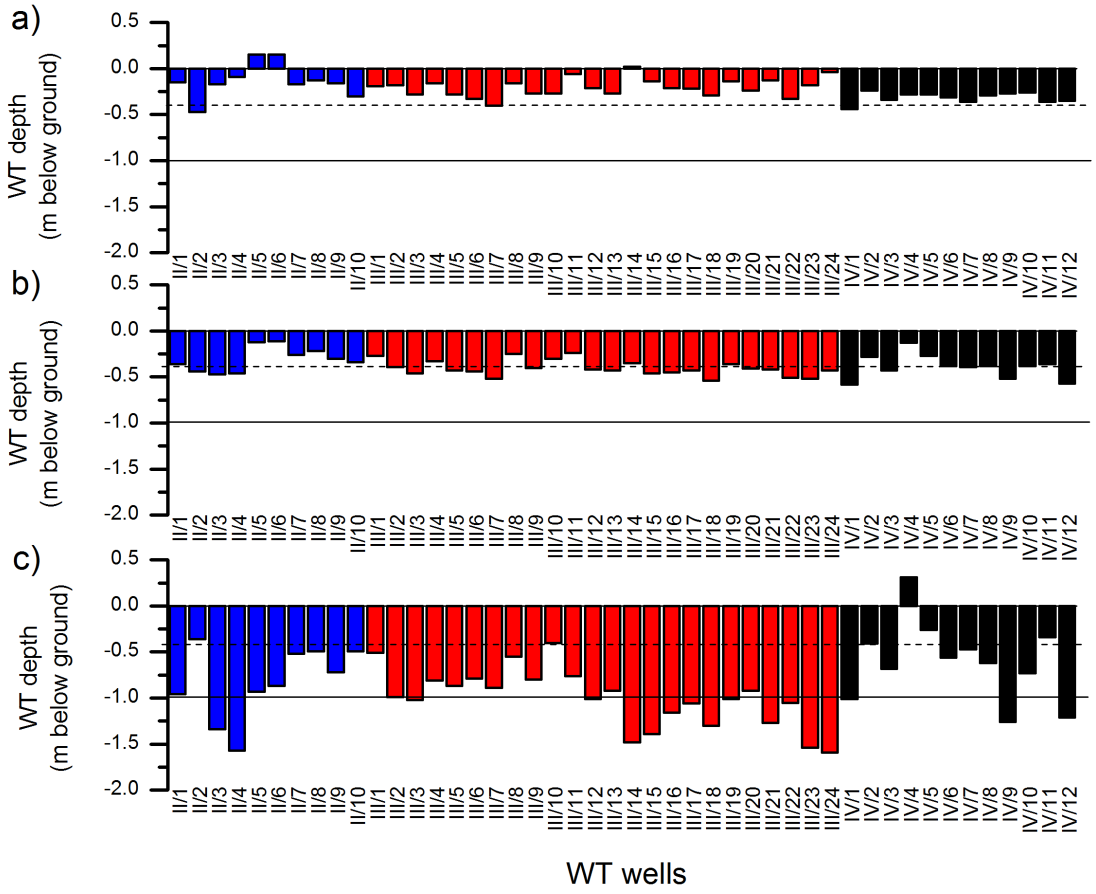

Figure 6.4 Mean water table (WT) depth according to the position of the linear fit by the STL trend line for monitoring wells at plot II (blue), plot III (red), and plot IV (black) in the past (1997; a), at present (2012; b), and according to the forecast (2055; c). The black dashed line and the solid line indicate 0.4 and 1 m below ground, respectively.

When forecasting the development under the ambient meteorological conditions, WT positions are assumed to be on average −0.83, −1.00, and −0.60 m below ground in 2055 at plots II, III, and IV, respectively (Fig. 6.4c). Drier summers and mild winters would certainly push the WT development in this direction but, because soil water extraction by plant roots is limited to a certain depth, Fig. 6.4c presents a worst-case scenario. Taking into account

the seasonal component derived by the STL analysis procedure (Fig. 6.S1 in the supplemental material shows three examples), we observed an increasing seasonality along 42 out of 46 monitoring wells from 2007 to 2012 and 18 out of 46 monitoring wells even show an increase of the seasonal component from 2003 onwards. Only 1 out of 46 monitoring wells shows a decreasing seasonal component and 3 out of 46 neither an increase nor a decrease. These findings highlight that differences between mean WT depths in the summer- and wintertime might drift apart in the future. Figure 6.5 underlines these findings. It is evident that WT depth development shows a strong seasonality and more than 40% of all wells show a significant decrease in July. Furthermore, one out of five wells shows a decreasing trend in April and June, which further indicates an extension of the hydroperiod for some monitoring wells.

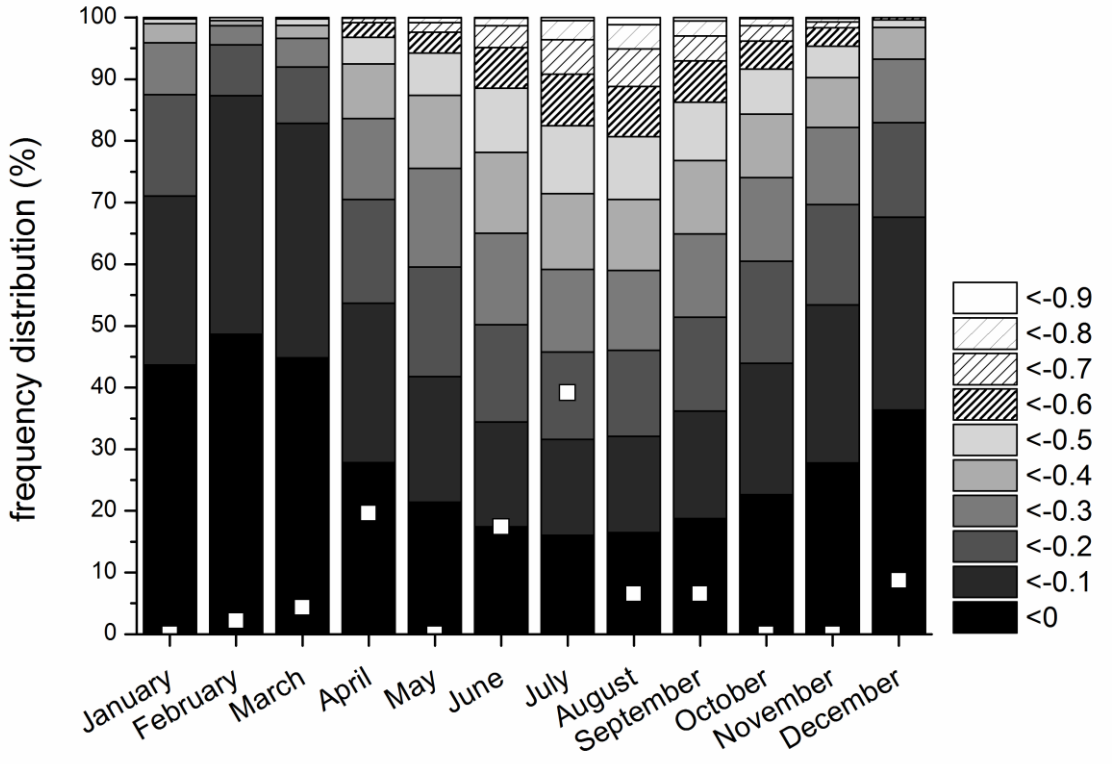

Figure 6.5 Mean frequency distribution histogram of water table (WT) depths for monitoring wells (n = 46) on monthly basis. The white rectangles denote the relative fraction of monitoring wells that show a significant decreasing trend within the individual months of the time series. Verification of a decreasing trend was evaluated using the Mann–Kendall trend test on the 5% probability scale.

Best management practices

Obviously, recent trends in groundwater data indicate that the development is contradicting to the re-wetting goals. The process of enhanced seasonality with an extension of the

hydroperiod might be accelerated and proceed in the future when the CWB changes toward drier summers as predicted by the meteorological forecast. It is therefore advisable to validate the restoration management and adapt it in certain ways to mitigate the impact of climate change. Martinez-Martinez et al. (2014) modelled the impact of wetland areas (50, 100, 250, and 500 ha), depths (15, 30, 61, and 91 cm), and wetland placement on streamflow characteristics using the Soil and Water Assessment Tool (SWAT). Increasing the wetland area (250 and 500 ha), rather than depth, resulted in greater streamflow reduction while the smallest area (50 ha) had negligible impacts on average daily streamflow. Hence, a best management practice (BMP) for the Bastauwiesen would be to (a) connect the recently separated plots II (192 ha), III (181 ha), and IV (79 ha), which would result in a size of > 500 ha. Enhancing the amount of water that is retained within the Bastauwiesen is desired to minimize the WT draw-down at the beginning of the vegetation period (March to May of each year). The (b) removal of levees along the channelized river Bastau would result in more frequent flooding and support an additional water supply for plot II, III, and IV. Finally, (c) considering the Water Framework Directive (WFD) as a major EU policy to enhance the water quality standards of various member states, synergy effects and incentives for wetland restoration that include the construction of meanders, oxbows, and riparian zones might be accomplished (Verhoeven, 2014).

Conclusions

In this study, we analyzed time series data (1997–2012) of WT depth development along a formerly drained mesotrophic fen in Northern Germany by applying the seasonal trend decomposition (STL) procedure. The impact of wetland restoration is contradicting to the re-wetting goals because 84% of all monitoring wells (n = 46) along the study site Bastauwiesen show a decreasing trend. The development of WT depths indicates a lowering by 20 cm within the monitoring period according to the trend lines. Especially under a changing climate with drier summers, the transformation of previously drained and arable land back to the previous non-anthropogenic situation based on the re-wetting goals (e.g. which plants should develop) is difficult to achieve. It is very likely that the proposed meteorological forecast with a decrease of the CWB for both RCP scenarios favors an extension of the hydroperiod and increases the seasonality of annual WT depth development. To derive certain patterns of the individual plots, a density of one monitoring well per 0.103 km^2 yielded good results with a monthly measuring interval. A higher temporal resolution on hourly basis is recommended to differentiate plot specific properties such as the specific yield. We showed that restoration management is important but has to be validated continuously to guarantee success, especially under the aspect of climate change.

Acknowledgements

We kindly thank Biologische Station Minden-Lübbecke e.V. for providing the data of the groundwater monitoring campaign.

Supplemental Material

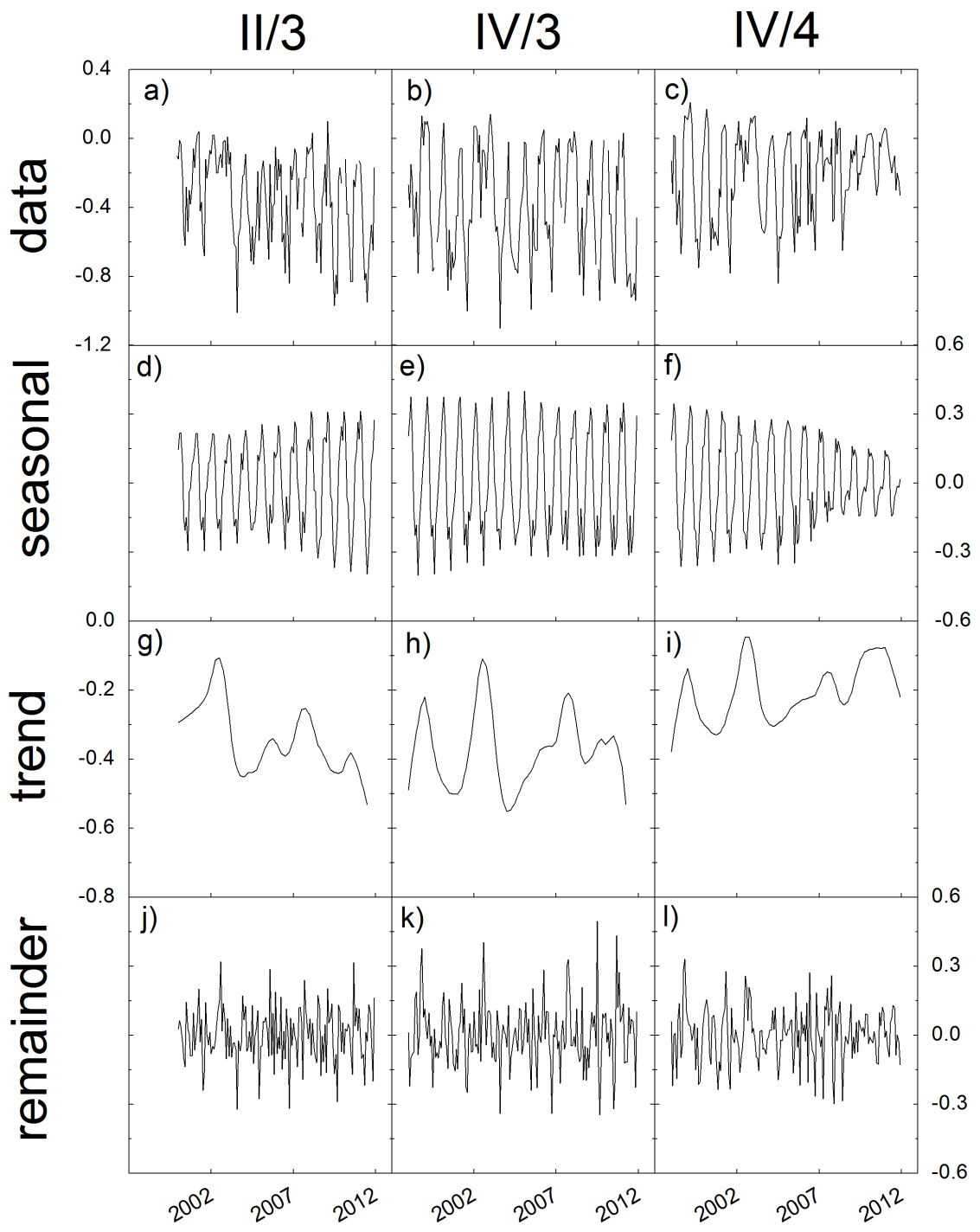

Figure 6.S1 Results of the STL analysis for well II/3, IV/3, and IV/4 with the raw data (a to c), the seasonal component (d to f), the trend component (g to i), and the remainder (j to l). Please note the increase (d), neither an increase nor a decrease (e), and the decrease (f) of the seasonal component starting from 2003 to 2012.

References

Allen M.R. and Ingram W.J., Constraints on future changes in climate and the hydrologic cycle, Nature 419, 2002, 224–232.

Brülisauer A. and Klötzli F., Notes on the ecological restoration of fen meadows, ombrogenous bogs and rivers: definitions, techniques, problems, Bull. Geobot. Inst. ETH 1998, 47–61.

Cleveland R., Cleveland W., McRae J. and Terpenning I., STL: A seasonal-trend decomposition procedure based on loess, J. Off. Stat. Stat. 6, 1990, 3–73.

Deutscher Wetterdienst (DWD), Daten der Klimastationen des Deutschen Wetterdienstes, 2009, Offenbach; Germany.

Freeman C., Lock M.A. and Reynolds B., Fluxes of CO_2, CH_4 and N_2O from a Welsh peatland following simulation of water table draw-down: potential feedback to climatic change, Biogeochemistry 19, 1992, 51–60.

Holden J., Wallage Z.E., Lane S.N. and McDonald A.T., Water table dynamics in undisturbed, drained and restored blanket peat, J. Hydrol. 402, 2011, 103–114.

Kasimir-Klemedtsson Å., Klemedtsson L., Berglund K., Martikainen P., Silvola J. and Oenema O., Greenhouse gas emissions from farmed organic soils: a review, Soil Use Manag. 13, 1997, 245–250.

Kirk G., The Biogeochemistry of Submerged Soils, 2004, John Wiley & Sons; Hoboken, NJ, USA.

Koirala S., Yeh P.J.F., Hirabayashi Y., Kanae S. and Oki T., Global-scale land surface hydrologic modeling with the representation of water table dynamics, J. Geophys. Res. – Atmos. 119, 2014, 75–89.

Laine J., Silvola J., Tolonen K., Alm J., Nykänen H., Vasander H., Sallantaus T., Savolainen I., Sinisalo J. and Martikainen P.J., Effect of water-level drawdown on global climatic warming: northern peatlands, Ambio 25, 1996, 179–184.

Löpmeier F.J., Berechnung der Bodenfeuchte und Verdunstung mittels agrarmeteorologischer Modelle, Z. Bewaesserun. 29, 1994, 157–167.

Maljanen M., Sigurdsson B.D., Guðmundsson J., Óskarsson H., Huttunen J.T. and Martikainen P.J., Greenhouse gas balances of managed peatlands in the Nordic countries – present knowledge and gaps, Biogeosciences 7, 2010, 2711–2738.

Manabe S. and Wetherald R.T., Reduction in summer soil wetness induced by an increase in atmospheric carbon-dioxide, Science 232, 1986, 626–628.

Martinez-Martinez E., Nejadhashemi A.P., Woznicki S.A. and Love B.J., Modeling the hydrological significance of wetland restoration scenarios, J. Environ. Manage. 133, 2014, 121–134.

Moore T.R. and Knowles R., The influence of water table levels on methane and carbon dioxide emissions from peatland soils, Can. J. Soil Sci. 69, 1989, 33–38.

Orlowsky B., Gerstengarbe F.W. and Werner P.C., A resampling scheme for regional climate simulations and its performance compared to a dynamical RCM, Theor. Appl. Climatol. 92, 2008, 209–223.

Potsdam Institute For Climate Research Impact (PIK), STARS Klimaszenarien. Potsdam, Germany, 2013.

Price J.S., Hydrology and microclimate of a partly restored cutover bog, Quebec, Hydrol. Process. 10, 1996, 1263–1272.

Price J.S. and Maloney D.A., Hydrology of a patterned bog-fen complex in southeastern Labrador, Canada, Nord. Hydrol. 25, 1994, 313–330.

Price J.S., Heathwaite A.L. and Baird A.J., Hydrological processes in abandoned and restored peatlands: an overview of management approaches, Wetl. Ecol. Manag. 11, 2003, 65–83.

Radcliffe D.E. and Simunek J., Soil Physics with HYDRUS – Modeling and Applications, 2010, CRC Press; Boca Raton, FL, USA.

Reddy K.R. and DeLaune R.D., Biogeochemistry of Wetlands – Science and Applications, 2008, CRC Press; Boca Raton, FL, USA.

Schouwenaars J.M., The impact of water management upon groundwater fluctuations in a disturbed bog relict, Agric. Water Manag. 14, 1988, 439–449.

Shah N., Nachabe M. and Ross M., Extinction depth and evapotranspiration from ground water under selected land covers, Ground Water 45, 2007, 329–338.

Shamsudduha M., Chandler R.E., Taylor R.G. and Ahmed K.M., Recent trends in groundwater levels in a highly seasonal hydrological system: the Ganges-Brahmaputra-Meghna Delta, Hydrol. Earth Syst. Sci. 13, 2009, 2373–2385.

Shantz M.A. and Price J.S., Hydrological changes following restoration of the Bois-des-Bel peatland, Quebec, 1999–2002, J. Hydrol. 331, 2006, 543–553.

Tiemeyer B., Lennartz B. and Vegelin K., Hydrological modelling of a re-wetted peatland on the basis of a limited dataset for water management, J. Hydrol. 325, 2006, 376–389.

Verhoeven J.T.A., Wetlands in Europe: perspectives for restoration of a lost paradise, Ecol. Eng. 66, 2014, 6–9.

Yu K.W. and Patrick W.H., Redox window with minimum global warming potential contribution from rice soils, Soil Sci. Soc. Am. J. 68, 2004, 2086–2091.

Yue S., Pilon P. and Cavadias G., Power of the Mann–Kendall and Spearman's rho tests for detecting monotonic trends in hydrological series, J. Hydrol. 259, 2002, 254–271.

Chapter 7 Comprehensive discussion

Discussion

The previous chapters showed results of the temporal and spatial E_H variability monitored by Pt electrodes (Chapter 2) and introduced the simultaneous application of Mn and Fe redox bars as an alternative approach to monitor and characterize the soil redox status (Chapter 3 to 5). A characterization of the soil redox status is mandatory as climate change likely affects the position of the WT depth development (Chapter 6) with implications to biogeochemical processes. The formulated Objectives a) to e) are summarized and illustrated in Fig. 7.1, which major findings will be discussed in the following.

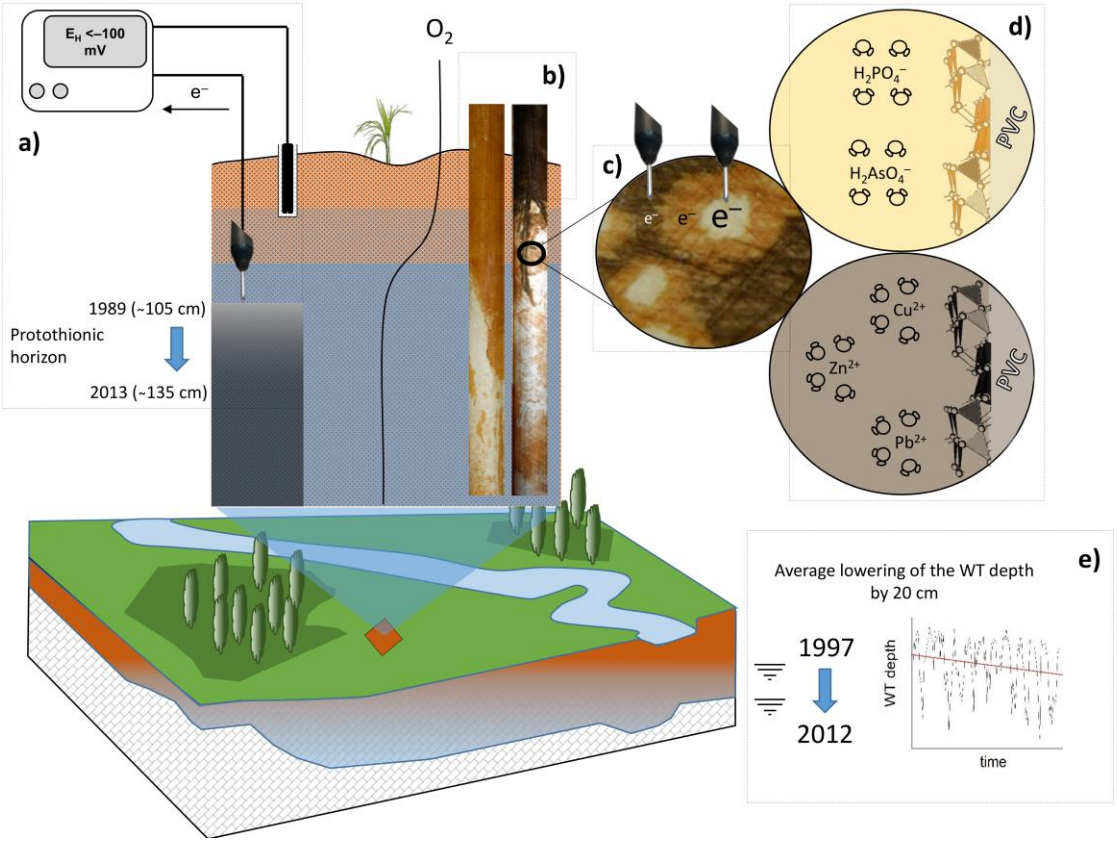

Figure 7.1 Illustration and major results for the formulated objectives within this thesis: a) Comparison of the E_H dynamics between two monitoring campaigns (1990 to 1993; 2011 to 2014) using permanently installed Pt electrodes; b) Manufacturing and evaluation of Mn redox bars; c) Monitoring and differentiation into weakly and moderately reducing soil conditions by Mn and Fe redox bars; d) Investigation of selective element sorption to the oxide coating of redox bars; e) Evaluation of the WT depth development under the aspect of climate change.

Objective a)

Comparison of the E_H dynamics between two monitoring campaigns (1990 to 1993; 2011 to 2014) using permanently installed Pt electrodes

A unique characteristic of the study site Speicherkoog during the former (1990 to 1993) and during the latter (2011 to 2014) monitoring campaign was the wide range of fluctuation in the WT level. Near-surface groundwater and WT depths of –200 cm below ground were recorded for both periods (Fig 2.1). The relationship between the period of water saturation and E_H was shown for groundwater (Cogger et al. 1992; Mansfeldt 2003), perched-water (Vepraskas and Wilding 1983), flooding (Shrestha et al. 2014), and irrigation (Meek and Grass 1975). All results had in common that an extension of the period of water saturation favored the onset of reduction and were therefore negatively correlated with E_H. Obviously, this has an impact on the stability of $Mn^{III,IV}$ and Fe^{III} oxides. The E_H-pH diagram in Fig. 7.2 displays the mean E_H values in 60 and 100 cm during the hydrological summer and winter at Polder Speicherkoog for the period from 2011 to 2014. Whereas oxidizing soil conditions ($Mn^{III,IV}$ and Fe^{III} oxides remain stable) at a mean WT depth of –110 cm below ground prevailed in the summer, weakly ($Mn^{III,IV}$ oxide reduction) and moderately (Fe^{III} oxide reduction) reducing soil conditions at a mean WT depth of –39 cm below ground were measured during winter. Hence, the annual fluctuating WT with the subsequent onset of either reduction or aeration changed the depths in 60 and 100 cm from a potential source for Mn^{2+} and Fe^{2+} in the winter to a potential sink by re-oxidation of these reduced species (e.g. to MnO_2 and $Fe_5HO_8 \cdot 4H_2O$) in the summer. These differences were not apparent for the E_H observation depths in 10 and 30 cm (continuous sink) and 150 cm (continuous source) between the hydrologic summer and winter from 2011 to 2014. Additionally, a shift of the redox class distribution towards oxidizing soil conditions (calculated from E_H data in Fig. 2.3) was evident on the decadal scale between 1990 to 1993 and 2011 to 2014 in 60 (+18%), and 100 (+84%) cm, which extended the period to be a potential sink for manganous Mn and ferrous Fe in these depths. It is obvious that a delineation of these trends are important with implications for agricultural practice (aeration status) and soil formation (development of redoximorphic features).

An exclusive discussion of the E_H development solely based on the fluctuation of the WT is not meaningful because other external parameters (e.g. soil temperature) and soil properties (e.g. SOM, pH, soil mineralogy) affect the E_H. For instance, bacteria in water saturated soil environments are the principal dynamic agent influencing the E_H (Fiedler et al. 2007) but the microbial activity depends not only on the soil temperature but also on the pH. To make it even more complicated, the direct or indirect impact on the E_H development acts on different time-scales. Changes of the WT depth can be instantaneously within

minutes to hours, whereas soil temperature and SOM content change more slowly. The interaction of these factors alters the E_H development and has an impact on $Mn^{III,IV}$ and Fe^{III} oxide reduction rates.

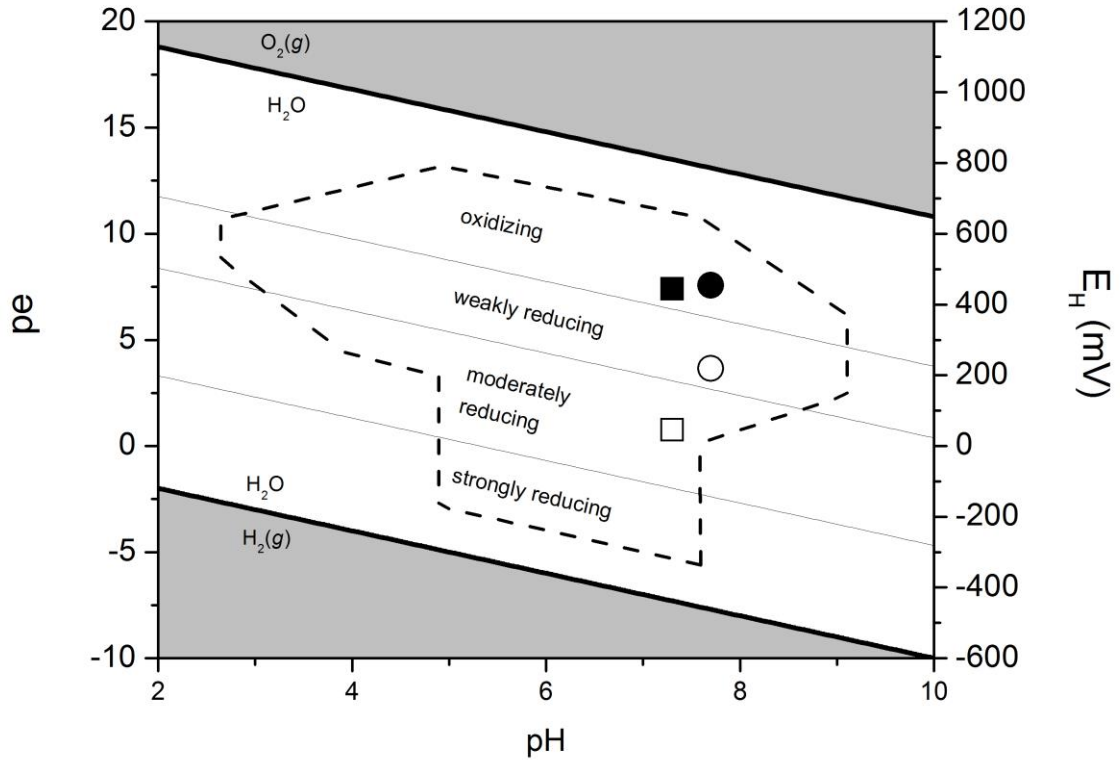

Figure 7.2 E_H-pH diagram with the stability region of water (white area), with common E_H and pH values measured in natural waters (dashed line; modified from (Essington 2015), and with the redox classes (at pH 7) of oxidizing (E_H > 400 mV), weakly reducing (E_H 400 to 200 mV), moderately reducing (E_H 200 to –100 mV), and strongly reducing (E_H < –100 mV) soil conditions. The diagram also includes the mean E_H values of Polder Speicherkoog recorded during the hydrologic winter (open symbols; November to April of each year) and summer (solid symbols; May to October of each year) in 60 (squares) and 100 (circles) cm during the study period from 2011 to 2014.

Various studies demonstrated the relationship between soil temperature and E_H. Meek and Grass (1975) reported that a 5 °C increase in soil temperature went along with a 50 mV decrease. Clay et al. (1990) and Farrell et al. (1991) also observed this on a daily basis. Typically, temperature maxima followed E_H minima with diurnal variations by 30 to 50 mV demonstrating an inverse relationship of E_H with soil temperature. It was hypothesized that either temperature induced changes of the microbial activity or root respiration was responsible for this pattern (Fiedler 2000). At Polder Speicherkoog, diurnal E_H variations were also observed with up to 100 mV and the diurnal E_H amplitude was enhanced in 10 and 20 cm compared with 30, 60, and 100 cm (data not shown). This finding leads to the assumption that root respiration is responsible because the distribution of roots is denser

in the topsoil than in the subsoil. However, E_H fluctuations up to 5 mV were also found in 150 cm that cannot be explained by this process because roots are absent and soil temperatures remained constant throughout the year. In this regard, a process not considered so far is the temperature dependence of the internal electrolyte solution (3 M KCl) within the Ag/AgCl reference electrode. Approximately, a 1 °C increase goes along with a 1 mV decrease (Galster 1991). Diurnal E_H patterns might therefore be a mixture of biologically mediated processes and remnants of technical constraints. However, daily E_H variations of 5 mV have no impact on the reduction of $Mn^{III,IV}$ and Fe^{III} oxides and readings more precise than ±10 mV (Mueller et al. 1985) little significance. Other authors proposed that even E_H variations up to ±40 to 50 mV (McKenzie et al. 1960; Pfisterer and Gribbohm 1989) have little informative value. Therefore, the use of redox classes is encouraged over the use of numerical values (Chapter 2). A direct comparison of soil temperatures between both monitoring periods was not possible at Polder Speicherkoog because soil temperatures were monitored exclusively for the period during 2011 to 2014. However, considering the forecast of rising air temperatures it can be expected that soil temperatures are also prone to increase in the future. Houle et al. (2012) estimated the soil temperature development until 2100 at three forested sites in Quebec and computed an increase between 1.9 and 3.3 °C for the period from 2070 to 2099. The increase during the growing season was up to 5 °C. Without doubt, a 5 °C increase has impact on $Mn^{III,IV}$ and Fe^{III} oxide reduction rates and is likely to affect the E_H development because O_2 is exhausted more rapidly in the soil during water logging.

Apart from the impact of the WT depth and soil temperature on the E_H dynamics, the reduced C in the SOM pool is the primary electron donor in the soils environment and alters the E_H development. Its content is not stable over time and in a transient state. Wetlands are suitable habitats and net accumulators of SOM over decadal to millennial timescales because decomposition is impeded by flooding and water saturation (Schlesinger and Emily 2013). However, under aerobe conditions SOM degradation is accelerated and forms by various intermediate products heterogeneous, polyfunctional organic molecules defined as humic substances (HS) (Strawn et al. 2015). Humic substances are redox active due to a variety of functional units (Piepenbrock et al. 2014) with E^0 values between +150 to –300 mV at pH 7 (Aeschbacher et al. 2011), enabling to donate or accept electrons depending on the soil milieu. The process is called electron shuttling and plays a key role in many biogeochemical redox reactions. Piepenbrock et al. (2014) demonstrated that HS contributed significantly to biogenic Fe^{III} oxide reduction in marine sediments. The process was of importance for short-range-ordered Fe^{III} oxides (e.g. ferrihydrite) but not accountable for more crystalline oxide minerals (e.g. goethite). The relevance of electron shuttling

by HS must be further investigated to verify or falsify this process to be important to alter the E_H dynamics under field conditions. In 24-years of soil formation at Polder Speicherkoog, the SOM content remained at a similar level (Table 2.1) but simultaneous to long-term E_H monitoring, changes of the SOM inventory (quantity and quality) over time are essential because of the dependency and interaction of both parameters.

Redox potential measurements by Pt electrodes are micro-aggregate dependent and susceptible to changes in the soil mineralogy. A major difference in terms of the mineralogical composition between the two monitoring campaigns was the lowering of the sulfide-bearing *Protothionic* soil horizon from 105 to 135 cm (illustrated in Fig. 7.1a). A diminishing of monosulfidic S contents in 150 cm from 275 (in 1989) to 112 mg S^{2-}-S kg^{-1} (in 2013) underlined this finding. The sulfide was associated with Fe to form monosulfidic Fe minerals (FeS), which were highly unstable and rapidly oxidized in the presence of O_2 (Nordstrom 1982). Lower E_H readings from 1990 to 1993 (minimum E_H –207 mV) compared with the period from 2011 to 2014 (82 mV) in 100 cm depth were likely due to FeS being oxidized to the metastable S^0 and further to SO_4^{2-}. This has impact on the measured E_H and is characteristic of the FeS-S^0 redox couple (Whitfield 1974). At present, the distance between the E_H observation depth in 100 cm to the sulfide-bearing horizon in 135 cm indicates that this process is not important but must be considered relevant for the monitoring period from 1990 to 1993.

Oxidation of reduced species (e.g. Mn^{2+}, Fe^{2+}, and S^{2-}) is a proton-producing process with impact on the pH of the soil solution. The reverse process was shown during the microcosm experiment in Chapter 3 (Fig. 3.2), where a lowering of the E_H from 300 mV to 80 mV resulted in a pH increase from pH 6.8 to 7.8 because reduction is a proton-consuming process. Rezanezhad et al. (2014) installed pH microelectrodes in an automated soil column experiment with a variable WT and found differences of one pH unit over the course of the experiment. For simplicity and in most applications, the soil pH is portrayed as a state variable and inherent of temporal changes but obviously, fluctuations in the range of one pH unit have impact on biogeochemical processes. The only attempt to monitor pH simultaneous to E_H readings was performed by Unger et al. (2008). However, their automated system detected erroneous readings with pH values in the range from negative values to greater than 14 and without any relationship to E_H. Time-resolved *in situ* pH measurements would certainly help to understand the temporal and spatial variability of E_H. Especially to answer questions related to diurnal E_H variability under oxidizing soil conditions. In this regard, measuring the E_H for the O_2/H_2O system depends more on pH (a change of 59 mV per pH unit) and to a lesser extent on O_2 partial pressure (a change of 15 mV per tenfold change in O_2 pressure) (Glinski and Stepniewski 1985).

Objective b)

Manufacturing and evaluation of Mn redox bars

A central aspect of this thesis was to adapt and improve the already established IRIS method that solely comprises Fe redox bars. A broad range of peer-reviewed scientific articles (Castenson and Rabenhorst 2006; Jenkinson and Franzmeier 2006; Rabenhorst 2010, 2012; Rabenhorst and Burch 2006; Rabenhorst et al. 2008; Rabenhorst et al. 2010) have demonstrated the effectiveness and acceptance of this methodology in the scientific community. Moreover, this approach entered the framework of the US Hydric Soil Technical Standard as a means of proving reducing conditions and to classify land categories. In the following, emphasis is given to the (i) synthesis of $Mn^{III,IV}$ oxides, (ii) manufacturing of Mn redox bars and (iii) field-installation for monitoring purposes.

(i) Synthesis of minerals

The idea to manufacture Mn redox bars evolved by a new method to synthesize birnessite under ambient pressure and temperature (Händel et al. 2013), which was in contrast to older methods that required high temperatures (60 to 400 °C), long reaction times (up to 90 days), and strong acids and bases in closed systems (Ching et al. 1997; Ma et al. 1999; McKenzie 1971). As a major advantage, it was possible to synthesize birnessite within three working days (one day for the washing procedure and two days for the freeze-drying step) and in sufficient contents (typically one batch within an 800 mL beaker yielded 3.5 g) to start experimenting on how to coat white PVC bars. To summarize it, differences for the synthesis between $Mn^{III,IV}$ and Fe^{III} oxides account for the mineralogical alteration (none vs. at least 7 days), storage of the minerals (freeze dried powder vs. minerals in suspension), and the crystallite size (8 to 11 nm vs. several hundred nm), respectively. Synthesized $Mn^{III,IV}$ oxides did not transform into more crystalline phases by a rearrangement of the crystal lattice because mineralogical alteration did not proceed after the freeze-drying process. This is an important issue for users who manufacture redox bars at multiple times. Even slight changes of the $Mn^{III,IV}$ oxide properties impact their function as electron acceptor (e.g. by alteration of the crystallite size) and might affect depletion patterns along the PVC surface. This was different to the synthesis of Fe^{III} oxides due to the short half-life of the suspension. Preparation of the Fe^{III} oxide suspension was achieved by titrating a 1 M KOH solution to a 0.5 M $FeCl_3$ solution (Rabenhorst and Burch 2006). The original $FeCl_3$ solution was very acidic but Fe^{III} oxides started to precipitate above pH 4. At this point, the formed minerals consisted of pure 2-line ferrihydrite (slightly modified by Schwertmann and Cornell (2000)). The crystallite size of newly formed ferrihydrite was estimated to be 1 nm (Rabenhorst et al. 2008) that demonstrated poor adhesion to the

PVC surface and hence little durability (Rabenhorst and Burch 2006). Rabenhorst and Burch (2006) verified that 30 to 40% goethite content must be present to facilitate a durable Fe^{III} oxide coating. This can be achieved by titrating the Fe^{III} oxide suspension to pH 12 by a 1 M KOH solution to progressively transform ferrihydrite into goethite. The goethite minerals had a lath-shaped habitus with 20 to 50 nm in width and several hundred nm in length and were therefore considerably larger than ferrihydrite and birnessite. They formed a reinforcing network that locked the remaining ferrihydrite minerals together (Rabenhorst et al. 2008). It is obvious that the mineralogical composition has effect on the depletion patterns along Fe redox bars because ferrihydrite is reduced at higher E_H (E^0 = –71 mV at pH 7) than goethite (E^0 = –230 mV at pH 7). The mineralogical transformation can be slowed down when the paint was stored at 5 °C but cannot be completely stopped. Therefore, Fe redox bars manufactured from a distinct suspension must be manufactured within a narrow period of time to guarantee uniform mineral characteristics, a problem not associated with the manufacturing of Mn redox bars.

(ii) Manufacturing

Besides the mineral composition, the content of $Mn^{III,IV}$ and Fe^{III} oxides applied to the PVC surface was also important to compare depletion patterns along redox bars manufactured by individual users. Jenkinson (2002) recommended Fe redox bars having a double coating whereas Rabenhorst et al. (2010) used Fe redox bars with a single coat. Obviously, twice as much Fe^{III} oxide applied to the PVC surface of redox bars required longer installation times in the soil to achieve the same depletion patterns compared with a single coating under soil reducing conditions. Manganese redox bars manufactured in Chapter 3 and used in Chapter 4 and 5 comprised a single $Mn^{III,IV}$ oxide coating but for some PVC bars, pale brownish areas were likely due to an inhomogeneous roughening practice. If the appearance of the coating was uneven, a second $Mn^{III,IV}$ oxide coat was applied. A sufficient roughening practice was very important for a good adherence of the $Mn^{III,IV}$ oxides to the PVC surface, otherwise a lotus-effect was observed. As stated, “it is fundamental to roughening the PVC surface as long as the original smooth surface is not visible anymore” (Chapter 3). There were no further information about the bonding mechanism to the PVC surface but the analogy of $Mn^{III,IV}$ oxides that remained in the perforated PVC surface to silt that remained in the finger ridges seems appropriate. Universal procedures (e.g. by sand blasting, coating techniques) to reproducible apply a defined coating to the PVC surface are desired (e.g. defined by µM Mn or Fe cm^{-2} PVC surface) and subject to further research.

(iii) Field-Installation

So far, all monitoring applications used PVC pipes or tubes for the installation of Fe redox bars (Bryant et al. 2008; Jenkinson and Franzmeier 2006; Rabenhorst and Burch 2006). To minimize loss of the oxide coating, an uncoated PVC pipe, having the same dimensions, was installed in advance, removed from the soil, and carefully replaced by the coated pipe (Bryant et al. 2008). Alternatively a soil probe or auger was used for the push probe (Jenkinson and Franzmeier 2006). The problem of using hollow PVC materials is that O_2 from the atmosphere is potentially transferred to the end of the tube or pipe analogous to aerenchyma inside plant roots. To circumvent this problem, redox bars manufactured within this thesis were composed of solid PVC bars that did not promote the transfer of O_2 into a formerly reducing soil environment. It is encouraged to sharpen the PVC bar at one side to minimize a collapsing of the borehole during installation.

Objective c)

Monitoring and differentiation into weakly and moderately reducing soil conditions by Mn and Fe redox bars

(i) Monitoring

Chapter 4 demonstrated that Mn and Fe redox bars were capable of characterizing the soil redox status with two to five times enhanced $Mn^{III,IV}$ oxide over Fe^{III} oxide removal. A finding in accordance with the thermodynamic properties of the applied minerals. Manganese oxide removal was especially favorable in the capillary fringe where the soil pores were not fully water saturated but high water contents prevailed. The period of water saturation was the main trigger to stimulate the onset of reduction and was negatively correlated with E_H (Mansfeldt 2003) and with the percentage oxide removal along redox bars (Fig. 4.2). Hence, as longer water saturation prevailed as more reducing the soil environment was and as more $Mn^{III,IV}$ and Fe^{III} oxide removal occurred showing the white PVC underneath. Hindersmann and Mansfeldt (2014) demonstrated in microcosm experiments that water saturation must prevail for 160 h at 7 °C, 10 h at 15 °C, and 7 h at 25 °C to achieve weakly reducing soil conditions, and Vaughan et al. (2009) showed that water saturation must prevail for at least 480 h at 1.0 to 3.9 °C and for 48 h at > 9 °C to achieve moderately reducing soil conditions. Hence, suitable conditions to reductively dissolve $Mn^{III,IV}$ oxides (e.g. birnessite) and Fe^{III} oxides (e.g. ferrihydrite) were accelerated at higher soil temperatures. These findings were important for the understanding of depletion patterns along Mn and Fe redox bars. Elevated soil temperature intensified and low temperature hampered the impact by the period of water saturation for the onset of reduction and

subsequently for depletion patterns along redox bars. For instance, high precipitation in June along with elevated soil temperatures (15.5 °C) favored oxide removal of Mn redox bars from plot A with up to 50% in the topsoil (0 to 25 cm) and only minor depletion in the subsoil. In contrast, no oxide removal was observed in the top of the Mn and Fe redox bar from March to May when soil temperatures were lower.

Generally, $Mn^{III,IV}$ oxide removal was highest at plot C (periodically flooded) and ranged between 32.4% and complete removal in the topsoil and entire removal of the oxide coating for the subsoil throughout the study period (Table 4.2). The complete $Mn^{III,IV}$ oxide removal at plot C indicated that the installation time of 30 days was too long for an adequate characterization of the soil redox status in predominantly water saturated soil environments. Hence, weekly monitoring of the soil redox status by Mn redox bars is encouraged, which contributes to a better temporal understanding of soil reducing conditions. Though, characterization of the E_H dynamics that occured within 24 h from moderately reducing towards oxidizing soil conditions (Fig. 2.5) cannot be assessed by either Mn or Fe redox bars. Despite this shortcoming, the use of redox bars over Pt electrodes had some advantages: redox bars reflected the distribution of soil reducing conditions over the complete bars length that represented a **continuum** (Fig. 7.2b) whereas E_H readings by Pt electrodes reflected discrete **point measurements** (Fig. 7.2a). This renders Pt electrodes more susceptible to soil heterogeneity and to a misinterpretation of E_H data when the Pt tip dipped into a soil aggregate assuming reducing conditions in an already aerobic soil environment. The susceptibility to microsite variability was underlined by the active surface area because electron transfer reactions occured along 329 cm^2 at redox bars (50 cm length, 21 mm Ø) compared with 0.16 cm^2 at the tip of Pt electrodes (0.5 cm length, 5 mm Ø).

Overall, the oxide removal along Mn and Fe redox bars was coherent with environmental boundary conditions (e.g. setting of the WT depth, soil temperature) and soil properties (SOM content), a prerequisite to characterize the temporal and spatial distribution of the soil redox status. The simultaneous use of Mn and Fe redox bars is especially helpful at study sites where soils do not develop redoximorphic features. Reasons for the absence of *gleyic* or *stagnic* color patterns are (i) low Fe contents and failure to develop concretions and mottles, (ii) low contents of SOM and lack of a readily available electron donor, (iii) low chroma in color, (iv) alkaline soil horizons preventing Fe^{III} oxide reduction, and (v) the presence of redox buffers (e.g. NO_3^-) that prevent the utilization of $Mn^{III,IV}$ and Fe^{III} oxides as terminal electron acceptors.

(ii) Weakly and moderately reducing soil conditions

Initially, Jenkinson and Franzmeier (2006) noticed darker brown areas along previously field-installed Fe redox bars, which they attributed to a re-deposition of Fe^{III} oxides while the bar was in the soil. Indeed, the remaining Fe^{III} oxide coating along Fe redox bars installed at plot C in June differed slightly after an installation time of 30 days compared with the original Fe^{III} oxide coating (Fig. 4.3b). The differences were only marginal restricting a quantification by image analysis. When we started working with Mn redox bars, we noticed areas along the $Mn^{III,IV}$ oxide coating that differed significantly in color after 30 days of installation. These zones were verified by X-ray fluorescence spectroscopy and element analysis by inductively coupled plasma mass spectrometry as precipitated Fe^{III} oxides (Chapter 4) and later on by energy-dispersive X-ray spectroscopy (Chapter 5; Fig. 5.6). Because of remarkable differences in color, zones along Mn redox bars of remaining $Mn^{III,IV}$ oxide coatings (Fig. 7.3b), Fe^{III} oxide precipitates (Fig. 7.3c), and complete oxide removal (Fig. 7.3d) can be more easily differentiated by image and retouching tools (e.g. GIMP v.2.8.4). Consequently, a differentiation and quantification of zones along redox bars affected by oxidizing (E_H > 300 mV; $Mn^{III,IV}$ and Fe^{III} oxides remain stable), weakly reducing (E_H 300 to 100 mV; $Mn^{III,IV}$ oxides are reduced and Fe^{III} oxides remain stable), and moderately reducing soil conditions (E_H 100 to −100 mV; Fe^{III} oxides are reduced) was possible. These zones were very small in scale (< 10 mm) and emphasized that E_H varied considerably at short distances by three redox classes. Obviously, placement of the Pt electrode tip into the center of an aggregate (E_H < –100 mV) or in the outside (E_H > 300 mV) alters the E_H reading significantly (illustrated in Fig. 7.1c).

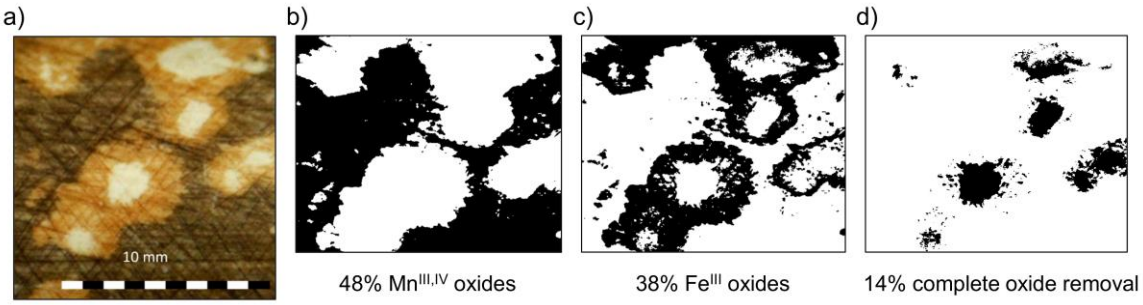

Figure 7.3 Detailed image of a previously field-installed Mn redox bars (a), percentage area of $Mn^{III,IV}$ oxide removal (b), Fe^{III} oxide formation (c), and complete oxide removal (d).

A monitoring of weakly and moderately reducing soil conditions is therefore possible but the applicability and reproducibility must be standardized. In this regard, two constraints are mentioned: first of all, a uniform application procedure is important because a variable thickness (= content) of $Mn^{III,IV}$ oxides is responsible whether or not the white PVC shines

underneath or is completely visible under soil reducing conditions (analogue to the **poise** of a system at which a change of E_H occurs). Further, a color change by the reaction with Fe^{2+} from soil solution is altered because a surplus of oxidant ($Mn^{III,IV}$ oxide) retards a color change towards brownish Fe^{III} oxides by the reaction with the reductant (ferrous Fe^{2+}) (see Chapter 5, Eq. [1]). Secondly, image analysis must progress in tandem with coating procedures. It is desirable to develop a user interface based on digital analysis, which allows the assessment of the depletion patterns in a reproducible, cost-efficient and fast manner. The application of a line-scan camera mounted on a rail is encouraged. Disadvantages of a handheld camera can be compensated by this approach because of a constant distance to the redox bar, defined illumination when mounted inside a dark chamber, and a lengthwise pixel re-composition afterwards that counteracts shading-effects by the three dimensional object.

Objective d)

Investigation of selective element sorption to the oxide coating of redox bars

As outlined in the introduction, $Mn^{III,IV}$ and Fe^{III} oxides are important soil constituents and besides the contribution as electron acceptors under anaerobic respiration, they act as scavenger for nutrients (Peretyazhko and Sposito 2005) and trace metals (Della Puppa et al. 2013) in the soils environment. The element content sorbed to the oxide coating depended on two factors: first, the element concentration in soil solution itself, and second, available sorption sites by the oxide surface. The availability of sorption sites was positively correlated with the contents of oxides applied to redox bars and hence, a depletion of the oxide coating under soil reducing conditions decreased the sorption capacity for elements in soil solution (e.g. defined as µM As m^{-2} oxide surface). Subsequently, redox bars were non-equivalent to suction cups for the monitoring of total element concentrations in soil solution because (i) both factors were difficult to differentiate and (ii) suction cups gather soil solution from the bulk soil whereas the sorption of elements to the oxide surface took place at the pore scale. Besides this restriction, Mn redox bars enabled to investigate temporally and spatially diverse Fe^{III} oxide-forming processes by the collection of *in situ* precipitated Fe^{III} oxides. The percentage area of Fe^{III} oxide formation can be quantified and monitored over time that approximated the depth-dependent distribution of ferrous Fe^{2+} in soil solution (Fig. 4.4a and Fig. 7.3c). Rabenhorst et al. (2010) used Fe redox bars to document and measure semi-quantitatively S^{2-} concentrations in marsh soil pore water that was in conformity to the approach to collect Fe^{III} oxides naturally formed along Mn redox bars. A major disadvantage of the former approach is the requirement of a scanner in the field because FeS formed along the Fe^{III} oxide coating was meta-stable and rapidly

oxidized within minutes (example shown in Fig. 4.4f). In contrast, Fe^{III} oxides along Mn redox bars remained stable over time and the oxide patterns can be digitally analyzed in the laboratory without pressure of time. For a precise terminology and to differentiate between *in situ* formed Fe^{III} oxides along Mn redox bars and synthesized Fe^{III} oxides in the laboratory, it was reasonable to use the terms “field”- and “lab”- Fe^{III} oxides, respectively.

A unique feature of the study site where redox bars were installed were elevated As contents of 111 mg kg^{-1} in the topsoil (Table 5.3) originating from the weathering of fossil bog Fe in shallow groundwater that was relocated upwards by capillary rise in the summertime (Mansfeldt and Overesch 2013). The As contents exceeded by far background values for topsoil in Germany and considering sand loess as parent material with 7 mg As kg^{-1} soil (Utermann et al. 2008), as well as trigger values for the pathway soil → plant by 50 mg As kg^{-1} (BBodSchV 1999). The vast majority of As (> 95%) was associated with poorly- and well-crystallized Fe^{III} oxides (Mansfeldt and Overesch 2013) as revealed by the sequential extraction procedure according to Wenzel et al. (2001). Hence, a competition with other soil constituents for As adsorption was neglible at the study site and it can be expected that As sorption along “field”- and “lab”-Fe^{III} oxides occured. Indeed, selective extraction of either $Mn^{III,IV}$ or Fe^{III} oxide coatings along previously field-installed Mn redox bars revealed that As (and elements such as P, Mo, and V) was enriched along Fe^{III} oxides compared with $Mn^{III,IV}$ oxides (Table 5.2). This finding was in agreement with various studies in literature (e.g. Bowell 1994; Goldberg et al. 1998; Peacock and Sherman 2004; Peretyazhko and Sposito 2005). Because Fe^{III} oxides exhibit a high point of zero charge along with low pH values of 4.5 present at the study site, favorable sorption of oxyanions to the protonated functional groups occurred. It is assumed that sorption of oxyanions to “field”- and “lab”-Fe^{III} oxides gets neglible as closer the soil pH shifts towards the point of zero charge from Fe^{III} oxides, which needs to be tested in further field experiments. Besides minor differences in color, both types of Fe^{III} oxides possessed different Fe_o/Fe_d ratios with a constant value of 0.76 for “lab”- and > 0.99 for “field”-Fe^{III} oxides throughout the study period. Hence, variations of the mineralogy were evident in terms of crystallinity that alters the sorption capacity of a mineral (Wang et al. 2013) and was further proven by elevated element loadings of As and P to “field”- over “lab”-Fe^{III} oxides (Fig. 5.5). Changing redox conditions renders Gleysols natural laboratories to study the mineral (trans)formation of Fe^{III} oxides (Mansfeldt et al. 2012) with redox bars as a supplemental tool to study and monitor the element sorption behavior (Fig. 7.1d).

Objective e)

Evaluation of the WT depth development under the aspect of climate change

The position of the WT was responsible for the E_H dynamics, altered the depletion of the $Mn^{III,IV}$ and Fe^{III} oxide coating along redox bars by the onset of reduction, and triggered the element relocation into the topsoil by capillary rise and subsequent sorption to the remaining oxide coating (Fig. 7.1a, b, c, d). Enduring periods of water saturation went along with peat accumulation in wetlands over centuries (Reddy and DeLaune 2008), whereas peak values of CO_2 release by microbial oxidation of SOM occured during WT draw-down (Rezanezhad et al. 2014) that might counteract accumulation rates. Hence, a temporal or permanent dislocation of the WT has impact on many biogeochemical processes. For instance, Leppelt et al. (2014) identified the WT as the main driver to stimulate N_2O release from organic soils and demonstrated that anthropogenic management by drainage accounts for 85% of N_2O emissions in Europe. The authors emphasized the reduction potential of N_2O emission when re-wetting measures of formerly drained wetlands were performed. Obviously, there is a potential for wetland restoration in Europe because 80% of the original wetland area was lost due to conversion to agricultural uses in the past millennium (Verhoeven 2014). One example of a wetland restoration management was discussed in Chapter 6 and its success evaluated by analyzing time series data of WT depth readings from 1997 to 2012. Application of a trend decomposition procedure revealed decreasing trends at 84% of all monitoring wells (n = 46; Fig. 6.1) that equaled a lowering of the WT depth by 20 cm according to the position of the trend line. Hence, the WT depth development is contradicting to the re-wetting goals. It is expected that rising air temperatures and variable precipitation patterns alter the climatic water balance towards more negative values in the summer and positive in the winter that favors an earlier and more intense WT draw-down. This development is already verifiable by the STL procedure because an increase of the seasonal component was detected along 42 out of 46 monitoring wells from 2007 to 2012 (exemplified in Fig. 6.S1d). These results imply for the future development that the position of the WT depth during summer- and wintertime might drift apart. Seasonal WT fluctuations were also observed at the study site Speicherkoog (Chapter 2) and Lavesum (Chapter 4) with WT fluctuations from ponding water in winter up to 200 cm below ground in summer.

Quantification of the oxide removal along Mn and Fe redox bars was also indicative to deliver information of the WT depth and can be used to depict trends over time. Jenkinson and Franzmeier (2006) proposed the term upper depletion depth (UDD) to indicate enhanced removal of Fe^{III} oxide coatings. In Fig. 4.3b, the UDD along Fe redox bars correlated well with the mean WT depth demonstrating only minor Fe^{III} oxide removal above the

groundwater surface. In contrast, the UDD along Mn redox bars correlated better with the maximum rose of the WT during the installation time of Mn redox bars with enhanced $Mn^{III,IV}$ oxide removal in the capillary fringe (illustrated in Fig. 7.1b). Furthermore, depth- and time-dependent $Mn^{III,IV}$ oxide removal gives insight about potential N transformation pathways because the reductive dissolution of $Mn^{III,IV}$ oxides under weakly reducing soil conditions is the range of N_2O formation by denitrification processes (Yu and Patrick 2004; Yu et al. 2001). The formation of N_2O is very variable in space and time as verified by Shrestha et al. (2014) by measuring N_2O concentrations and E_H along a river floodplain during a flood pulse. In their study, the E_H decreased rapidly from oxidizing to weakly reducing soil conditions during the flood event and increased again after the peak discharge within 48 hours. The authors characterized the drying phase after the flood as “hot moments” because N_2O emission increased from 17 to 40 mg $N\text{-}N_2O$ kg^{-1} day^{-1}. Short-term monitoring by Mn redox bars on a weekly basis certainly helps to delineate potential hot spots of N_2O emission but further studies are required to link the percentage oxide removal under weakly reducing soil conditions with N_2O measurements.

Chapter 8 References

References

Chapter 1 and 7

Aeschbacher, M., Vergari, D., Schwarzenbach, R.P. and Sander, M. (2011) Electrochemical analysis of proton and electron transfer equilibria of the reducible moieties in humic acids. Environmental Science & Technology. 45: 8385–8394.

BBodSchV (1999) Federal Soil Protection and Contaminated Sites Ordinance (Bundes-Bodenschutz- und Altlastenverordnung - BBodSchV) from 12.07.1999. BGBl. I pp. 1554–1582.

Bohn, H.L. (1970) Comparison of measured and theoretical Mn^{2+} concentrations in soil suspensions. Soil Science Society of America Proceedings. 34: 195–197.

Bohn, H.L. (1971) Redox potentials. Soil Science. 112: 39–45.

Bouma, J. (1983) Hydrology and soil genesis of soils with aquic moisture regimes. In: Wilding, L.P., Smeck, N.E. and Hall, G.F., (Eds.), Pedogenesis and soil taxonomy. I. concepts and interactions. Elsevier, Amsterdam, Netherlands.

Bowell, R.J. (1994) Sorption of arsenic by iron oxides and oxyhydroxides in soils. Applied Geochemistry. 9: 279–286.

Brümmer, G. (1974) Redoxpotentiale und Redoxprozesse von Mangan-, Eisen und Schwefelverbindungen in hydromorphen Böden und Sedimenten. Geoderma. 12: 207–222.

Bryant, K., Wilson, P.R., Biggs, A.J.W., Brough, D.M. and Burgess, J.W. (2008) Soil indicators of Queensland wetlands: statewide assessment and methodology. In: Department of Natural Resources and Water. Brisbane, Australia.

Canfield, D.E., Thamdrup, B. and Hansen, J.W. (1993) The anaerobic degradation of organic matter in Danish coastal sediments: iron reduction, manganese reduction, and sulfate reduction. Geochimica et Cosmochimica Acta. 57: 3867–3883.

Castenson, K.L. and Rabenhorst, M.C. (2006) Indicator of reduction in soil (IRIS): evaluation of a new approach for assessing reduced conditions in soil. Soil Science Society of America Journal. 70: 1222–1226.

Chapelle, F.H., McMahon, P.B., Dubrovsky, N.M., Fujii, R.F., Oaksford, E.T. and Vroblesky, D.A. (1995) Deducing the distribution of terminal electron-accepting processes in hydrologically diverse groundwater systems. Water Resources Research. 31: 359–371.

Childs, C.W. (1981) Field-tests for ferrous iron and ferric-organic complexes (on exchange sites or in water soluble forms) in soils. Australian Journal of Soil Research. 19: 175–180.

Ching, S., Petrovay, D.J., Jorgensen, M.L. and Suib, S.L. (1997) Sol-gel synthesis of layered birnessite-type manganese oxides. Inorganic Chemistry. 36: 883–890.

Clay, D.E., Clapp, C.E., Molina, J.A.E. and Linden, D.R. (1990) Soil tillage impact on the diurnal redox-potential cycle. Soil Science Society of America Journal. 54: 516–521.

Cogger, C.G., Kennedy, P.E. and Carlson, D. (1992) Seasonally saturated soils in the Puget lowland II. measuring and interpreting redox potentials. Soil Science. 154: 50–58.

Cornell, R.M. and Schwertmann, U. (2003) The iron oxides: structure, properties, reactions, occurences, and uses. second ed. Wiley-VCH, Weinheim, Germany.

Dalkmann, P., Dresemann, T.F., Siebe, C., Mansfeldt, T., Amelung, W. and Siemens, J. (2014) Release of pharmaceuticals under reducing conditions in a wastewater-irrigated mexican soil. Journal of Environmental Quality. 43: 1926–1932.

DeLaune, R.D. and Reddy, K.R. (2005) Redox potential. In: Hillel, D., (Ed.), Encyclopedia of soils in the environment. Academic Press, San Diego, CA, USA.

Della Puppa, L., Komárek, M., Bordas, F., Bollinger, J.-C. and Joussein, E. (2013) Adsorption of copper, cadmium, lead and zinc onto a synthetic manganese oxide. Journal of colloid and interface science. 399: 99–106.

Essington, M.E. (2015) Soil and water chemistry: an integrative approach. second ed. CRC Press, Boca Raton, FL, USA.

Fakih, M., Davranche, M., Dia, A., Nowack, B., Petitjean, P., Chatellier, X. and Gruau, G. (2008) A new tool for in situ monitoring of Fe-mobilization in soils. Applied Geochemistry. 23: 3372–3383.

Farrell, R.E., Swerhone, G.D.W. and van Kessel, C. (1991) Construction and evaluation of a reference electrode assembly for use in monitoring in situ soil redox potentials. Communications in Soil Science and Plant Analysis. 22: 1059–1068.

Fiedler, S. (2000) In situ long-term-measurement of redox potential in redoximorphic soils. In: Schüring, J., Schulz, H.D., Fischer, W.R., Böttcher, J. and Duijnisveld, W.H.M., (Eds.), Redox: fundamentals, processes, and applications. Springer, Heidelberg, Germany.

Fiedler, S., Vepraskas, M.J. and Richardson, J.L. (2007) Soil redox potential: importance, field measurements, and observations. In: Sparks, D.L., (Ed.), Advances in Agronomy. Academic Press, San Diego, CA, USA.

Galster, H. (1991) pH measurement: fundamentals, methods, applications, instrumentation. VCH, Weinheim, Germany.

Gillespie, L.J. (1920) Reduction potentials of bacterial cultures and of water-logged soils. Soil Science. 9: 199–216.

Glinski, J. and Stepniewski, W. (1985) Soil aeration and its role for plants. CRC Press, Boca Raton, FL, USA.

Goldberg, S., Chunming, S. and Forster, H.S. (1998) Sorption of molybdenum on oxides, clay minerals, and soils: mechanisms and models. In: Jenne, E.A., (Ed.), Adsorption of metals by geomedia. Academic Press, San Diego, CA, USA.

Händel, M., Rennert, T. and Totsche, K.U. (2013) A simple method to synthesize birnessite at ambient pressure and temperature. Geoderma. 193–194: 117–121.

Hindersmann, I. and Mansfeldt, T. (2014) Trace element solubility in a multimetal-contaminated soil as affected by redox conditions. Water, Air, & Soil Pollution. 225: 1–20.

Houle, D., Bouffard, A., Duchesne, L., Logan, T. and Harvey, R. (2012) Projections of future soil temperature and water content for three southern Quebec forested sites. Journal of Climate. 25: 7690–7701.

IUSS Working Group WRB (2014) World reference base for soil resources 2014. FAO, Rome, Italy.

James, B.R. and Brose, D.A. (2012) Oxidation-reduction phenomena. In: Huang, P.M., Yuncong, L. and Sumner, M.E., (Eds.), Handbook of soil science: properties and processes. CRC Press, Boca Raton, FL, USA.

Jenkinson, B.J. (2002) Hydrology of sandy soils in northwest Indiana and iron oxide indicators to identify hydric soils. PhD, Purdue University, West Lafayette.

Jenkinson, B.J. and Franzmeier, D.P. (2006) Development and evaluation of iron-coated tubes that indicate reduction in soils. Soil Science Society of America Journal. 70: 183–191.

Kirk, G. (2004) The biogeochemistry of submerged soils. John Wiley & Sons, Chichester, England.

Komárek, M., Vaněk, A. and Ettler, V. (2013) Chemical stabilization of metals and arsenic in contaminated soils using oxides – a review. Environmental Pollution. 172: 9–22.

Leppelt, T., Dechow, R., Gebbert, S., Freibauer, A., Lohila, A., Augustin, J., Drösler, M., Fiedler, S., Glatzel, S., Höper, H., Järveoja, J., Lærke, P.E., Maljanen, M., Mander, Ü., Mäkiranta, P., Minkkinen, K., Ojanen, P., Regina, K. and Strömgren, M. (2014) Nitrous oxide emission budgets and land-use-driven hotspots for organic soils in Europe. Biogeosciences. 11: 6595–6612.

Lindsay, W.L. (1979) Chemical equilibria in soils. John Wiley & Sons, Inc., New York, NY, USA.

Loganathan, P. and Burau, R.G. (1973) Sorption of heavy metal ions by a hydrous manganese oxide. Geochimica et Cosmochimica Acta. 37: 1277–1293.

Ma, Y., Luo, J. and Suib, S.L. (1999) Syntheses of birnessites using alcohols as reducing reagents: effects of synthesis parameters on the formation of birnessites. Chemistry of Materials. 11: 1972–1979.

Mansfeldt, T. (1993) Redoxpotentialmessungen mit dauerhaft installierten Platinelektroden unter reduzierenden Bedingungen. Zeitschrift für Pflanzenernährung und Bodenkunde. 156: 287–292.

Mansfeldt, T. (2003) In situ long-term redox potential measurements in a dyked marsh soil. Journal of Plant Nutrition and Soil Science. 166: 210–219.

Mansfeldt, T. (2004) Redox potential of bulk soil and soil solution concentration of nitrate, manganese, iron, and sulfate in two Gleysols. Journal of Plant Nutrition and Soil Science. 167: 7–16.

Mansfeldt, T. and Blume, H.-P. (2002) Organic sulfur forms in mineral top soils of the marsh in Schleswig-Holstein, Northern Germany. Journal of Plant Nutrition and Soil Science. 165: 255–260.

Mansfeldt, T. and Overesch, M. (2013) Arsenic mobility and speciation in a Gleysol with petrogleyic properties: a field and laboratory approach. Journal of Environmental Quality. 42: 1130–1141.

Mansfeldt, T., Schuth, S., Häusler, W., Wagner, F., Kaufhold, S. and Overesch, M. (2012) Iron oxide mineralogy and stable iron isotope composition in a Gleysol with petrogleyic properties. Journal of Soils and Sediments. 12: 97–114.

Martin, S.T. (2005) Precipitation and dissolution of iron and manganese oxides In: Grassian, V.H., (Ed.), Environmental Catalysis. CRC Press, Boca Raton, FL, USA.

Matern, K. and Mansfeldt, T. (2015) Molybdate adsorption by birnessite. Applied Clay Science. 108: 78–83.

McKenzie, L.J., Whiteside, E.P. and Erickson, A.E. (1960) Oxidation-reduction studies on the mechanism of B horizon formation in Podzols. Soil Science Society of America Journal. 24: 300–305.

McKenzie, R.M. (1971) The synthesis of birnessite, cryptomelane, and some other oxides and hydroxides of manganese. Mineralogical Magazine. 38: 493–502.

Meek, B.D. and Grass, L.B. (1975) Redox potential in irrigated desert soils as an indicator of aeration status. Soil Science Society of America Journal. 39: 870–875.

Morse, J.W. and Luther III, G.W. (1999) Chemical influences on trace metal-sulfide interactions in anoxic sediments. Geochimica et Cosmochimica Acta. 63: 3373–3378.

Mueller, S.C., Stolzy, L.H. and Fick, G.W. (1985) Constructing and screening platinum microelectrodes for measuring soil redox potential. Soil Science. 139: 558–560.

National Technical Committee for Hydric Soils (2015) Hydric soils technical note 11: hydric soils technical standard and data submission requirements for field indicators of hydric soils. http://www.nrcs.usda.gov/wps/portal/nrcs/detail/soils/home/?cid=nrcs 142p2_ 053973 (accessed 27 Jan. 2016).

Negra, C., Ross, D.S. and Lanzirotti, A. (2005) Oxidizing behavior of soil manganese: interactions among abundance, oxidation state, and pH. Soil Science Society of America Journal. 69: 87–95.

Nordstrom, D.K. (1982) Aqueous pyrite oxidation and the consequent formation of secondary iron minerals. In: Kittrick, J.A., Fanning, D.S. and Hosner, L.P., (Eds.), Acid sulfate weathering. Soil Science Society of America Madison, WI, USA.

Owens, P.R., Wilding, L.P., Miller, W.M. and Griffin, R.W. (2008) Using iron metal rods to infer oxygen status in seasonally saturated soils. CATENA. 73: 197–203.

Patrick, W.H. and Turner, F.T. (1968) Effect of redox potential on manganese transformation in waterlogged soil. Nature. 220: 476–478.

Peacock, C.L. and Sherman, D.M. (2004) Vanadium(V) adsorption onto goethite (α-FeOOH) at pH 1.5 to 12: a surface complexation model based on ab initio molecular geometries and EXAFS spectroscopy. Geochimica et Cosmochimica Acta. 68: 1723–1733.

Peretyazhko, T. and Sposito, G. (2005) Iron(III) reduction and phosphorous solubilization in humid tropical forest soils. Geochimica et Cosmochimica Acta. 69: 3643–3652.

Pfisterer, U. and Gribbohm, S. (1989) Zur Herstellung von Platinelektroden für Redoxmessungen. Zeitschrift für Pflanzenernährung und Bodenkunde. 152: 455–456.

Piccolo, A., Celano, G., Arienzo, M. and Mirabella, A. (1994) Adsorption and desorption of glyphosate in some European soils. Journal of Environmental Science and Health. 29: 1105–1115.

Picek, T., Šimek, M. and Šantrůčková, H. (2000) Microbial responses to fluctuation of soil aeration status and redox conditions. Biology and Fertility of Soils. 31: 315–322.

Piepenbrock, A., Schröder, C. and Kappler, A. (2014) Electron transfer from humic substances to biogenic and abiogenic Fe(III) oxyhydroxide minerals. Environmental Science & Technology. 48: 1656–1664.

Ponnamperuma, F.N. (1972) The chemistry of submerged soils. Advances in Agronomy. 24: 29–96.

Ponnamperuma, F.N., Tianco, E.M. and Loy, T. (1967) Redox equilibria in flooded soils: I. the iron hydroxide systems. Soil Science. 103: 374–382.

Rabenhorst, M.C. (2010) Visual assessment of IRIS tubes in field testing for soil reduction. Wetlands. 30: 847–852.

Rabenhorst, M.C. (2012) Simple and reliable approach for quantifying IRIS tube data. Soil Science Society of America Journal. 76: 307–308.

Rabenhorst, M.C., Bourgault, R.R. and James, B.R. (2008) Iron oxyhydroxide reduction in simulated wetland soils: effects of mineralogical composition of IRIS paints. Soil Science Society of America Journal. 72: 1838–1842.

Rabenhorst, M.C. and Burch, S.N. (2006) Synthetic iron oxides as an indicator of reduction in soils (IRIS). Soil Science Society of America Journal. 70: 1227–1236.

Rabenhorst, M.C., Megonigal, J.P. and Keller, J. (2010) Synthetic iron oxides for documenting sulfide in marsh pore water. Soil Science Society of America Journal. 74: 1383–1388.

Rabenhorst, M.C., Ming, D.W., Morris, R.V. and Golden, D.C. (2008) Synthesized iron oxides used as a tool for documenting reducing conditions in soils. Soil Science. 173: 417–423.

Reddy, K.R. and DeLaune, R.D. (2008) Biogeochemistry of wetlands - science and applications. CRC Press, Boca Raton, FL, USA.

Rennert, T. and Mansfeldt, T. (2005) Iron-cyanide complexes in soil under varying redox conditions: speciation, solubility and modelling. European Journal of Soil Science. 56: 527–536.

Rezanezhad, F., Couture, R.M., Kovac, R., O'Connell, D. and Van Cappellen, P. (2014) Water table fluctuations and soil biogeochemistry: an experimental approach using an automated soil column system. Journal of Hydrology. 509: 245–256.

Ringrose-Voase, A.J. and Humphreys, G.S. (1993) Soil micromorphology: studies in management and genesis. Elsevier, Amsterdam, Netherlands.

Schieber, J. (2011) Iron sulfide formation. In: Reitner, J. and Thiel, V., (Eds.), Encyclopedia of Geobiology. Springer, Heidelberg, Germany.

Schlesinger, W.H. and Emily, S.B. (2013) Biogeochemistry: an analysis of global change. third ed. Academic Press, Amsterdam, Netherlands.

Schuth, S., Hurraß, J., Münker, C. and Mansfeldt, T. (2015) Redox-dependent fractionation of iron isotopes in suspensions of a groundwater-influenced soil. Chemical Geology. 392: 74–86.

Schwertmann, U. and Cornell, R.M. (2000) Iron oxides in the laboratory - preparation and characterization. second ed. Wiley-VCH, Weinheim, Germany.

Schwertmann, U. and Taylor, R.M. (1989) Iron oxides. In: Dixon, J.B. and Weed, S.B., (Eds.), Minerals in soil environments. Wiley-VCH, New York, NY, USA.

Scott, A.D. and Evans, D.D. (1955) Dissolved oxygen in saturated soil. Soil Science Society of America Journal. 19: 7–12.

Scott, M.J. and Morgan, J.J. (1990) Energetics and conservative properties of redox systems. In: Melchior, D.C. and Bassett, R.L., (Eds.), Chemical modeling of aqueous systems II. American Chemical Society, Washington, DC, USA.

Shrestha, J., Niklaus, P.A., Pasquale, N., Huber, B., Barnard, R.L., Frossard, E., Schleppi, P., Tockner, K. and Luster, J. (2014) Flood pulses control soil nitrogen cycling in a dynamic river floodplain. Geoderma. 228–229: 14–24.

Smedley, P.L. and Kinniburgh, D.G. (2002) A review of the source, behaviour and distribution of arsenic in natural waters. Applied Geochemistry. 17: 517–568.

Strawn, D.G., Bohn, H.L. and O'Connor, G.A. (2015) Soil chemistry. fourth ed. John Wiley & Sons, Ltd., Hoboken, NJ, USA.

Tebo, B.M., Johnson, H.A., McCarthy, J.K. and Templeton, A.S. (2005) Geomicrobiology of manganese(II) oxidation. Trends in Microbiology. 13: 421–428.

Unger, I.M., Muzika, R.M., Motavalli, P.P. and Kabrick, J. (2008) Evaluation of continuous in situ monitoring of soil changes with varying flooding regimes. Communications in Soil Science and Plant Analysis. 39: 1600–1619.

Utermann, J., Fuchs, M. and Düwel, O. (2008) Flächenrepräsentative Hintergrundwerte für Arsen, Antimon, Beryllium, Molybdän, Kobalt, Selen, Thallium, Uran und Vanadium in Böden Deutschlands aus länderübergreifender Sicht. In: Bundesanstalt für Geowissenschaften und Rohstoffe, Hannover, Germany

Vaughan, K.L., Rabenhorst, M.C. and Needelman, B.A. (2009) Saturation and temperature effects on the development of reducing conditions in soils. Soil Science Society of America Journal. 73: 663–667.

Vepraskas, M.J. and Wilding, L.P. (1983) Aquic moisture regimes in soils with and without low chroma colors. Soil Science Society of America Journal. 47: 280–285.

Verhoeven, J.T.A. (2014) Wetlands in Europe: perspectives for restoration of a lost paradise. Ecological Engineering. 66: 6–9.

Wang, Xiaoming, Liu, Fan, Tan, Wenfeng, Li, Wei, Feng, Xionghan and Sparks, D.L. (2013) Characteristics of phosphate adsorption-desorption onto ferrihydrite: comparison with well-crystalline Fe (hydr)oxides. Soil Science. 178: 1–11.

Wenzel, W.W., Kirchbaumer, N., Prohaska, T., Stingeder, G., Lombi, E. and Adriano, D.C. (2001) Arsenic fractionation in soils using an improved sequential extraction procedure. Analytica Chimica Acta. 436: 309–323.

Whitfield, M. (1974) Thermodynamic limitations on the use of the platinum electrode in E_H measurements. Limnology and Oceanography. 19: 857–865.

Yu, K.W. and Patrick, W.H. (2004) Redox window with minimum global warming potential contribution from rice soils. Soil Science Society of America Journal. 68: 2086–2091.

Yu, K.W., Wang, Z.P., Vermoesen, A., Patrick, W.H. and Van Cleemput, O. (2001) Nitrous oxide and methane emissions from different soil suspensions: effect of soil redox status. Biology and Fertility of Soils. 34: 25–30.

Zausig, J., Stepniewski, W. and Horn, R. (1993) Oxygen concentration and redox potential gradients in unsaturated model soil aggregates. Soil Science Society of America Journal. 57: 908–916.

Zhou, Q., Maurice, P.A. and Cabaniss, S.E. (2001) Size fractionation upon adsorption of fulvic acid on goethite: equilibrium and kinetic studies. Geochimica et Cosmochimica Acta. 65: 803–812.

Eigenbeteiligung an den Veröffentlichungen

1. **Dorau, K.**, Mansfeldt, T. 2016. Comparison of redox potential dynamics in a diked marsh soil: 1990 to 1993 versus 2011 to 2014. *Journal of Plant Nutrition and Soil Science* 179(5), 641–651.
   Erhebung der Daten im Labor: 60%
   Auswertung und Interpretation: 95%
   Verfassen der Publikation: 95%

2. **Dorau, K.**, Mansfeldt, T. 2015. Manganese-Oxide-Coated Redox Bars as an Indicator of Reducing Conditions in Soils. *Journal of Environmental Quality* 44, 696–703.
   Erhebung der Daten im Labor: 90%
   Erhebung der Daten im Gelände: 80%
   Auswertung und Interpretation: 90%
   Verfassen der Publikation: 75%

3. **Dorau, K.**, Eickmeier, M., Mansfeldt, T. 2016. Comparison of manganese and iron oxide-coated redox bars for characterization of the redox status in wetland soils. *WETLANDS* 36, 133–141.
   Erhebung der Daten im Gelände: 80%
   Auswertung und Interpretation: 95%
   Verfassen der Publikation: 95%

4. **Dorau, K.**, Mansfeldt, T. 2015. Manganese and iron oxide-coated redox bars as a tool to study the in situ sorption behavior of elements in wet soils. *Journal of Soils and Sediments* 16(3), 976–986.
   Erhebung der Daten im Labor: 60%
   Auswertung und Interpretation: 95%
   Verfassen der Publikation: 95%

5. **Dorau, K.**, Gelhausen, H., Esplör, D., Mansfeldt, T. 2015. Wetland restoration management under the aspect of climate change at a mesotrophic fen in Northern Germany. *Ecological Engineering* 84, 84–91.
   Auswertung und Interpretation: 95%
   Verfassen der Publikation: 95%

Köln, February 2017 Kristof Dorau

Erklärung

Ich versichere, dass ich die von mir vorgelegte Dissertation selbständig angefertigt, die benutzten Quellen und Hilfsmittel vollständig angegeben und die Stellen der Arbeit − einschließlich Tabellen, Karten und Abbildungen −, die anderen Werken im Wortlaut oder dem Sinn nach entnommen sind, in jedem Einzelfall als Entlehnung kenntlich gemacht habe; dass diese Dissertation noch keiner anderen Fakultät oder Universität zur Prüfung vorgelegen hat; dass sie −abgesehen von unten angegebenen Teilpublikationen −noch nicht veröffentlicht worden ist, sowie, dass ich eine solche Veröffentlichung vor Abschluss des Promotionsverfahrens nicht vornehmen werde. Die Bestimmungen der Promotionsordnung sind mir bekannt. Die von mir vorgelegte Dissertation ist von Prof. Dr. Tim Mansfeldt betreut worden.

[1] Dorau, K., Mansfeldt, T. Comparison of redox potential dynamics in a diked marsh soil: 1990 to 1993 versus 2011 to 2014. *Journal of Plant Nutrition and Soil Science* 179(5), 641–651.

[2] Dorau, K., Mansfeldt, T. 2015. Manganese-Oxide-Coated Redox Bars as an Indicator of Reducing Conditions in Soils. *Journal of Environmental Quality* 44, 696–703.

[3] Dorau, K., Eickmeier, M., Mansfeldt, T. 2016. Comparison of manganese and iron oxide-coated redox bars for characterization of the redox status in wetland soils. *WETLANDS* 36, 133–141.

[4] Dorau, K., Mansfeldt, T. 2015. Manganese and iron oxide-coated redox bars as a tool to study the in situ sorption behavior of elements in wet soils. *Journal of Soils and Sediments* 16(3), 976–986.

[5] Dorau, K., Gelhausen, H., Esplör, D., Mansfeldt, T. 2015. Wetland restoration management under the aspect of climate change at a mesotrophic fen in Northern Germany. *Ecological Engineering* 84, 84–91.

Köln, February 2017 Kristof Dorau